TACKLING MULTI-REFERENCE SYSTEMS WITH QUANTUM MONTE CARLO METHODS

Von der Fakultät für Mathematik, Informatik und Naturwissenschaften der RWTH

Aachen University zur Erlangung des akademischen Grades einer Doktorin der

Naturwissenschaften genehmigte Dissertation

vorgelegt von

Jil Schultze, M.Sc.

aus

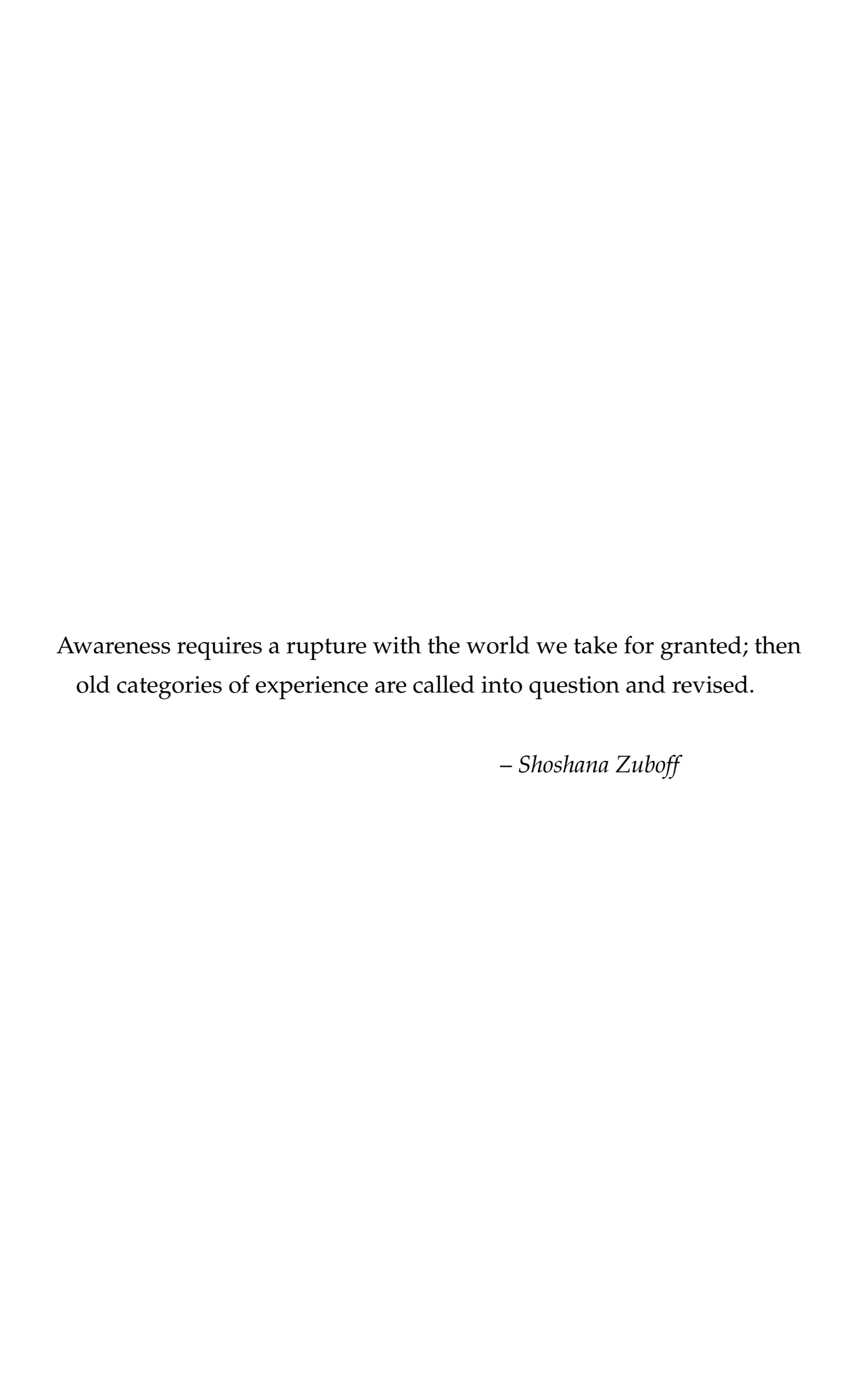
Luxemburg, Luxemburg

Berichter: Prof. Dr. Arne Lüchow

Prof. Dr. Christoph Bannwarth

Tag der mündlichen Prüfung: 08.12.2023

Diese Dissertation ist auf den Internetseiten der Universitätsbibliothek verfügbar.



Eidesstattliche Erklärung

Ich, Jil Schultze, erkläre hiermit, dass diese Dissertation und die darin dargelegten Inhalte die eigenen sind und selbstständig, als Ergebnis der eigenen originären Forschung, generiert wurden. Hiermit erkläre ich an Eides statt

- 1. Diese Arbeit wurde vollständig oder größtenteils in der Phase als Doktorand dieser Fakultät und Universität angefertigt;
- 2. Sofern irgendein Bestandteil dieser Dissertation zuvor für einen akademischen Abschluss oder eine andere Qualifikation an dieser oder einer anderen Institution verwendet wurde, wurde dies klar angezeigt;
- 3. Wenn immer andere eigene- oder Veröffentlichungen Dritter herangezogen wurden, wurden diese klar benannt;
- 4. Wenn aus anderen eigenen- oder Veröffentlichungen Dritter zitiert wurde, wurde stets die Quelle hierfür angegeben. Diese Dissertation ist vollständig meine eigene Arbeit, mit der Ausnahme solcher Zitate;
- 5. Alle wesentlichen Quellen von Unterstützung wurden benannt;
- 6. Wenn immer ein Teil dieser Dissertation auf der Zusammenarbeit mit anderen basiert, wurde von mir klar gekennzeichnet, was von anderen und was von mir selbst erarbeitet wurde;
- 7. Ein Teil oder Teile dieser Arbeit wurden zuvor veröffentlicht und zwar in:
 - J. Ludovicy, K. Haghighi Mood, A. Lüchow, Full Wave Function Optimization with Quantum Monte Carlo—A Study of the Dissociation Energies of ZnO, FeO, FeH, and CrS, J. Chem. Theory Comput. **2019**, *15*, 5221-5229.
 - J. Ludovicy, R. Dahl, A. Lüchow, Toward Compact Selected Configuration Interaction Wave Functions with Quantum Monte Carlo—A Case Study of C₂, J. Chem. Theory Comput. **2023**, 19, 2792-2803.

Aachen, 11. Juli 2023

Parts of this thesis have been published in the following posters and books:

- Jil Ludovicy and Arne Lüchow, Full Wave Function Optimization of Transition Metal Compounds with Quantum Monte Carlo, poster at the 10th Triennial Congress of the International Society for Theoretical Chemical Physics, Tromsø, Norway, July 2019.
- Arne Lüchow, Many-Body Methods for Real Materials, *Lecture Notes of the Autumn School on Correlated Electrons* 2019, 4.1-4.25, Jülich, Germany, September 2019.
- Jil Ludovicy and Arne Lüchow, Toward Compact Selected Configuration Interaction Wave Functions with Quantum Monte Carlo—A Case Study of C₂, poster at the 58th Symposium on Theoretical Chemistry, Heidelberg, Germany, September 2022.

The work of the following students, supervised by me, is partly used in this thesis:

- Hannah A. Graß, Investigation of CIPSI Wave Function Impact of the Jastrow Factor and the Expansion Size on the Nodal Surface, Bachelor Thesis, RWTH Aachen University, July 2021.
- Robin Dahl, On the Impact of Initital Orbitals on CIPSI-Jastrow Wave Functions, Bachelor Thesis, RWTH Aachen University, July 2022.

Acknowledgements

I would like to dedicate a few words to the following people as a token of my gratitude.

Arne Lüchow. Thank you for your support and for making the realization of this thesis possible. Your enthusiasm for research as well as your dedication is a true inspiration.

Christoph Bannwarth. Thank you for co-supervising this thesis and for the many fruitful discussions, whether work-related or not.

Leonard Reuter. We worked together in the AK Lüchow for our bachelor, master, and doctoral theses. Thank you for being a great colleague and an even better friend. I cherish the many laughs, the Hüpfen and beach volleyball sessions, and, of course, your myriad (almost always correct) facts and stories.

Colleagues. Thank you to Kaveh Haghighi Mood, Michael Heuer, Vladimir Terzi, Michel Heinz, and Sonja Keimes for creating such an agreeable working atmosphere. To you and the colleagues of the other working groups: thank you for the numerous coffee breaks, the barbecues, the Irish pub visits, the cake meetings, and, overall, simply a great time at the IPC.

Students. Thank you to Tim Schramm, Christopher Roeper, Tom Höfken, Nils van Staalduinen, Hannah Grass, and Robin Dahl for your contributions to this work and for your commitment while working in our group.

Pascale and Patrick. My dear parents. Thank you for your endless support and always enabling me to pursue my goals.

Tim. My wonderful husband. You are my greatest source of inspiration. Thank you for always being there. Here's to many adventures ahead.



Abstract

For nearly a century, the quest to accurately describe the correlation of electrons has been pursued by scientists. However, the challenging task of recovering both dynamic and static electron correlation, which is crucial for systems dominated by multiple configurations, has been encountered. In the last few decades, researchers have developed a multitude of methods carefully tailored to capture both types of correlation. Among the techniques capable of addressing this challenge are quantum Monte Carlo methods, known for their ability to provide accuracy beyond mean-field theory. The objective of this work is to explore the effectiveness and accuracy of the multi-reference diffusion Monte Carlo (MR-DMC) approach for various systems exhibiting multi-reference character. In the first part of this work, we focus on the late transition metal compounds, utilizing initial full valence complete active space self-consistent field wave functions. Accurate bond dissociation energies are reported for a variety of transition metal dimers, demonstrating close agreement with experimental results. The optimization of molecular orbitals using variational Monte Carlo in the presence of a Jastrow correlation function is identified as a key factor contributing to this success. Additionally, spectroscopic constants are investigated by fitting a Morse potential to the recorded MR-DMC potential energy curves, resulting in a good agreement with experimental and theoretical data. In the second part, we shift our attention to selected configuration interaction approaches, with a primary emphasis on a rigorous investigation of the ground state of the carbon dimer using truncated CIPSI*-Jastrow wave functions. The influence of the Jastrow factor on the redistribution of importance among the different configurations is discussed. Furthermore, accurate MR-DMC absolute energies and bond dissociation energies for the carbon dimer are presented. Lastly, a selected configuration interaction algorithm in conjunction with a Jastrow correlation function is introduced.

^{*}configuration interaction using a perturbative selection made iteratively

Contents

A	bstra	ct		xi			
1	on	1					
2	Intr	Introducing Quantum Mechanics					
	2.1	The S	chrödinger Equation	6			
	2.2	The B	orn-Oppenheimer Approximation	8			
	2.3	The V	ariational Principle	9			
3	Har	tree-Fo	ck Theory	11			
4	The	Pursui	it of Electronic Correlation	13			
	4.1	Post-I	Hartree-Fock Methods	13			
		4.1.1	Configuration Interaction	13			
		4.1.2	Multi-Reference Configuration Interaction	14			
		4.1.3	Multi-Configurational Self-Consistent Field	15			
		4.1.4	Selected Configuration Interaction	16			
	4.2	Densi	ty Functional Theory	17			
	4.3	Explic	cit Treatment	19			
5	Qua	ntum l	Monte Carlo Methods	21			
	5.1	Unde	rlying Foundations	21			
		5.1.1	Statistical Analysis of Random Variables	22			
		5.1.2	Monte Carlo Integration	23			
		5.1.3	Importance Sampling	24			
		5.1.4	Metropolis-Hastings Algorithm	25			
	5.2	Wave	Function Form	26			
		5.2.1	Jastrow Correlation Function	26			
		5.2.2	Configuration State Functions	28			
5.3 Variational Monte Carlo				31			

	5.4	Wave I	Function Parametrization and Optimization
		5.4.1	Variance Minimization
		5.4.2	Energy Minimization
			5.4.2.1 Linear Method
			5.4.2.2 Newton Method
			5.4.2.3 Perturbative Method
	5.5	Diffusi	on Monte Carlo
		5.5.1	Importance Sampling DMC
		5.5.2	Fermion Sign Problem
	5.6	Effectiv	ve Core Potentials
6	Trar	nsition N	Metal Compounds 47
	6.1	With H	Iydrogen
		6.1.1	FeH
		6.1.2	СоН 55
	6.2	With F	irst-Row Elements
		6.2.1	NiC
		6.2.2	FeC
		6.2.3	FeO
	6.3	With S	econd-Row Elements
		6.3.1	CrS
		6.3.2	NiSi
	6.4	Spectro	oscopic Constants
	6.5	Comp	atational Approach
7	Sele	ected Co	onfiguration Interaction 73
	7.1	Statisti	cal Analysis of CI Coefficients
	7.2	Using	the Linear Optimization Method
	7.3	CIPSI-	Jastrow Wave Functions
		7.3.1	Truncated CIPSI-Jastrow Wave Functions 83
		7.3.2	Comparison of Determinant and CSF Expansions 85
		7.3.3	Influence of Different Jastrow Factors
		7.3.4	Comparison to the Literature
		7.3.5	CI Coefficients
		7.3.6	Bond Dissociation Energy
		7.3.7	Choice of Initial Orbitals
		7.3.8	Selected CI in the Presence of a Jastrow Factor

	7.3.9 Computational Approach	104
	7.4 Jastrow-sCI Scheme	105
8	Conclusion	111
Bi	bliography	113
Ac	cronyms	133
A	CIPSI Algorithm	A-1
В	Integral Form of the Schrödinger Equation	A-3
C	Symmetry of Diatomic Molecules	A-5
D	Transition Metal Compounds	A-7
E	Selected Configuration Interaction	A-11

1 Introduction

"NOTHING IN LIFE IS TO BE FEARED, IT IS ONLY TO BE UNDERSTOOD. NOW IS THE TIME TO UNDERSTAND MORE, SO THAT WE MAY FEAR LESS." – *Marie Curie*

The chemistry and physics of a system are fully determined by quantum mechanics, that is—in the non-relativistic approximation—by the solutions to the Schrödinger equation. Unfortunately, the exact solutions are only known for very few systems, so that for the majority of quantum chemical problems, we have to make do with approximate descriptions. The source of all "evil" here is the simultaneous interaction of all particles involved, the so-called many-body problem. In this thesis, we concentrate on the solutions to the stationary, electronic Schrödinger equation, which means that we can limit our focus to the electronic many-body problem, also known as the electron correlation. The approximation of the electron correlation is an unavoidable aspect of quantum chemical calculations and typically constitutes the largest source of error. [1]

The first calculations for homonuclear bonds involving electron correlation were published by Walter Heitler and Fritz London^[2] in 1927. The authors were able to provide a correct description of the covalent bond in H₂ only after including electron correlation into the wave function. In his work on the ground state of the helium atom in 1929, Egil A. Hylleraas^[3] accounted for the electron correlation by means of an explicitly correlated wave function. Since these first attempts to include electronic correlation in electronic structure calculations, nearly a century of research has been invested in obtaining an accurate description of the electron correlation.

For fermionic systems, there are two different types of correlation: the Fermi and the Coulomb correlation. The former arises from the symmetry requirements of the exact wave function imposed by the Pauli exclusion principle, while the latter is due to electron repulsion. The Fermi correlation can be accounted for exactly if the symmetry requirements of the wave function are satisfied, which is achieved, for example, by us-

ing an SD as the wave function ansatz. The Coulomb interaction, on the other hand, must be approximated and is usually described by a linear combination of SDs.

The Coulomb correlation can be further divided into static and dynamic electron correlation. Consider, for example, the boron atom in its ground state. The 2*p* electron can occupy any of the triply degenerate p orbitals, and all three configurations, i.e. $2p_x^1, 2p_y^1$ and $2p_z^1$, contribute equally to the wave function. This type of correlation, in which several important configurations must be retained in the wave function for an accurate description, is called static electron correlation, while the systems are usually referred to as multi-reference systems. The dynamic correlation then comprises the remainder of the correlation resulting from the dynamics of the electrons. The MCSCF method is a conventional approach used for handling static electron correlation. The first MCSCF calculations of atoms were published in 1939 by Douglas R. Hartree and co-workers.^[4] Nowadays, CASSCF—belonging to the MCSCF approaches—is the method of choice when studying multi-reference systems. Despite intensive algorithmic development and enormous advancements in computer hardware in recent decades, CASSCF calculations are still "only" feasible today for small actives spaces correlating 20 electrons in 20 orbitals ($\approx 4 \times 10^9 \; \text{SDs})^{[5]}$, using massively parallel implementations. However, Head-Gordon and co-workers^[6] have shown that CASSCF-like calculations are possible with approximate FCI solvers for about 50 electrons in 50 active orbitals.

Dynamic electron correlation is always required in order to achieve high accuracy, whereas static electron correlation is only important for systems dominated by more than one configuration. However, both types of correlation are physically equivalent and result from Coulomb interactions. Therefore, a strict separation of static and dynamic electron correlation is generally not possible. Nevertheless, much research has been invested in a rigorous partitioning of these correlation types.^[7–9]

The aim of this work is to achieve an accurate representation of multi-reference systems using QMC methods, more specifically VMC and DMC. Unlike conventional *ab initio* electronic structure methods, these techniques are vastly parallel and exhibit favorable scaling with the system size. First, we will turn to a thorough investigation of transition metal dimers. The accuracy of the MR-DMC approach using full valence CASSCF initial wave functions will be evaluated in terms of bond dissociation energies. The performance of single-, which include common methods such as DFT and CC, but also DMC, and multi-reference approaches is discussed for a selection of transition metal dimers. Further assessment of the applied method is derived from spectroscopic

constants obtained from a Morse fit to MR-DMC potential energy curves. The second part of this thesis focuses on different sCI approaches in the framework of QMC. First, a statistical analysis of CI coefficients optimized with VMC is performed. Then, different Jastrow-sCI ansatzes are evaluated in terms of applicability and accuracy. Finally, an exhaustive analysis of the ground state of C_2 using truncated CIPSI-Jastrow wave functions is performed. This investigation includes a discussion of the effects of the Jastrow factor on the CI picture. Additionally, the CIPSI-Jastrow-DMC absolute and bond dissociation energies of C_2 are compared with highly accurate data from the literature. The influence of the choice of the initial orbitals for the generation of the CIPSI wave functions is evaluated. Eventually, a Jastrow-sCI scheme based on an energy contribution criterion is presented.

2 Introducing Quantum Mechanics

"The task is not to see what has never been seen before, but to think what has never been thought before about what you see everyday." – *Erwin Schrödinger*

Scientists, at the end of the 19th century, felt that everything had been manifested in the realm of physics. Little did they know, however, that trying to, amongst others, solve the mysteries of the black body radiation and the photoelectric effect would open a new world: the world of quantum theory. Within the scope of about 25 years, the world went from the separate realms of particles and waves to the formulation of modern quantum mechanics.

A quantum system can be described by the quantum states that it can assume. These quantum states are mathematically represented by state vectors $|\Psi\rangle$ that are elements of an abstract vector space. The position space analog to a state vector is called wave function:

$$\langle \mathbf{x} | \Psi \rangle \equiv \Psi(\mathbf{x}). \tag{2.1}$$

According to the Copenhagen interpretation of quantum mechanics, and more precisely Born's rule^[12], the probability density corresponds to the square of the absolute value of the wave function:

$$p = |\Psi(\mathbf{x})|^2 = \Psi^*(\mathbf{x})\Psi(\mathbf{x}) \tag{2.2}$$

In this probabilistic interpretation, the measurement outcome of a system is always given with a certain probability, which is linked to p and thus to the wave function

describing the system.

The postulates of quantum mechanics entail that not all wave functions are allowed. The wave functions used throughout this work originate from the L^2 —ensuring square integrability—Hilbert space with the following inner product

$$\langle f|g\rangle = \int f^*(\mathbf{x})g(\mathbf{x})d\mathbf{x}.$$
 (2.3)

2.1 The Schrödinger Equation

The wave function—being a central quantity in quantum mechanics—can be obtained as a solution to the Schrödinger equation for stationary states^[13]

$$\hat{H}\Psi = E\Psi, \tag{2.4}$$

with the Hamiltonian \hat{H} as total energy operator. Eq. (2.4) corresponds to an eigenvalue problem with Ψ as the eigenvector to the corresponding eigenvalue E.

The Hamiltonian—in the non-relativistic framework—describes the kinetic and potential energy of the system at hand:

$$\hat{H} = \hat{T} + \hat{V}. \tag{2.5}$$

The kinetic and potential energy operators for the electrons and nuclei are defined (in a.u.) in Eqs. (2.6) and (2.7), respectively. The vectors ${\bf r}$ and ${\bf R}$ describe the Cartesian coordinates of the individual particles. The Laplace operator Δ corresponds to the sum of the second partial derivatives with respect to the Cartesian coordinates: $\Delta = \left(\frac{\partial^2}{\partial x^2} + \frac{\partial^2}{\partial y^2} + \frac{\partial^2}{\partial z^2}\right).$

$$\hat{T} = \hat{T}_{e} + \hat{T}_{n}$$

$$= -\frac{1}{2} \sum_{i} \Delta_{i} - \frac{1}{2} \sum_{I} \frac{1}{m_{I}} \Delta_{I}$$
(2.6)

$$\hat{V} = \hat{V}_{en} + \hat{V}_{ee} + \hat{V}_{nn}
= -\sum_{I} \sum_{i} \frac{Z_{I}}{|\mathbf{r}_{i} - \mathbf{R}_{I}|} + \sum_{i} \sum_{j>i} \frac{1}{|\mathbf{r}_{i} - \mathbf{r}_{j}|} + \sum_{I} \sum_{J>I} \frac{Z_{I}Z_{J}}{|\mathbf{R}_{I} - \mathbf{R}_{J}|}$$
(2.7)

The derivation of the Schrödinger equation, which is considered a fundamental concept in quantum chemistry, will be briefly discussed in the following. The discovery that a particle also exhibits wave-like properties is central to the rationale. In his reasoning, Schrödinger probably^[14] started with the standing wave equation with Ψ as wave amplitude:

$$\frac{\mathrm{d}^2\Psi}{\mathrm{d}x^2} + \frac{4\pi^2}{\lambda^2}\Psi = 0. \tag{2.8}$$

By inserting de Broglie's relation between a particle's momentum p and its wavelength $\lambda = h/p$ into Eq. (2.8), one obtains:

$$\frac{d^2\Psi}{dx^2} + \frac{4\pi^2 \cdot p^2}{h^2}\Psi = 0.$$
 (2.9)

Through the connection between the momentum p and the total energy E (via the kinetic energy T)

$$p^2 = 2mT = 2m(E - V), (2.10)$$

the energy is introduced into the wave equation:

$$\frac{\mathrm{d}^2\Psi}{\mathrm{d}x^2} + \frac{1}{\hbar^2} [2m(E - V)]\Psi = 0. \tag{2.11}$$

By rearranging Eq. (2.11), one obtains the (one-dimensional) time-independent Schrödinger equation:

$$\left[-\frac{\hbar^2}{2m} \frac{\mathrm{d}^2 \Psi}{\mathrm{d}x^2} + V \right] \Psi = E \Psi \tag{2.12}$$

2.2 The Born-Oppenheimer Approximation

The Schrödinger equation is a high-dimensional partial differential equation that can only be exactly solved—in its original form—for very few systems and some toy systems. Max Born and J. Robert Oppenheimer proposed in 1927^[15] to reduce the dimensionality of the problem by separating the motion of the electrons and the nuclei.

In the *clamped nuclei* approximation, the kinetic energy operator of the nuclei is removed from the Hamiltonian, justified by the large mass difference between electrons and nuclei. The resulting Hamiltonian

$$\hat{H}_{\text{elec}} = \hat{T}_{\text{e}} + \hat{V} \tag{2.13}$$

is usually referred to as electronic Hamiltonian.

The exact solution to the Schrödinger equation—including electrons and nuclei—can be written in the basis of the eigenfunctions of the electronic Hamiltonian $\psi_n(\mathbf{r}; \mathbf{R})$:

$$\Psi(\mathbf{r},\mathbf{R}) = \sum_{n=0}^{\infty} \psi_n(\mathbf{r};\mathbf{R}) f_n(\mathbf{R}), \qquad (2.14)$$

with the respective coefficients $f_n(\mathbf{R})$. In the Born-Oppenheimer approximation, the sum in Eq. (2.14) is reduced to the first term, the wave function thus being simplified to (omitting the subscript 0)

$$\Psi(\mathbf{r}, \mathbf{R}) \equiv \psi(\mathbf{r}; \mathbf{R}) f(\mathbf{R}), \tag{2.15}$$

which achieves the separation of the electronic and nuclear motion. The eigenfunctions of the electronic Schrödinger equation ψ thus only depend parametrically on the nuclear coordinates. In the second part of the Born-Oppenheimer approximation, the Schrödinger equation for the nuclear motion is retrieved.

2.3 The Variational Principle

The electronic Schrödinger equation is still very complex which is why mathematical tools are needed to find approximate solutions. One approach is the Rayleigh-Ritz method which makes use of the variational principle.

The Ritz quotient gives the expectation value of the Hamiltonian

$$E[\Psi] = \frac{\langle \Psi | \hat{H} | \Psi \rangle}{\langle \Psi | \Psi \rangle} \ge E_0, \tag{2.16}$$

transforming Eq. (2.4) from a partial differential equation into an integral problem.

The variational principle states that one always obtains an upper bound to the exact ground state energy E_0 . Additionally, E_0 is only attained if Ψ corresponds to the exact ground state wave function.

In the Rayleigh-Ritz (variational) method, the wave function $\Psi(\mathbf{r}; \mathbf{c})$ is parametrized and the Ritz quotient is minimized with respect to the parameter vector \mathbf{c} . The lowest possible energy is reached for the optimal set of parameters \mathbf{c}_{opt} :

$$E(\mathbf{c}_{\text{opt}}) = \min_{\mathbf{c}}(E(\mathbf{c})). \tag{2.17}$$

3 Hartree-Fock Theory

"ARITHMETIC IS BEING ABLE TO COUNT UP TO TWENTY WITHOUT TAKING OFF YOUR SHOES." – *Mickey Mouse*

The electron-electron interaction \hat{V}_{ee} in Eq. (2.7) spoils the separation of the electronic Hamiltonian into a sum of one-particle operators, which would reduce the dimensionality of the Schrödinger equation—from 3N (including the spin: 4N) dimensions—to N three- (four-) dimensional equations. In the Hartree-Fock (HF) theory, pioneered shortly after the formulation of quantum mechanics by Douglas R. Hartree^[16] and Vladimir Fock^[17], this challenge is addressed by introducing an independent-particle model, which assumes that the electrons move in a mean-field, independently of the positions of all other electrons. By accounting for the electron-electron interaction in an averaged manner, it becomes possible to express the Hamiltonian as a sum of one-electron operators, the Fock operators.

Mathematically, this can be achieved by employing a Slater determinant (SD) as an approximation for the exact wave function. This is the *only* approximation in the HF formalism. An important advantage of using an SD as wave function lies in its inherent anti-symmetric nature, essential for the description of fermions. The anti-symmetry of the wave function emerges from the Pauli exclusion principle, which states that, upon the exchange of the coordinates of two identical particles, the wave function must change sign. Additionally, another attribute of the exact wave function is retained: the SD prevents two same spin electrons from approaching one another—known as the Fermi hole—since this would result in the determinant, and thus also the probability density, becoming zero. In the HF theory, the SD is constructed from orthonormal spin orbitals.

The constraint—ensuring the orthonormality of the spin orbitals—minimization (via the Lagrange multipliers method) of the energy, a functional of the SD, by means of the variational method results in the Hartree-Fock equations. They constitute a pseudo-eigenvalue problem, since the molecular orbitals (MOs)—solutions to the HF equations—are needed to construct the Fock operators. Thus, an iterative approach, known as the self-consistent field (SCF) method, is needed to solve the equations. The HF equations provide the ideal orbitals for a Slater determinant.

The MOs that represent the solutions to the HF equations are, as of yet, not known. One way to tackle this problem is to expand these unknown functions into linear combinations of (known) basis functions. Applying this technique to the HF formalism, using atomic orbitals as basis functions, is attributed to Clemens C. J. Roothaan^[18] and George G. Hall^[19]. The resulting Roothaan-Hall equations transform the original coupled integro-differential problem into a generalized matrix eigenvalue problem, making the solution by means of a computer feasible. Since the use of a finite basis is unavoidable for practical applications, a further approximation is introduced by the Roothaan-Hall formalism.

Since the HF method makes use of the variational principle, extending the basis set size must lead to lower energies. In the limit of a complete basis, the lowest possible HF solution is obtained. This is called the Hartree-Fock limit. The correlation energy is defined as the difference between the HF limit and the exact, non-relativistic solution to the Schrödinger equation.

4 The Pursuit of Electronic Correlation

"Humans think in stories, and we try to make sense of the world by telling stories." – Yuval Noah Harari

Despite being able to retrieve 99% of the total energy, the HF formalism falls short of recovering the remaining 1% that is essential for the description of chemically and physically relevant properties. Nearly a century has, hitherto, been devoted to this task. One distinguishes between two types of correlation: static and dynamic electron correlation. The former comes into play in case a system comprises degenerate or quasi-degenerate configurations, while the latter arises from the electronic motion itself. This distinction is rather arbitrary, it is, however, often a helpful conceptual tool. In this part of the thesis, different approaches that aim at retrieving the correlation energy are discussed.

4.1 Post-Hartree-Fock Methods

The ambition of post-Hartree-Fock methods is to account for the missing electron correlation in the HF theory. The approaches, described below, all have in common that they a) abide by the variational principle and b) aim at including the electron correlation through linear combinations of SDs.

4.1.1 Configuration Interaction

The configuration interaction (CI) method is a straightforward approach to include dynamic correlation in quantum chemical calculations. In this method, the wave function is expressed as a linear combination of configuration state functions (CSFs) (as

described in section 5.2.2), with the CI coefficients optimized to obtain a minimum energy. Each configuration corresponds to an *n*-tuple excitation from the HF reference. Unlike the HF theory, the MOs are not optimized in the CI formalism.

This form of the wave function is—in theory—able to provide the exact solution to the Schrödinger equation. In practice, the necessary introduction of a basis puts the exact solution out of reach. The CI method suffers from slow convergence due to the exponential growth in the number of determinants with the number of electrons and basis set size. As a result, including all possible excitations (limited by a finite basis) in the wave function, which is referred to as full configuration interaction (FCI), is only feasible for small systems and small basis sets. This approach would recover 100% of the correlation energy within the given basis set. The result of a CI calculation can only be as "good" as the zeroth-order wave function.

To apply the CI method in practice, it is necessary to reduce the number of excited determinants. One common approach is to truncate the CI basis by limiting the excitation level. Including only singly excited determinants in the expansion does not improve upon the HF determinant, as the matrix elements between the reference and the singly excited determinants are—according to the Brillouin theorem—equal to zero. The double excitations, which are the first excitations connected to the HF reference, contribute the most to the correlation energy, making the CISD method the preferred choice in practice. Truncating CI expansions comes, however, at the cost of losing size consistency, arising from an unequal treatment of a system and its respective fragments.

4.1.2 Multi-Reference Configuration Interaction

The multi-reference configuration interaction (MRCI) method is based on excitations out of a reference space, similar to the single-reference CI approach. However, the main difference between the two methods lies in the definition of the reference space. In MRCI, the reference space is typically built from a linear combination of SDs. This allows for a more accurate description of systems with degenerate or quasi-degenerate ground states, for which a single-determinant zeroth-order wave function cannot provide a correct characterization.

The reference wave functions for MRCI can for example be obtained from multi-configuration self-consistent field (MCSCF) calculations, see next section. Often even singles and dou-

bles MRCI already yields more configurations than can be computationally handled. Further truncations or approximations are therefore required. One strategy is to only take into consideration a pre-defined set of orbitals for the generation of the excited determinants.

4.1.3 Multi-Configurational Self-Consistent Field

The general MCSCF theory was introduced by Roy McWeeny^[20] in 1955.

The MCSCF method allows for the treatment of static correlation by incorporating dominant electron configurations in the wave function, resulting in qualitatively correct wave functions. Unlike the CI method, not only the expansion coefficients but also the MOs are optimized in the MCSCF method to avoid any biases toward a specific configuration. Orbital rotations are used to optimize the orbital parameters because they ensure the orthogonality of the orbitals during the optimization process.^[21]

The MCSCF method requires selecting the configurations that are relevant to the problem, which is a challenge in itself. One approach to address this challenge is through the complete active space self-consistent field (CASSCF) method—pioneered by Roos, Taylor, and Siegbahn^[22]—which necessitates a classification of the orbitals. The inactive MOs are doubly occupied in all configurations, while all possible excitations are carried out for the active orbitals. The approach is called *complete* active space because all possible configurations are included in the active space. This concept is important for the treatment of static electron correlation. Since no occupation restrictions apply to the active orbitals (usually a set of degenerate or quasi-degenerate orbitals), they are included in the wave function with all possible occupation patterns, with the consequence that all important configurations are retained in the wave function.^[14,21] The virtual orbitals remain empty in all configurations. The CASSCF technique is schematically depicted in Fig. 4.1.

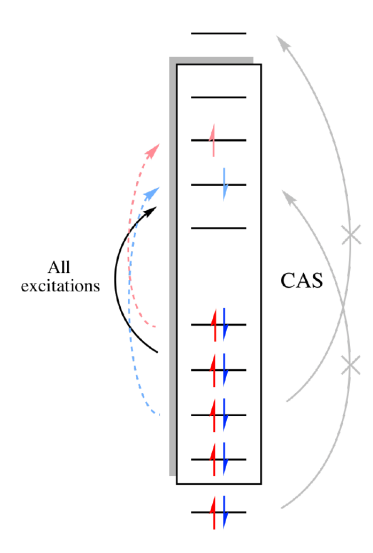


Fig. 4.1: Partition of CAS orbitals with the allowed excitations. The graph is taken from Ref. 23.

The CASSCF method can—in principle—capture static and dynamic electron correlation. However, the FCI nature of the active space limits calculations to a small number of electrons and orbitals (in the active space). Since retrieving the dynamic correlation requires excitations into higher-lying orbitals, CASSCF mostly accounts for the static electron correlation. The CAS(n, m) notation—meaning that n electrons are distributed to m orbitals—will be used throughout this thesis for the CASSCF calculations.

4.1.4 Selected Configuration Interaction

In the (multi-reference) methods presented above, the selection of configurations was either done via excitation criteria or via the choice of orbitals a scientist deems important. These techniques undoubtedly include configurational "deadwood"^[24], symbolizing configurations that do not significantly contribute to the correlation energy.

The selected configuration interaction (sCI) methods—while relying on the usual principles of CI—constitute an alternative class of methods that iteratively probe the FCI space (within a given basis) and choose important configurations based on different criteria, such as determinant amplitudes or energy contributions. sCI methods have gained increasing interest over the last decades, with popular approaches including full configuration interaction quantum Monte Carlo (FCIQMC)^[25], adaptive sampling CI (ASCI)^[26], and semi-stochastic heat-bath CI (SHCI)^[27].

In this thesis, the configuration interaction using a perturbative selection made iteratively (CIPSI) method, which was pioneered by Huron, Malrieu, and Rancurel^[28,29], is used. CIPSI determines the energy contribution of a determinant α (absent from the reference space) via second-order perturbation theory using an Epstein-Nesbet^[30,31] zeroth-order Hamiltonian

$$\delta e_{\alpha}^{(2)} = \frac{\langle \Psi_0^{(n)} | \hat{H} | \alpha \rangle}{E_0^{(n)} - \langle \alpha | \hat{H} | \alpha \rangle},\tag{4.1}$$

with $E_0^{(n)}$ and $\Psi_0^{(n)}$ as the *n*-th iteration ground state energy and wave function, respectively. A more detailed description of the CIPSI algorithm can be found in appendix A.

4.2 Density Functional Theory

Density functional theory (DFT) is, today, the most applied method in electronic structure theory. The methods, presented above, all draw on wave functions, which are high-dimensional objects with at least 3N degrees of freedom, to solve the Schrödinger equation. Falling back on the three-dimensional electronic density to characterize the ground state would severely reduce the complexity of the problem. Pierre Hohenberg and Walter Kohn^[32] proved in 1964 that the ground state of a system can be fully and equivalently described as well by the ground state wave function as by the ground state electronic density. In other words, the information required for the construction of the Hamiltonian, namely the number of electrons and nuclei, as well as the nuclear positions and atomic numbers, can be extracted from the electronic density. All the information enshrined in the high-dimensional wave function is thus also present in the electronic density. As a consequence, the exact ground state energy can be written as a functional of the exact ground state electronic density.

In a second theorem, Hohenberg and Kohn proved a variational principle for the density

$$E^{\rm HK}[\rho] \ge E^{\rm HK}[\rho_0] \equiv E_0, \tag{4.2}$$

with the exact ground state electronic density ρ_0 and its corresponding energy E_0 . The key problem of DFT is, however, that the mathematical form of this energy functional remains unknown.

It was only with the development of the Kohn-Sham (KS) formalism that DFT became important in chemistry. In its original, orbital-free form, DFT struggled to describe the electronic kinetic energy, which is—following the virial theorem—as large in value as the total energy of a system, and should, therefore, be determined accurately. The KS formalism, which was developed by Walter Kohn and Lu J. Sham^[33], assumes that the electronic density of a real system with interacting electrons is equivalent to the electronic density of a fictitious system with non-interacting electrons. Orbitals, more precisely Kohn-Sham spin orbitals $\{\phi_i\}$, are then re-introduced for the description of the kinetic energy functional. The DFT energy $E_{\rm DFT}[\rho]$ is defined as

$$E_{\text{DFT}}[\rho] = T_{\text{KS}}[\{\psi_i\}] + \int v(\mathbf{r})\rho(\mathbf{r})d\mathbf{r} + J[\rho] + E_{\text{xc}}[\rho], \tag{4.3}$$

where $T_{KS}[\{\psi_i\}]$ corresponds to the kinetic energy functional of the non-interacting electrons, $J[\rho]$ to the Coulomb energy, and $E_{xc}[\rho]$ to the exchange-correlation energy functional, which includes exchange and correlation effects, a correction for the kinetic energy (for interacting electrons), as well as the correction of the self-interaction error (hidden in $J[\rho]$). The second term on the right-hand side of Eq. (4.3), also known as the external potential, is system dependent and describes the electron-nucleus interaction.

The exact form of the exchange-correlation functional is, unfortunately, not known. The pursuit of accurate approximations constitutes a highly active field of research with a wide range of functionals tailored to all kinds of problems having been developed to date. One class of functionals, known as hybrid functionals, include the (exact) HF exchange $E_{\rm x}^{\rm HF}$ to some extent:

$$E_{\rm xc}^{\rm hybrid} = (1-a)E_{\rm x} + aE_{\rm x}^{\rm HF} + E_{\rm c} \tag{4.4}$$

In this thesis, the B3LYP^[34–36] and the PBE0^[37,38] functionals with a = 0.2 and a = 0.25, respectively, are employed.

Similar to the HF theory, the Kohn-Sham equations are solved iteratively by means of the SCF approach. The Ritz method is employed to minimize the energy, the final DFT energy is, however, not variational due to the approximations made in the exchange-correlation functional, resulting in an alteration of the Hamiltonian. A major drawback of DFT is that its accuracy can—in contrast to wave function-based methods—not be systematically improved.

4.3 Explicit Treatment

Another ansatz to account for the electron correlation is based on explicitly including the electron-electron distance in the wave function. This approach is able to provide highly accurate results, the explicit treatment complicates, however, the evaluation of the integrals enormously, limiting it to small systems.

The idea of including the inter-electronic distance in the wave function was first applied by Egil A. Hylleraas in 1929—shortly after the formulation of quantum mechanics—to describe, and very successfully so, the ground state of the helium atom.^[3] This Hylleraas-CI method has, however, to date only been applied to systems with a maximum of ten electrons^[39] due to the very high numerical complexity of the problem.

When one intends to include the inter-electronic distance r_{ij} in the wave function, which has the greatest effect—in terms of the Coulomb interaction—for small distances, one must discuss the behavior of the wave function for the coalescence of (charged) particles. Kato, who analyzed this in 1957 for the coalescence of two particles^[40], deduced (from the Schrödinger equation) the singular character of the many-body wave function at these coalescence points. This discontinuity of the derivative of the wave function for the coalescence of two electrons is described by

$$\left. \frac{\partial \hat{\Psi}}{\partial r_{ij}} \right|_{r_{ij}=0} = \frac{1}{2} \Psi(r_{ij}=0), \tag{4.5}$$

with $\hat{\Psi}$ denoting spherical averaging.

Tackling the problems that follow from the explicit treatment of electron correlation has

been subject to intense research with considerable progress having been made since the mid-2000s, see review by Kong *et al.*^[41] for details. Promising R12/F12 methods include MP2-R12^[42] as well as various coupled cluster (CC) (e.g. CCSD(R12)^[43,44], CCSD-F12x^[45]), and multi-reference (e.g. R_{12} -MRCI^[46,47], MRMP2-F12^[48]) approaches.

Another class of methods that can—rather easily—employ explicitly correlated wave functions are the quantum Monte Carlo (QMC) methods, since the required integrals are evaluated in a stochastic way, see next section. The explicit treatment of electron-electron interactions is usually accounted for in QMC by so-called Jastrow correlation functions (defined below) and allows for very accurate results. A similar approach employing a transcorrelated Hamiltonian in FCIQMC was recently developed. [49,50]

5 Quantum Monte Carlo Methods

"THIS WILL ALL MAKE SENSE WHEN I AM OLDER." – Olaf

In QMC, the use of random number sequences (Monte Carlo) is paired with quantum mechanics to tackle quantum chemical and physical problems. Quantum Monte Carlo methods distinguish themselves from (most) methods, presented above, through their stochastic—contrary to deterministic—nature. They can, on the one hand, be employed to simulate truly random processes and, on the other hand, to stochastically evaluate multi-dimensional integrals. For the latter application, they offer a way to solve problems with very high dimensionality (very large Hilbert spaces), where standard analytical and numerical approaches fail.

QMC methods are among the most rigorous techniques when an accuracy beyond mean-field theory is required. They have some advantages compared to traditional electronic structure methods. First of all, QMC scales favorably with the system size as $\mathcal{O}(N^3)$ and is inherently parallel. Furthermore, the memory requirements for QMC calculations are comparably low. And, finally, the accuracy—in terms of the statistical uncertainty—of QMC calculations can be tuned by means of the sample size.^[11]

Various reviews about QMC methods^[10,11,51,52] are readily available in the literature, which is why only the concepts relevant to this thesis will be presented in this part.

5.1 Underlying Foundations

The foundations for both QMC methods used in this thesis, namely variational Monte Carlo (VMC) and diffusion Monte Carlo (DMC), will be provided below. Both techniques correspond to real-space QMC methods.

5.1.1 Statistical Analysis of Random Variables

The expectation value of a (one-dimensional) function f(x), distributed according to the probability density function p(x), can be calculated as follows

$$\langle f \rangle_p \equiv \int f(x)p(x)\mathrm{d}x.$$
 (5.1)

A probability density function is uniquely defined by its moments

$$\langle x^k \rangle_p \equiv \int x^k p(x) \mathrm{d}x,$$
 (5.2)

with the first moment (k = 1) describing the mean value of x. The expectation values in Eq. (5.3) correspond to the central moments of p.

$$\langle (x - \bar{x})^k \rangle_p \equiv \int (x - \bar{x})^k p(x) dx$$
 (5.3)

The second central moment (k=2) is also known as the variance σ^2 of the probability density function. The standard deviation σ is obtained as the square root of the variance.

If the form of probability density is not known—which is often the case—the expectation value of Eq. (5.1) can be obtained as the mean of the $f(X_i)$ values, with the $\{X_i\}$ corresponding to a set of random variables that are distributed according to p(x):

$$\langle f \rangle_p = \lim_{M \to \infty} \frac{1}{M} \sum_{i=1}^M f(X_i)$$
 (5.4)

Let us imagine a (finite) sample $\{X_1, X_2, \dots, X_M\}$ of size M, again distributed as p(x). The arithmetic mean can be used as an estimator for the sample mean

$$S_M \equiv \frac{1}{M} \sum_{i=1}^M X_i. \tag{5.5}$$

The sample mean S_M is itself a random variable. The *central limit theorem* states that—for large M—the sample mean distribution converges toward a Gaussian distribution, independent of the form of the initial probability density function. For N independent sample means S_i , one can thus write

$$\bar{x} = \frac{1}{N} \sum_{i=1}^{N} S_i, \tag{5.6}$$

which corresponds to the mean value of x, denoted as \bar{x} . The variance of the mean of the samples $\sigma_{\bar{x}}^2$ can then be calculated—using Bessel's correction—as

$$\sigma_{\bar{x}}^2 = \frac{\sigma^2}{N-1},\tag{5.7}$$

with σ^2 corresponding to the variance of the S_i . The standard deviation is then defined as

$$\sigma_{\bar{x}} = \frac{\sigma}{\sqrt{N-1}}.\tag{5.8}$$

The central limit theorem is fundamental for the Monte Carlo methods since the standard deviation can only be interpreted as an approximation error if the sample mean is normally distributed. As a consequence (for large enough *independent* samples), the probability of finding the S_i within one standard deviation (of the mean value) corresponds to 68%, within two standard deviations to 95%, and within three standard deviations to 99.7%.^[51]

5.1.2 Monte Carlo Integration

Monte Carlo integration can be employed to evaluate a definite integral of the following form

$$I = \int_{\Omega} f(x)p(x)dx. \tag{5.9}$$

p(x) can act as a probability density function if $p(x) \ge 0$ over the domain Ω and

$$\int_{\Omega} p(x) \mathrm{d}x = 1. \tag{5.10}$$

By drawing a sample (of size M) out of p(x), the value of I can be estimated using Eq. (5.5):

$$S_M = \frac{1}{M} \sum_{i=1}^{M} f(x_i)$$
 (5.11)

Using the sample mean as an estimator for the expectation value of the integral in Eq. (5.9) is known as Monte Carlo integration. The law of large numbers ensures that

$$\lim_{M \to \infty} S_M = I. \tag{5.12}$$

As can be seen from Eq. (5.8), the statistical uncertainty of I can be reduced by increasing the sample size or by reducing the sample variance.

5.1.3 Importance Sampling

Importance sampling paves the way to reduce the sample variance. In the Monte Carlo integration described above, sampling can be inefficient since areas with both large and small integrand values are equally sampled. In importance sampling Monte Carlo, a new probability density function $\tilde{p}(x)$ is introduced. Eq. (5.9) is then altered to

$$I = \int_{\Omega} \frac{f(x)p(x)}{\tilde{p}(x)} \tilde{p}(x) dx.$$
 (5.13)

The density $\tilde{p}(x)$ is chosen such that the fluctuations of the fraction in Eq. (5.13) are minimal, leading to a reduction of the variance. The expectation value of I can then be estimated as

$$\tilde{S}_{M} = \frac{1}{M} \sum_{i=1}^{M} \frac{f(x_{i})p(x_{i})}{\tilde{p}(x_{i})}.$$
(5.14)

This weighting of the sample results in a higher density of the sample points in regions where f is large and a lower one where f is small. The reduction in variance directly implies that a smaller sample can be utilized to achieve the desired level of accuracy.

5.1.4 Metropolis-Hastings Algorithm

The question that remains, until now, unanswered is how to draw a sample out of an arbitrary density function. This can be achieved by means of the Metropolis-Hastings algorithm^[53,54] which makes use of a Markov chain. In a Markov process, the probability of moving to a new state only depends on the current state, not on the history of the states that have been visited. This process requires only two components: an initial state and a matrix that describes the transition probability from the initial state \mathbf{R}_i to the final state \mathbf{R}_f .

The *detailed balance* condition is imposed to construct the transition matrix (here $A(\mathbf{R}_f|\mathbf{R}_i)T(\mathbf{R}_f|\mathbf{R}_i)$), with $\rho(\mathbf{R})$ as its stationary distribution (that one wishes to sample):

$$A(\mathbf{R}_f|\mathbf{R}_i)T(\mathbf{R}_f|\mathbf{R}_i)\rho(\mathbf{R}_i) = A(\mathbf{R}_i|\mathbf{R}_f)T(\mathbf{R}_i|\mathbf{R}_f)\rho(\mathbf{R}_f).$$
(5.15)

In Eq. (5.15), a two-step process is adopted for the transition matrix. The matrix T is used to propose a new step, while A describes the probability with which this new step is accepted. The acceptance matrix A is defined as follows:

$$A(\mathbf{R}_f|\mathbf{R}_i) = \min\left\{1, \frac{T(\mathbf{R}_i|\mathbf{R}_f)}{T(\mathbf{R}_f|\mathbf{R}_i)} \frac{\rho(\mathbf{R}_f)}{\rho(\mathbf{R}_i)}\right\}.$$
 (5.16)

The choice of the proposal matrix T is less straightforward, but one has a higher degree of freedom. T should be chosen such that the proposed moves are large without, however, dispensing with high acceptance probabilities. Additionally, reducing the serial

correlation between the sample points should be considered for the choice of *T*.

In the original work by Metropolis *et al.*^[53], T was chosen to be symmetric, i.e. $T(\mathbf{R}_f|\mathbf{R}_i) = T(\mathbf{R}_i|\mathbf{R}_f)$. Hastings^[54] later generalized the algorithm to $T(\mathbf{R}_f|\mathbf{R}_i) \neq T(\mathbf{R}_i|\mathbf{R}_f)$, resulting in an improved efficiency.

Translated to our real-space methods, the distribution $\rho(\mathbf{R})$ corresponds to the probability density function $\Psi_T^2(\mathbf{R})/\int \Psi_T^2(\mathbf{R})d\mathbf{R}$ and an approximate Green's function, see Ref. 55, is employed for the proposal matrix T.

A disadvantage of the Metropolis-Hastings algorithm is the serial correlation of the sample points. The importance of having independent samples was shown in 5.1.1.

5.2 Wave Function Form

QMC methods usually rely on having—in terms of accuracy and efficiency—suitable approximate wave functions. The advantage of stochastically evaluating integrals is, however, that one is rather flexible in the choice of the wave function form.

In this work, so-called Slater-Jastrow-type trial wave functions, constructed from a Jastrow correlation function $e^{U(\mathbf{R})}$ and a linear combination of CSFs $|\Phi_i\rangle$, are employed:

$$\Psi_{\mathrm{T}}(\mathbf{R}) = \mathrm{e}^{U(\mathbf{R})} \cdot \sum_{i} c_{i} \Phi_{i}(\mathbf{R}). \tag{5.17}$$

5.2.1 Jastrow Correlation Function

The name of the Jastrow factor can be traced back to the physicist Robert Jastrow who introduced the idea of using functions that include the inter-electronic distances in order to capture the electron correlation.^[56]

The product approach in Eq. (5.17) together with the exponential form of the Jastrow factor—making it totally symmetric with respect to electron permutations—entail that it does not change the nodes of the wave function. The Jastrow factor describes the

correlated motion of electrons, thus accounting for the short-range dynamic electron correlation. It is usually expanded into different many-body terms

$$U = U_{\text{ee}}^{(2)} + U_{\text{en}}^{(2)} + U_{\text{een}}^{(3)} + \dots, \tag{5.18}$$

with "e" denoting the electrons and "n" the nuclei. The superscripts indicate how many particles are involved for each term. It has been shown that the improvement which is achieved by including Jastrow terms of an even higher order (than indicated in Eq. (5.18)) is minor compared to the increase in computational expenditure.^[57]

The ee term yields the highest contribution to the electron correlation. However, it also introduces an excessive repulsion of the electrons, especially near the nuclei where the electron density is large. This effect is corrected by the en term. The three-body term provides a much smaller, yet non-negligible, contribution to the electron correlation.

The potential energy diverges if two particles coalesce due to its inverse dependence on the inter-particle distances ($1/r_{ij}$ and $1/r_{il}$). The correct behavior of the wave function at the coalescence points of two particles is determined by the cusp conditions. The condition for the coalescence of two electrons has been introduced in section 4.3. A similar condition can be formulated for the coalescence of an electron with a nucleus, the slope of the wave function being proportional to the atomic number Z:

$$\left. \frac{\partial \hat{\Psi}}{\partial r_{iI}} \right|_{r_{iI}=0} = -Z_I \Psi(r_{iI}=0). \tag{5.19}$$

When accurate MOs are used for the construction of the SD, the electron-nucleus cusp condition is approximately fulfilled. Since the $U_{\text{ee}}^{(2)}$ and $U_{\text{en}}^{(2)}$ terms describe the respective cusps, the three-body term $U_{\text{een}}^{(3)}$ should be constructed cusp-less.

The Jastrow factor is obtained as sums over all pairs with the functions f, g_I , and h_I corresponding to polynomials that depend on the inter-particle (scaled) distances:

$$U = \sum_{i < j} f(\bar{r}_{ij}) + \sum_{I,i} g_I(\bar{R}_{Ii}) + \sum_{I,i < j} h_I(\bar{R}_{ij}, \bar{R}_{Ii}, \bar{r}_{Ij}).$$
 (5.20)

For the Jastrow factor employed in this work, the polynomials are expressed as power series using the scaled distances, first introduced by Boys and Handy^[58]:

$$\bar{r} = \frac{\alpha r}{1 + \alpha r}.\tag{5.21}$$

Eq. (5.21) is used for both, the electron-electron and electron-nucleus distances. The parameter α is kept fixed at a value of one. The Jastrow factor will be denoted as sm*FGH* throughout this thesis, with *F*, *G*, and *H* corresponding to the order of the electron-electron, the electron-nucleus, and the electron-electron-nucleus polynomials, respectively. "sm" stands for **S**chmidt and **M**oskowitz, since the generic Jastrow, used in this thesis^[59,60], is based on their work.^[61] Further details on the Jastrow factor employed in this thesis are given in Ref. 60.

Concerning the wave function optimization, see below, not all Jastrow parameters have to be optimized, some are fixed due to the cusp conditions.

5.2.2 Configuration State Functions

The CSFs constitute the anti-symmetric part of the Slater-Jastrow wave function. A configuration state function corresponds to a linear combination of SDs. The coefficients of the determinants are determined by the spin and, where applicable, spatial symmetry of the considered state. The SDs are in turn constructed from orthonormal single-particle orbitals. Each MO ϕ_i is expanded into a basis of single-particle functions χ_{μ} :

$$\phi_i = \sum_{\mu=1}^{N_{\rm bf}} a_{i,\mu} \chi_{\mu}.$$
 (5.22)

The basis functions employed in this work are either Slater-type orbitals (STOs) (for all-electron calculations) or Gaussian-type orbitals (GTOs) (for effective core potential (ECP) calculations). The former have the advantage that they intrinsically impose the electron-nucleus cusp.

A correct wave function has to be an eigenfunction of both the \hat{S}^2 and \hat{S}_z operators for

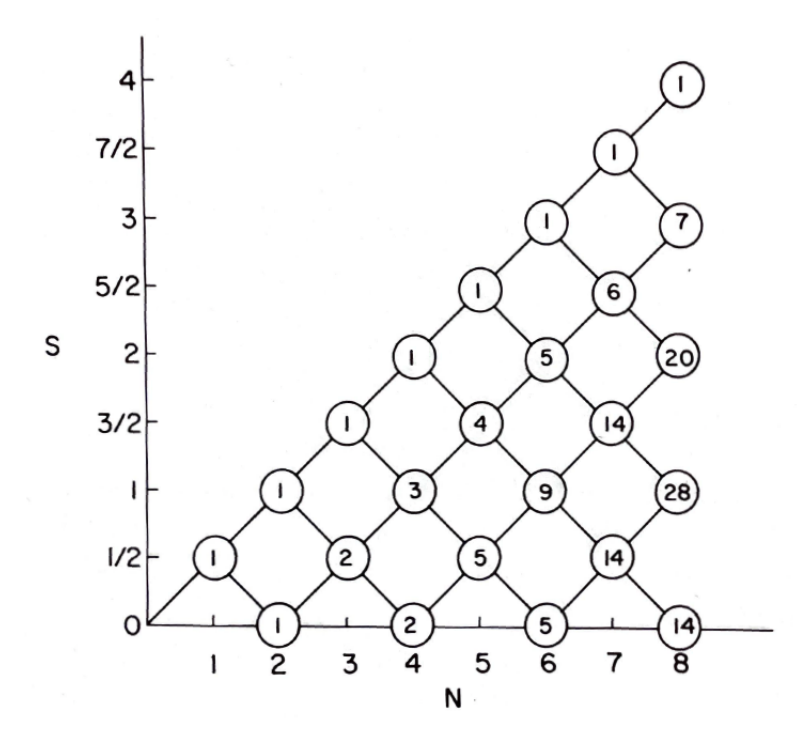


Fig. 5.1: Spin quantum number *S* as a function of the number of electrons *N*. The number of independent spin eigenfunctions, for a given number of electrons and the resultant spin quantum number, is indicated within the circle. The diagram is taken from Ref. 63.

any stationary state. If a wave function is not an eigenfunction of the square of the total spin operator, the wave function does not correspond to a pure spin state and is said to be spin contaminated. CSFs are inherently eigenfunctions of \hat{S}^2 and \hat{S}_z .

One way to construct these spin eigenfunctions is through a genealogical construction, introduced by Kotani and co-workers. ^[62] In this scheme, the spin functions $X(N, S, M_S; k)$ are obtained by successively coupling electron spins. When adding an electron to a state with quantum number S, the addition theorem of angular momenta allows for two final states with quantum numbers $S + \frac{1}{2}$ and $S - \frac{1}{2}$, respectively. In order to achieve an N electron state with quantum number S, one can either start from an (N-1) electron spin function with $S + \frac{1}{2}$ (substraction) or from an (N-1) electron spin function belonging to $S - \frac{1}{2}$ (addition). ^[63]

A branching diagram^[64], see Fig. 5.1, can be used to visualize the spin function construction procedure. The figure in the circle indicates the number of independent spin functions (or CSFs) for given N and S values. Note that the number of independent spin functions grows very fast with the number of electrons. The number of degenerate spin functions for a given (N, S) tuple corresponds to the possible routes that lead from the origin to the desired point in the branching diagram. For instance, two independent

spin functions can be constructed for N=4 and S=0 (singlet state), the moving patterns being as follows ("/" stands for moving up, while "\" designates moving down in the diagram):

It is sufficient to perform the construction of the spin functions for the highest spin component ($M_S = S$) of each state. [63] The *addition* formula—corresponding to moving up in the branching diagram—is then given as

$$X(N, S, S; k) = X(N - 1, S - \frac{1}{2}, S - \frac{1}{2}; k')\alpha(N).$$
 (5.23)

The construction of the spin eigenfunctions using the *substraction* formula—equivalent to moving down in the branching diagram—is a bit more tedious, see Eq. (5.24).

$$X(N,S,S;k) = \left[-X(N-1,S+\frac{1}{2},S-\frac{1}{2};k')\alpha(N) + (2S+1)^{1/2}X(N-1,S+\frac{1}{2},S+\frac{1}{2};k')\beta(N) \right] (2S+1)^{-1/2}$$
(5.24)

The genealogy of the construction scheme is reflected in the Eqs. (5.23) and (5.24) since they display which (N-1) spin function is used to generate the N electron function. As for the construction of the (N-1) spin function, one can tell from which (N-2) it originates, and so on.^[63]

In practice, within the framework of spin-free quantum mechanics, a product of spin-up and spin-down determinants is used in order to reduce the computational cost. This is possible since the Slater matrix of an SD can always be subjected to a block diagonalization into spin-up and spin-down sub-matrices without loss of general validity. The employed Hamiltonian, and thus the propagators in QMC, have no explicit spin dependence. The spins $m_{s,i}$ of the n electrons can, therefore, be chosen randomly as long as their sum equals the total quantum number M_S :

$$\sum_{i}^{n} m_{s,i} = M_{S}. {(5.25)}$$

As a consequence, one can equivalently assign the spins to the individual electrons and evaluate the spin functions $\alpha(m_s)$ and $\beta(m_s)$ for the given m_s values:

$$lpha(m_s) = egin{cases} 1 & ext{if } m_s = 1/2 \ 0 & ext{if } m_s = -1/2 \end{cases}, egin{cases} eta(m_s) = egin{cases} 0 & ext{if } m_s = 1/2 \ 1 & ext{if } m_s = -1/2 \end{cases}.$$

The product form is then obtained by a re-labelling of the electron indices. [65]

5.3 Variational Monte Carlo

All the ingredients needed for VMC have been introduced in the previous sections. Let us define a mathematical entity, called *walker*, that corresponds to a 3n-dimensional vector $\mathbf{R} = (\mathbf{r}_1, \mathbf{r}_2, \dots, \mathbf{r}_n)$ containing the Cartesian coordinates of all n electrons, with $\mathbf{r}_i = (x_i, y_i, z_i)$.

In the VMC method, the Ritz quotient, see Eq. (2.16), is evaluated by means of Monte Carlo integration. The VMC energy is given as

$$E_{\text{VMC}}(\mathbf{R}) = \frac{\langle \Psi_{\text{T}}(\mathbf{R}) | \hat{H} | \Psi_{\text{T}}(\mathbf{R}) \rangle}{\langle \Psi_{\text{T}}(\mathbf{R}) | \Psi_{\text{T}}(\mathbf{R}) \rangle} = \frac{\int |\Psi_{\text{T}}(\mathbf{R})|^2 \frac{\hat{H}\Psi_{\text{T}}(\mathbf{R})}{\Psi_{\text{T}}(\mathbf{R})} d\mathbf{R}}{\int |\Psi_{\text{T}}(\mathbf{R})|^2 d\mathbf{R}} = \int E_{\text{L}}(\mathbf{R}) \rho_{\text{T}}(\mathbf{R}) d\mathbf{R}, \quad (5.26)$$

with $\rho_T(\mathbf{R}) = |\Psi_T(\mathbf{R})|^2/\int |\Psi_T(\mathbf{R})|^2 d\mathbf{R}$ corresponding to the probability density and $E_L(\mathbf{R}) = \hat{H}\Psi_T(\mathbf{R})/\Psi_T(\mathbf{R})$ to the *local energy*. If $\Psi_T(\mathbf{R})$ is an eigenfunction of the Hamiltonian, the local energy is constant.

A sample of size M, $\{\mathbf{R}_k\}_{k=1,\dots,M}$, is drawn out of the probability density with the Metropolis-Hastings algorithm and the VMC energy is obtained as the sample mean of the local energy

$$E_{\text{VMC}}(\mathbf{R}) = \lim_{M \to \infty} \frac{1}{M} \sum_{k=1}^{M} E_{L}(\mathbf{R}_{k}) \approx \frac{1}{M} \sum_{k=1}^{M} E_{L}(\mathbf{R}_{k}).$$
 (5.27)

Note that the only requirements the trial wave function needs to satisfy for the evaluation of the energy are that it needs to be quadratically integrable and additionally, the quantities Ψ_T , $\nabla \Psi_T$, and $\Delta \Psi_T$ must be continuous.

5.4 Wave Function Parametrization and Optimization

The trial wave function can be optimized within the VMC framework. The wave function does not only depend on the positions of the electrons but also on the parameter vector $\mathbf{p} = \{\alpha, \mathbf{c}, \kappa\}$ which involves the Jastrow parameters α , the CI coefficients \mathbf{c} , and the orbital rotation parameters κ . The parametrized wave function is given as [66]

$$|\Psi_{\mathrm{T}}(\boldsymbol{\alpha}, \mathbf{c}, \boldsymbol{\kappa})\rangle = \hat{J}(\boldsymbol{\alpha})e^{\hat{\kappa}(\boldsymbol{\kappa})} \sum_{i=1}^{N_{\mathrm{CSF}}} c_i |C_i\rangle,$$
 (5.28)

where $e^{\hat{\kappa}(\kappa)}$ corresponds to the orbital rotation operator, see e.g. Ref. 21. $\hat{\kappa}$ is an anti-Hermitian operator, which makes the orbital rotation operator unitary, preserving the orthogonality of the orbitals (although that is not necessary for QMC). This parametrization for the optimization of the molecular orbitals is, amongst others, also used in MC-SCF.

The MO coefficients are the most challenging to optimize within VMC, since they are not linearly independent, resulting from the invariance of the SD when rows or columns (or multiples thereof) are exchanged. The MOs of a single-determinant ansatz are classified into *closed* (doubly occupied), *open* (singly occupied), and *virtual* (unoccupied) orbitals, with the only non-redundant orbital rotations involving *closed* \rightarrow *open*, *closed* \rightarrow *virtual*, and *open* \rightarrow *virtual*. On the other hand, for a CASSCF wave function, the non-redundant rotations are *inactive* \rightarrow *active*, *inactive* \rightarrow *virtual*, and *active* \rightarrow *virtual*. For sCI wave functions, some *active* \rightarrow *active* orbital rotations are additionally non-redundant. Only rotations between orbitals that transform according to the same irreducible representation have to be considered.

During a VMC calculation these different sets of parameters are optimized in order to minimize either the variance of the trial wave function's local energy or the mean of the local energy itself. For the exact wave function, both the variance and the energy minimization yield the same result.

5.4.1 Variance Minimization

The variance of the local energy (see Eq. (5.3) for k = 2) is given by Eq. (5.29) in a simplified form, with E_{ref} as an estimate of the mean of the energy, usually obtained from lower level *ab initio* calculations.

$$\sigma_n^2(\mathbf{p}) = \frac{1}{n} \sum_{k=1}^n (E_{L}(\mathbf{R}_k, \mathbf{p}) - E_{ref})^2$$
 (5.29)

The variance minimization corresponds to a non-linear least-squares minimization problem. In our code AMOLQC^[67], the algorithm *NL2SOL*, developed by Dennis *et al.*^[68], is used. The variance minimization is a very stable optimization because the variance is bounded from below (the exact wave function has a variance of zero). This is why it is usually used as a pre-optimization step for the energy minimization. The variance minimization requires a much smaller sample size, making it overall less time-consuming than the energy minimization.

5.4.2 Energy Minimization

Although the energy minimization is computationally more demanding, it is able to provide more accurate energy differences than the variance minimization.^[69]

There are different methods suitable for the minimization of the energy with respect to the different parameters. One distinguishes between the linear, Newton, and perturbative methods, which will be described in more detail in the following sections. The notation from the work of Toulouse and Umrigar^[66] is mostly adopted for the presentation of the optimization methods.

Efficient (stochastic) optimization methods are not only assessed by the number of iterations needed to reach convergence but also by the computational effort per iteration. It is thus of fundamental importance to have estimators with low variances for the computation of the quantities—such as the derivatives of the wave function and the local

energy with respect to the parameters—required for each optimization step. Low variance estimators allow for fewer evaluations, resulting in a reduced the computational effort.

5.4.2.1 Linear Method

For wave functions that only depend linearly on parameters—as in CI—the energy minimization is obtained, straightforwardly, by diagonalizing the Hamilton matrix in the space spanned by the parameters. In QMC, the linear method has been successfully applied to the optimization of linear parameters by Nightingale and Melik-Alaverdian.^[70] The method was later extended by Umrigar and co-workers^[66,71] to also optimize non-linear parameters. This can be achieved by expanding the parameter-dependent wave function to the first order in the parameters **p**:

$$\tilde{\Psi}_{\text{lin}}(\mathbf{p}) = \tilde{\Psi}_{\text{lin}}(\mathbf{p}_0 + \Delta \mathbf{p}) = \tilde{\Psi}(\mathbf{p}_0) + \sum_{i=1}^{N^{\text{opt}}} \Delta p_i \tilde{\Psi}_i(\mathbf{p}_0).$$
 (5.30)

The $\tilde{\Psi}_i$ describe the derivatives—orthogonal to $\tilde{\Psi}(\mathbf{p}_0)$ —of $\tilde{\Psi}(\mathbf{p})$ with respect to the parameters p_i . The wave function and parameter derivatives in Eq. (5.30) are normalized

$$\tilde{\Psi}(\mathbf{p}) = \frac{1}{\sqrt{\langle \Psi(\mathbf{p}) | \Psi(\mathbf{p}) \rangle}} \Psi(\mathbf{p}), \tag{5.31}$$

with the normalization constant depending on the parameter change. In the linear method, the eigenvalues E_{lin} and eigenvectors $\Delta \mathbf{p}$ (parameter changes) are the solutions to the following generalized matrix eigenvalue problem:

$$\mathbf{H} \cdot \Delta \mathbf{p} = E_{\text{lin}} \mathbf{S} \cdot \Delta \mathbf{p}. \tag{5.32}$$

The Hamiltonian **H** is diagonalized in the basis spanned by the current wave function $\tilde{\Psi}(\mathbf{p}_0)$ and its parameter derivatives $\tilde{\Psi}_i(\mathbf{p}_0)$. **S** corresponds to the overlap matrix.

Nightingale and Melik-Alaverdian have shown that using a non-symmetric Hamilton

matrix is advantageous since it satisfies the zero-variance property.^[70]

The linear method efficiently optimizes the Jastrow, CSF, and orbital parameters.^[66] For linear parameters, convergence is achieved within one iteration, while for the optimization of non-linear parameters, the process has to be repeated iteratively until convergence is reached.

The optimal parameter variations are obtained by solving Eq. (5.32) for the lowest *physical* eigenvalue. In practice, for finite Monte Carlo samples, the lowest eigenvalue may not provide the sought parameter change since spurious solutions can occur. This is prevented by recalculating the sample and its energy—with a much smaller sample—for a set of eigenvectors using the new parameters. For large sets of parameters (up to tens of thousands), storing the Hamilton and overlap matrices becomes cumbersome. With their blocked linear method, Zhao and Neuscamman^[72] were able to circumvent this memory bottleneck by blocking the Hamilton and overlap matrices.

5.4.2.2 Newton Method

The Newton method was first applied to energy minimization in VMC by Lin, Zhang, and Rappe in 2000.^[73] It was later improved in terms of robustness and efficiency by Umrigar and co-workers^[66,74], as well as by Sorella^[75]. The key challenge for efficient Newton methods lies in developing low variance estimators for the gradient and the Hessian.

In the Newton method, as described in Ref. 66, the energy is expanded in a Taylor series to the second-order around the current parameter vector \mathbf{p}^0

$$E^{(2)}(\mathbf{p}) = E_0 + \sum_{i}^{N^{\text{opt}}} g_i \Delta p_i + \frac{1}{2} \sum_{i,j}^{N^{\text{opt}}} h_{ij} \Delta p_i \Delta p_j.$$
 (5.33)

 E_0 corresponds to the VMC energy for the current parameter set, while the g_i and h_{ij} constitute the elements of the energy gradient and Hessian, respectively:

$$g_i = \frac{\partial E^{(2)}(\mathbf{p})}{\partial p_i} \bigg|_{\mathbf{p} = \mathbf{p}_0}, \quad h_{ij} = \frac{\partial^2 E^{(2)}(\mathbf{p})}{\partial p_i \partial p_j} \bigg|_{\mathbf{p} = \mathbf{p}_0}.$$
 (5.34)

The parameter change is then given as

$$\Delta \mathbf{p} = -\mathbf{h}^{-1} \cdot \mathbf{g}. \tag{5.35}$$

In practice, one usually solves the numerically more stable form $\mathbf{h} \cdot \Delta \mathbf{p} = \mathbf{g}$ of Eq. (5.35), which corresponds to a system of inhomogeneous linear equations.

Newton-like algorithms often suffer from limited convergence radii. The method, presented above, can for example be stabilized by updating the Hessian as follows

$$\mathbf{h}' = \mathbf{h} + \nu \mathbf{I},\tag{5.36}$$

with the positive constant ν adapted throughout the optimization. This approach ensures that the Hessian is positive definite. By increasing ν , one smoothly moves toward a steepest descent step.^[74]

The Newton method efficiently optimizes the Jastrow, CSF, and MO parameters. [66]

5.4.2.3 Perturbative Method

The perturbative optimization method^[66] and the energy fluctuation potential method^[76] are both variants of the stochastic reconfiguration method.^[77] In the approach formulated by Toulouse and Umrigar^[66], the parameter change is obtained as

$$\Delta p_i^{(1)} = -\frac{1}{\Delta \mathcal{E}_i} \sum_{j}^{N^{\text{opt}}} (\mathbf{S}^{-1})_{ij} H_{j0},$$
 (5.37)

with

$$H_{j0} = \langle \Psi_j | \hat{H} | \Psi_0 \rangle = \frac{g_j}{2}. \tag{5.38}$$

Eq. (5.37) is closely related to the Newton parameter variations, see Eq. (5.35), with an

approximate Hessian $h_{ij}^{\text{pert}} = \Delta \mathcal{E}_i/(\mathbf{S}^{-1})_{ij}$. The energy denominators $\Delta \mathcal{E}_i$ are determined as follows:

$$\Delta \mathcal{E}_i = \frac{\langle \Psi_i | \hat{H} | \Psi_i \rangle}{\langle \Psi_i | \Psi_i \rangle} - E_0 = \frac{H_{ii}}{S_{ii}} - H_{00}. \tag{5.39}$$

In both the linear and the Newton method, the parameter derivatives of the local energy $E_{\mathrm{L},i}$ are needed, which is especially demanding when ECPs are used. These derivatives are only needed in the perturbative optimization method for the computation of the energy denominators. It has been shown^[66,78] that rough estimates for the energy denominators are sufficient. In practice, they are thus only computed in the first step (with a smaller sample size) and then kept fixed throughout the subsequent iterations. For the parameter changes using the perturbative optimization method, only the overlap matrix and the gradient need to be calculated, which considerably reduces the computational effort. The perturbative optimization technique can be used to optimize the CI and orbital parameters, not however the Jastrow factor.^[66]

5.5 Diffusion Monte Carlo

The notation of Hammond, Lester, and Reynolds^[51] is mostly adopted here. The DMC technique is a stochastic projector method that solves the time-dependent Schrödinger equation—with a time-independent Hamiltonian—in imaginary time to extract the ground state

$$\frac{-\partial \Psi(\mathbf{R}, \tau)}{\partial \tau} = (\hat{H} - E_{\mathrm{T}})\Psi(\mathbf{R}, \tau), \tag{5.40}$$

where E_T is an arbitrary energy offset, see below. The time t has been replaced by an imaginary time variable $\tau = i \cdot t$. The formal solution of Eq. (5.40) can be expanded into a set of eigenfunctions $\psi_k(\mathbf{R})$ of the Hamiltonian

$$\Psi(\mathbf{R},\tau) = \sum_{k=0}^{\infty} C_k e^{-\tau(E_k - E_T)} \psi_k(\mathbf{R}), \qquad (5.41)$$

where the $C_k = \langle \psi_k | \Phi(t=0) \rangle$ depend on the initial condition. Note that the time and space variables have been separated in Eq. (5.41). Additionally, it becomes apparent why the time variable has been exchanged for an imaginary time. Using the original time variable, Eq. (5.41) would display an (undesired) oscillatory time behavior, while in the form presented here, an exponential time behavior is obtained. The ground state is projected out in the long time limit $(\tau \to \infty)$ since the excited states—having higher energy eigenvalues E_k —decay much faster. The rate at which convergence toward the ground state occurs is determined by the energy difference between the two lowest eigenstates.^[79]

In order to make the imaginary time-dependent Schrödinger equation feasible for Monte Carlo methods, it has to be transformed to an integral form (see appendix B):

$$\Psi(\mathbf{R}', \tau + \delta \tau) = \int G(\mathbf{R}', \mathbf{R}; \delta \tau) \Psi(\mathbf{R}, \tau) d\mathbf{R}$$
 (5.42)

with the Green's function defined as

$$G(\mathbf{R}', \mathbf{R}; \delta \tau) = \langle \mathbf{R}' | e^{-(\hat{H} - E_{\mathrm{T}})\delta \tau} | \mathbf{R} \rangle.$$
 (5.43)

The operator in Eq. (5.43) is called the time evolution operator. The Green's function corresponds to the position representation of the time evolution operator and describes the propagation between two electron arrangements in imaginary time.

The idea of DMC is to exploit the close resemblance of the time-dependent Schrödinger equation to a diffusion process. This connection becomes clear when rewriting Eq. (5.40) using the explicit form of the Hamiltonian.

$$\frac{\partial \Psi(\mathbf{R}, \tau)}{\partial \tau} = \frac{1}{2} \Delta \Psi(\mathbf{R}, \tau) + (E_{\mathrm{T}} - V(\mathbf{R})) \Psi(\mathbf{R}, \tau)$$
 (5.44)

The first term on the right-hand side of Eq. (5.44) is closely related to Fick's second law, while the second term can be interpreted as a first-order rate equation or branching process. Both processes can be simulated separately with QMC.^[51] To achieve this, the operator in Eq. (5.43) has to be factorized into a kinetic and a potential energy part:

$$e^{-(\hat{T}+\hat{V}-E_{\mathrm{T}})\tau} \approx e^{-\hat{T}\tau}e^{-(\hat{V}-E_{\mathrm{T}})\tau} \equiv G_{\mathrm{diff}}G_{\mathrm{by}} \tag{5.45}$$

with G_{diff} and G_{b} describing the Green's functions for both processes, respectively. This approach, called short time approximation, makes use of the Trotter-Suzuki formula^[80,81] and is only valid for small time steps because \hat{T} and \hat{V} do not commute. The first correction term corresponds to

$$G - G_{\text{diff}}G_{\text{b}} = \frac{1}{2} \left[\hat{V}, \hat{T} \right] \tau^2 + \mathcal{O}(\tau^3),$$
 (5.46)

introducing an error $\mathcal{O}(\tau^3)$, called time step bias. By performing several DMC calculations with different (small) time steps, the time step error can be removed by extrapolating the DMC energy to a zero time step.

Both processes provide exact solutions to their respective differential equations:

$$-\frac{\partial G_{\text{diff}}(\mathbf{R}', \mathbf{R}; \tau)}{\partial \tau} = \frac{1}{2} \Delta G_{\text{diff}}(\mathbf{R}', \mathbf{R}; \tau)$$

$$-\frac{\partial G_{\text{b}}(\mathbf{R}', \mathbf{R}; \tau)}{\partial \tau} = (E_{\text{T}} - V) G_{\text{b}}(\mathbf{R}', \mathbf{R}; \tau).$$
(5.47)

$$-\frac{\partial G_{b}(\mathbf{R}',\mathbf{R};\tau)}{\partial \tau} = (E_{T} - V)G_{b}(\mathbf{R}',\mathbf{R};\tau). \tag{5.48}$$

The solutions for the diffusion and the branching processes are given by the following equations:

$$G_{\text{diff}}(\mathbf{R}', \mathbf{R}; \tau) = (2\pi\delta\tau)^{-3N/2} e^{-(\mathbf{R}' - \mathbf{R})^2/2\tau}$$
 (5.49)

$$G_{\rm b}(\mathbf{R}',\mathbf{R};\tau) = e^{-(\frac{1}{2}[V(\mathbf{R})+V(\mathbf{R}')]-E_{\rm T})\tau}.$$
 (5.50)

Eq. (5.49) corresponds to a 3N-dimensional Gaussian distribution with variance τ . The diffusion part of Eq. (5.42) can thus be solved by a random walk process with the walkers being Gaussian distributed with a variance of τ .

The branching process, Eq. (5.50), on the other hand, is used to attribute a weight to

each walker. After a long propagation time, the weight differences between the walkers become substantial. To rectify this, a birth-death algorithm, which duplicates walkers with high weights (at the same position) while killing walkers with low weights, is adopted. Since the number of walkers can now fluctuate, a population control has to be introduced to prevent the population from either collapsing or exploding. To regulate the fluctuation of the walker population around a mean value, the reference energy E_T is utilized. However, its adjustment during the calculation leads to a population control error. [55]

It was previously mentioned that the ground state is only projected out in DMC in the long time limit. Eq. (5.45) is, however, only valid for $\tau \to 0$. Luckily, the time evolution operator, see Eq. (5.43), possesses the composition property. The long time is achieved by subsequently using the short-time functions multiple times.^[51]

5.5.1 Importance Sampling DMC

The technique presented above is also referred to as simple DMC and suffers from inefficiency mostly due to the divergence of the potential energy term in the branching process. This can be circumvented by using importance sampling, see section 5.1.3. Eq. (5.44) is multiplied by a guide function $\Psi_G(\mathbf{R})$, introducing the distribution $f(\mathbf{R},\tau) = \Psi(\mathbf{R},\tau)\Psi_G(\mathbf{R})$, which replaces the wave function. One then obtains the modified time-dependent Schrödinger equation

$$\frac{\partial f(\mathbf{R}, \tau)}{\partial \tau} = \frac{1}{2} \Delta f(\mathbf{R}, \tau) - \frac{1}{2} \nabla \cdot (f(\mathbf{R}, \tau) \mathbf{F}_{\mathbf{Q}}(\mathbf{R})) + (E_{\mathbf{T}} - E_{\mathbf{L}}(\mathbf{R})) f(\mathbf{R}, \tau), \tag{5.51}$$

with $F_Q(\mathbf{R}) = 2\nabla \Psi_G/\Psi_G$ corresponding to a vector field, called quantum force. This quantity directs the movement away from areas where $|\Psi_G|^2$ is small.^[51] For the diffusion and branching processes, the Green's functions are modified accordingly:

$$\tilde{G}_{\mathrm{dd}}(\mathbf{R}',\mathbf{R};\delta\tau) = (2\pi\delta\tau)^{-3N/2} e^{-(\mathbf{R}'-\mathbf{R}-1/2\delta\tau\mathbf{F}_{\mathrm{Q}}(\mathbf{R}'))^2/2\delta\tau}$$
(5.52)

$$\tilde{G}_{b}(\mathbf{R}',\mathbf{R};\delta\tau) = e^{-(\frac{1}{2}[E_{L}(\mathbf{R}) + E_{L}(\mathbf{R}')] - E_{T})\delta\tau}.$$
(5.53)

By introducing the guide function, an additional drift term occurs in the diffusion process, the subscript on the left-hand side of Eq. (5.52) being altered to *drift-diffusion*. As for the branching term, the potential energy has been replaced by the local energy, leading to a suppression of the branching process since $E_{\rm L}({\bf R})$ is nearly constant and does not fluctuate as strongly as the potential energy. [11,52] Importance sampling, resulting in an elevated walker density in regions where the guide function is large due to the drift velocity, increases the efficiency and reduces the variance.

5.5.2 Fermion Sign Problem

So far, the function is assumed to be strictly positive, arising from the comparison of the time-dependent Schrödinger with a diffusion process. As a consequence, following the spin-statistics theorem, the DMC method is only exact for bosons which are described by nodeless wave functions. In contrast to bosons, fermions necessitate the use of antisymmetric wave functions, resulting in an approximation that introduces nodes. This approximation, in which the guide function $\Psi_G(\mathbf{R})$ is used to enforce its nodes onto $\Psi(\mathbf{R},\tau)$, is referred to as fixed-node diffusion Monte Carlo (FN-DMC). The distribution $f(\mathbf{R},\tau)$ is only strictly positive if both $\Psi_G(\mathbf{R})$ and $\Psi(\mathbf{R},\tau)$ share the same nodes. Note that, without constraints, DMC converges to the bosonic ground state since this is the mathematical ground state of the electronic Hamiltonian.

The fixed-node approach introduces a systematic error, known as the node location error, since the exact nodes are only known for a few systems. The accuracy of the DMC solution, with the time step bias removed, solely depends on the nodes of the guide function.

The DMC energy is determined using a mixed estimator and calculated as a weighted average of the local energy over the walker sample.^[79]

Both the VMC and DMC methods obey the variational principle within the limit of all-electron calculations. Moreover, the VMC energy approaches the DMC energy by optimizing the Jastrow factor.

5.6 Effective Core Potentials

QMC methods are capable of producing energies within the "chemical accuracy" boundary (1 kcal/mol), as defined by John A. Pople^[83], at a reasonable computational cost.^[11] However, when dealing with systems that involve transition metals, the computational effort increases significantly since QMC methods scale less favorably with the atomic number, ranging from $\mathcal{O}(Z^{5.5})$ to $\mathcal{O}(Z^{6.5})$.^[51,84] For heavy atoms, where the atomic number is large, two issues arise. First, the high kinetic energy of the core electrons requires their time step to decrease in order to obtain accurate results. Second, the fluctuation of the local energy near the nucleus becomes significant as the atomic number increases, leading to a considerable amount of computing time being required for electrons that only play a secondary role in describing chemically relevant quantities such as bond dissociation or excitation energies.^[10,52]

One solution to this problem is to exclude the core electrons from the calculation using ECPs, which reduce the effective atomic number of an element by the number of electrons replaced by the ECP, and allow for easy inclusion of scalar relativistic effects. The ECP is designed to capture the effect of the core electrons and nuclei on the valence electrons.^[52]

To introduce a pseudopotential, the wave function must be separated into a product of core and valence functions, as shown in Eq. (5.54). The anti-symmetry operator \hat{A} ensures the anti-symmetry of the product, thereby satisfying the Pauli exclusion principle.

$$\Psi \approx \hat{\mathcal{A}}\Psi_{\text{core}}\Psi_{\text{val}} \tag{5.54}$$

The Schrödinger equation is then reduced to only include the valence electrons

$$\hat{H}_{\text{val}}\Psi_{\text{val}} = E_{\text{val}}\Psi_{\text{val}},\tag{5.55}$$

with the pseudo-Hamiltonian (in a.u.) for the valence electrons defined as

$$\hat{H}_{\text{val}} = -\frac{1}{2} \sum_{i} \Delta_{i} + \sum_{i < j} \frac{1}{r_{ij}} + \sum_{i, I} V_{\text{loc}}(R_{iI}) + \hat{W}.$$
 (5.56)

The $V_{loc}(R_{iI})$ terms correspond to the local part of the ECP and depend on the electron-nucleus distances. The operator \hat{W} is an angular momentum-dependent non-local operator which ensures the orthogonality of the valence states to the core states:

$$\hat{W} = \sum_{i,I} \sum_{l,m} V_l(R_{iI}) |Y_{lm}\rangle \langle Y_{lm}|.$$
(5.57)

The operator in Eq. (5.57) is a projection operator with the spherical harmonics Y_{lm} (centered at a given nucleus) as simultaneous eigenfunctions of the \hat{L}^2 and the \hat{L}_z operators. The operator projects the different angular momentum components (s, p, d, ...) out of a function (e.g. orbital), thereby allowing the different channels to be treated individually, or in other words: the different components see separate potentials.^[51] The operator \hat{W} should thus at the least include all the angular momentum quantum numbers of the removed electrons. There is, however, no constraint for the higher channels.

The actual form of the ECP corresponds to a sum of Gaussians, which facilitates the integration and have the advantage of not exhibiting singularities at the nuclei

$$V(r) = \sum_{k} A_k r^{-2+n_k} e^{-\alpha_k r^2},$$
(5.58)

with the parameters n_k , A_k , and α_k optimized to fulfill certain requirements. Various types of ECPs are available, including shape- and energy-consistent ECPs. The shape-consistent ECPs aim to accurately reproduce the core orbitals^[85,86], while the energy-consistent ones aim to reproduce the orbital energies of the valence electrons for an all-electron ansatz^[87].

The non-locality of the ECP poses a significant problem for QMC methods, as they are fully local approaches.^[88] This can be solved by using the trial wave function to localize the non-local operator:

$$W_{\rm loc} = \frac{\hat{W}\Psi_{\rm val}}{\Psi_{\rm val}}.$$
 (5.59)

In VMC, no approximation is made, since \hat{W} is applied to Ψ_{val} anyway for the evaluation of the local energy. The random walk simulation will converge to the correct distribution $|\Psi_{val}|^2$ even with \hat{W} as part of the Hamiltonian.^[51]

In the DMC formalism, the picture is rather different. A correct localization of the ECP would require the exact fixed-node solution. Since the exact wave function is usually not known, employing ECPs within DMC introduces an additional error, the ECP localization error. The exponential form of the propagator, see Eq. (5.43), complicates things; the non-local operator \hat{W} can neither be included in the diffusion process, it is not necessarily positive and, thus, cannot be interpreted as a probability density, nor can it be integrated into the branching process because the random walk is local. One way to tackle this problem is to remove it from the propagator by localizing it on the guide function, which is done within the *locality approximation*. The accuracy of the approximation depends on the quality of the guide function.

In both VMC and the locality approximation, the following integrals have to be calculated

$$\langle Y_{lm}(\theta_k, \phi_k) | \Psi_{\text{val}}(\mathbf{r}_1, ..., \mathbf{r}_n) \rangle = \iint Y_{lm}^*(\theta_k, \phi_k) \Psi_{\text{val}}(\mathbf{r}_1, ..., r_k, \theta_k, \phi_k, ..., \mathbf{r}_n) r_k^2 \sin \theta_k d\theta_k d\phi_k.$$
(5.60)

These integrals on the surface of a sphere with radius r_k are evaluated by means of Lebedev integration^[89,90] which can exactly integrate spherical harmonics up to a certain degree. The numerical integration is performed for several points—in this thesis: 12 for VMC and 18 for DMC^[88]—on a polyhedron. Note that, if one excludes the Jastrow factor from the localization of the ECP, the integrals in Eq. (5.60) can be solved analytically, as described by Hammond and co-workers^[91], which substantially lowers the computational expenditure. It has, however, been shown that by including the Jastrow factor in the localization procedure, better results in terms of energy can be obtained.^[92,93]

The drawback of the locality approximation is that, since the Hamiltonian is modified

(through the omission of a term), the DMC energy is not necessarily an upper bound to the exact ground state energy. [88,94] The T move approach [95,96] makes the DMC energy variational again, however, it does not eliminate the localization error. The error of the energy, introduced in DMC by the localization of the ECP, is quadratic in the accuracy of the guide wave function: $\propto (\Psi_{val} - \Phi_0)^2$.[88]

In this thesis, the energy-consistent HF ECPs by Burkatzki, Filippi, and $Dolg^{[97,98]}$ and their respective triple- ζ basis sets are employed. Mitas and co-workers^[99,100] recently developed a new generation of ECPs that are constructed from correlated calculations. These correlation-consistent effective core potentials (ccECPs) are designed to attain isospectrality between the ECP and the all-electron Hamiltonians and are able to include—to some degree—core-core and core-valence (CV) correlation.^[101] The ccECPs are used in this thesis as well.

Bachelet *et al.*^[102] proposed in 1989 an alternative approach for removing the core electrons which is based on a pseudo-Hamiltonian with a position-dependent effective mass tensor in the kinetic energy term, forgoing the use of non-local operators. However, the generation of this class of pseudopotentials proved numerically difficult^[103] and their use in QMC has therefore been rather sparse. In a recent study by Bennet *et al.*^[104], the authors successfully constructed a pseudo-Hamiltonian for cobalt and provided accurate atomic excitation energies, as well as rigorous binding energies for CoO at DMC level, which will undoubtedly renew the interest into this class of pseudopotentials.

6 Transition Metal Compounds

"THE COLD NEVER BOTHERED ME ANYWAY." – Elsa

Parts of this chapter are published in a condensed form in Ref. 105.

Reprinted (adapted) with permission from J. Ludovicy, K. Haghighi Mood, A. Lüchow, Full Wave Function Optimization with Quantum Monte Carlo—A Study of the Dissociation Energies of ZnO, FeO, FeH, and CrS, *J. Chem. Theory Comput.* **2019**, *15*, 5221-5229. Copyright 2019 American Chemical Society.

Transition metals and their compounds are chemical systems that are of great interest for catalytic processes, electrochemistry and biochemistry. [$^{106-109}$] These metals are particularly interesting systems due to their open d-shells, ability to exhibit multiple oxidation states, and tendency to possess magnetic properties. The high density of states surrounding these species renders an accurate description rather laborious.

An accurate understanding of how catalysts work is of great importance when it comes to elucidating and predicting catalytic processes. The study of transition metal compounds with high-level quantum chemical methods is justified since the bond-breaking of the metal and main group element plays a primary role for these processes. To achieve an accurate theoretical understanding of bond-breaking processes, it is important to study transition metal dimers as a first step, even though the ultimate goal may be to investigate bulk material properties or complete catalytic cycles. However, studying these small compounds with electronic structure theory is already challenging due to their strong correlation and complex electronic structures. [110–115] For the late transition metals, being of great interest especially for catalysis, the static electron correlation yields an important contribution to their properties. The development of efficient methods that are able to capture this part of the correlation thus constitutes a highly active field of research. Progress has been made by designing suitable DFT functionals [116,117] as well as by further developing multi-reference wave function-based methods, such

as multi-reference coupled cluster (MRCC)^[118].

Transition metal compounds have been thoroughly studied with various exhaustive benchmark studies providing accurate bond dissociation energies for most systems. In 2013, Zhang *et al.*^[112] tested 42 exchange-correlation functionals on a set of 70 molecules containing 3*d* transition metals. In another study, Xu *et al.*^[113] compared the performance of CC and KS DFT on bond dissociation energies of 20 transition metal dimers. Cheng *et al.*^[114] investigated the same 20 compounds by means of scalar relativistic CC calculations, focusing on the effects of electron correlation and basis set choice. At about the same time, Fang *et al.*^[119] published CCSD(T)/CBS bond dissociation energies and heats of formation for the same set of dimers. Additionally, Aoto *et al.*^[115] explored the dissociation energies as well as spectroscopic constants of 60 transition metal dimers using CC methods, discussing the impact of i.a. relativistic and multireference effects.

Transition metal compounds have, however, also been successfully studied with QMC in the past. Wagner and Mitas^[120] investigated transition metal oxides with FN-DMC. Petz and Lüchow^[121] reported accurate dissociation energies and ionization potentials for sulfide compounds with FN-DMC. Diedrich *et al.*^[122] studied transition metal carbonyls with regard to their dissociation energies with FN-DMC. Horváthová *et al.*^[123] presented energetics for transition metal organometallics employing QMC methods. Doblhoff-Dier *et al.*^[124] published dissociation energies of 3*d* transition metal compounds calculated with DMC. Finally, Haghighi Mood and Lüchow^[125] have shown that a multi-reference ansatz in combination with the optimization of the orbital parameters is necessary to predict the right ground state for and to reproduce the dissociation energy of FeS. In their study, the authors found that the re-optimization of the MOs in the presence of a Jastrow correlation function was the key to obtaining accurate results.

For several transition metal compounds, a rather large discrepancy between the theoretical and the experimental bond dissociation energies can still be observed. These compounds are believed to exhibit prominent multi-reference character, implying that the single-determinant approach is not capable of correctly describing them. In this part of the thesis, several of these transition metal dimers are therefore revisited with multi-reference diffusion Monte Carlo (MR-DMC). With this approach, the possibility to obtain sufficiently accurate DMC energies by retaining compact trial wave functions and by varying the nodal surface through orbital and CI optimization in the presence

of a Jastrow factor is to be explored.

6.1 With Hydrogen

6.1.1 FeH

Scientists have shown a great interest—both theoretically and experimentally—in molecular iron monohydride since the 1970s. [126–128] FeH is ubiquitous in our universe with a rigorous understanding of its properties being especially important to astrophysicists, trying to model stellar atmospheres. [129,130] Theoretical investigations on FeH have proven rather complex, with several studies [129,131,132] even suggesting a breakdown of the Born-Oppenheimer approximation.

FeH is revisited in this work because of the results of Truhlar and co-workers^[113], who performed DFT and CC calculations for a set of 20 transition-metal dimers. They reported a significant discrepancy in the experimental dissociation energy for, amongst others, FeH with both methods. The authors of that work also state a prominent multi-reference character for FeH. Additionally, Doblhoff-Dier *et al.*^[124] performed DMC calculations using KS orbitals for FeH and found a significant deviation to the experimental dissociation energy, suggesting that a single-reference approach is not able to correctly describe this system.

The $^4\Delta$ ground state of FeH was first determined by Beaton *et al.*^[133] with far-infrared laser magnetic resonance. The valence electronic configuration of FeH corresponds to $\sigma^2\pi^4\delta^2\sigma^1$.

In order to determine the equilibrium bond distance of FeH, a potential energy curve was recorded at the MR-DMC level for several bond distances, see Fig. 6.1. A fixed time step of $\tau = 0.001$ a.u., resulting in an acceptance ratio of 99% in DMC, was used for each data point. For every bond distance, the initial (full valence) CAS(9,7) wave functions—the active space being constructed from the 4s and 3d orbitals of the iron, and the 1s orbital of the hydrogen atoms—were optimized with respect to the VMC energy. All wave function parameters (Jastrow, MO, and CI) were included in the optimization. A more detailed description of the procedure and framework conditions is given in section 6.5. The potential energy curve was fitted with a Morse potential function [134],

the minimum of which yields the equilibrium bond distance, corresponding to $1.567 \, \text{Å}$ for FeH. Other spectroscopic constants, that can be extracted from the Morse fit as well, are discussed in section 6.4.

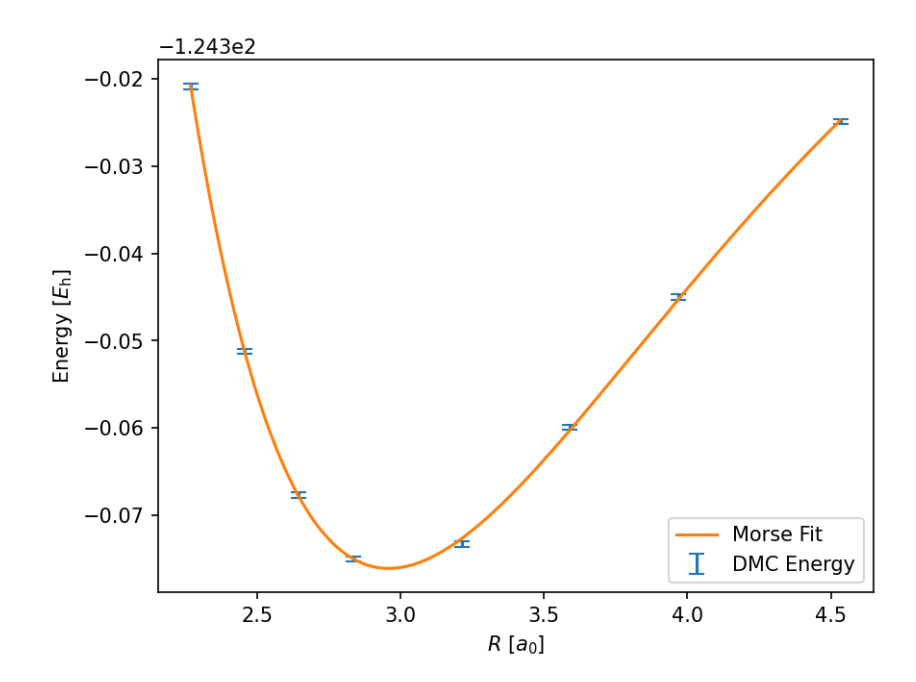


Fig. 6.1: FeH MR-DMC potential energy curve at the Jas+MO+CI optimization level with the corresponding Morse fit. A time step of $\tau=0.001$ a.u. was employed for each data point. An sm666 Jastrow factor was used.

One aim of this chapter is to investigate the accuracy of a single-reference—in contrast to a multi-reference—ansatz for transition metal compounds in the context of QMC. For the single-determinant results, HF and KS orbitals were employed, while CASSCF wave functions were chosen for the multi-reference approach. The VMC and time step extrapolated DMC energies, computed for the above-determined equilibrium bond distance of 1.567 Å are given in Tab. 6.1. The Slater-Jastrow wave functions were optimized alternately with respect to the Jastrow, MO, and CI parameters in order to minimize the variational energy. The parameters that are not optimized with VMC are taken from their respective *ab initio* calculations. ECPs were employed for all calculations, see section 6.5 for details about the computational approach.

Tab. 6.1: FeH VMC and DMC energies in E_h	at various optimization	levels, using different starting or-
bitals and BFD-VTZ/sm666.		

Ansatz	Orbitals	Optimization level	VMC energy	DMC energy
	HF	Jas	-124.2815(2)	-124.3443(5)
Single det	B3LYP	Jas	-124.2923(2)	-124.3519(5)
	opt	Jas+MO	-124.2948(2)	-124.3519(5)
CAS(9,7)	CAS	Jas	-124.2940(2)	-124.3548(5)
	CAS	Jas+CI	-124.3030(2)	-124.3647(5)
	opt	Jas+MO+CI	-124.3252(2)	-124.3802(5)

First of all, Tab. 6.1 shows that a systematic lowering of the VMC energies—at the Jastrow optimization level—is achieved from HF over KS B3LYP to CAS orbitals. The optimization of the molecular orbitals results in lower VMC energies for both, the singleand the multi-reference ansatzes, with the gain in energy being greater for the CAS orbitals. Optimizing the MOs in the presence of a Jastrow factor enables the coupling between the static and the dynamic electron correlation, which, as can be deduced from Tab. 6.1, has a significant impact on the energies. The change in energy is much smaller when KS orbitals are used, implying that they capture this effect at least to some extent. For the multi-reference ansatz, the optimization of the CI coefficients lowers the energy considerably, however, the effect is much smaller compared to the MO optimization. The quality of the nodal surface of the wave functions can be assessed through the DMC energies. For the single-determinant ansatz, the optimization of the MOs does not improve the nodal surface when KS orbitals are employed, indicating that these orbitals are already ideal before the optimization. Without the optimization of the antisymmetric part of the wave function (MO and CI parameters), the Jastrow correlation function has no impact on the nodal surface. The optimization of the CI coefficients lowers the DMC energy of the CAS(9,7) initial wave function by about 10 m E_h . The fully optimized wave function yields the best nodal surface with an energy that is lowered by another 15 m E_h , revealing the effect of the Jastrow correlation function, and thus of the dynamic correlation, on the nodal surface.

Tab. 6.2 contains the DMC bond dissociation energies for FeH for different ansatzes. The dissociation energies are obtained as the difference between the atomic and dimer energies in their respective ground states. The energies of the atomic species can be found in appendix D. Their DMC energies only differ within the statistical uncertainty

for the different starting orbitals and optimization levels. Throughout this chapter, only dissociation energies at the DMC level of theory are evaluated since it has been shown^[78] that their VMC counterparts are not competitive. Since the dissociation energies are to be compared to experimental data, it is important to include relativistic effects, the zero-point energy (ZPE), as well as the correlation between the core and valence electrons. This correlation effect—deemed important by other studies^[113,115] as well—is lost since ECPs, removing the core electrons, are used for the calculations. Scalar relativistic effects are intrinsically included through the ECP while the first-order spin-orbit (SO) coupling is taken from the literature. The SO correction for the atomic species is derived from experimental splittings^[135], see Tab. D.1 in the appendix. For FeH, the first-order SO correction is taken from Ref. 113 and amounts to -0.048 eV. The first-order SO coupling is always negative, thereby providing a stabilizing contribution to the energy. The ZPE is derived from the Morse fit and corresponds to 0.114(2) eV. Finally, the CV correlation contribution, see section 6.5 for details, amounts to 0.0675 eV.

Tab. 6.2: DMC dissociation energies of FeH in eV at various optimization levels, using different starting orbitals and BFD-VTZ/sm666. The energies are CV and SO corrected and the ZPE is included.

Ansatz	Orbitals	Optimization level	D_0
	HF	Jas	0.81(2)
Single det	B3LYP	Jas	1.02(2)
	opt	Jas+MO	1.02(2)
	CAS	Jas	1.10(2)
CAS	CAS	Jas+CI	1.37(2)
	opt	Jas+MO+CI	1.79(2)

The optimization levels in Tab. 6.2 refer to optimized parameters for the dimer. The dissociation energy for the KS nodes is significantly higher compared to the one for the HF nodes at the Jastrow optimization level. The optimization of the molecular orbital parameters shows no improvement of the dissociation energy when initial KS orbitals are used. For the multi-reference approach, even when dispensing with the re-optimization of the anti-symmetric part of the complete active space (CAS) guide function, a more accurate dissociation energy is obtained compared to the one from the fully optimized single-reference wave function, corroborating the multi-reference character of FeH. Additionally, a systematic improvement of the dissociation energy can be observed when including more sets of parameters in the optimization with VMC. The MO optimization

of the CAS wave function in the presence of a Jastrow correlation factor has the largest effect on the bond dissociation energy, it is increased by about 0.4 eV. This shows that the fixed-node error in DMC can be systematically reduced when accurate (optimized) wave functions are used.

Tab. 6.3: Calculated and measured bond dissociation energies (in eV) for FeH. The D_0 data refers to values obtained for 0 K.

Investigators	Method	D_{e}	D_0
This work	MR-DMC/BFD-VTZ (SO+CV)	1.90(2)	1.79(2)
This work	MR-DMC/ccECP-aug-cc-pVTZ (SO)	1.91(2)	1.80(2)
Schultz and Armentrout ^[136]	Mass Spectrometry		1.60(8) ^a
	DFT/B3LYP	2.10	
Jensen <i>et al</i> . ^[137]	DFT/BP86	2.41	
	DFT/PBE	2.30	
	CCSDT(2) _Q /apTZ-DK(3)-CV(3-DK) ^b	1.79	
Xu et al. ^[113]	DFT/B97-1-DK	2.00	
	DFT/M06-L-DK	2.17	
Aoto <i>et al.</i> ^[115]	CCSD(T)(CV)/CBS+ΔDK	1.95 ^c	
Cl (1 [114]	$CCSD(T)/CBS+\Delta T+\Delta Q+\Delta CV+\Delta SO^d$	1.95	
Cheng et al. ^[114]	Revised H abstraction reactions ^e	1.79(7)	1.69(7)
E 1 [119]	Revised H abstraction reactions ^e	1.72(13)	
Fang <i>et al.</i> ^[119]	CCSD(T)/PW91	1.95	
DeYonker and Allen ^[138]	FPA using CC (up to H excitations)		1.87
Shee <i>et al.</i> ^[139]	ph-AFQMC/CCcbs	1.81(7)	

^a Derived using the thermal correction 0.032 eV from DeYonker and Allen.^[138]

In Tab. 6.3, the best estimate of the dissociation energy of FeH, computed in this work, is compared to various experimental and theoretical data from the literature. For several of the systems, discussed in this work, a novel type of ECP was employed, in addition to the one from Burkatzki, Filippi, and Dolg (BFD). This new generation of ECPs,

^b From Table 10 of Ref. 113.

^c Best estimate value.

^d See Table 2 in Ref. 114. Value corresponds to cal $-\Delta_{\rm geo}$.

^e See text for details.

denoted as ccECP, stems from correlated calculations and thus accounts for core-core and—to some degree—core-valence correlation.^[99,100] The dissociation energy computed with this ECP is therefore only SO corrected. For FeH, both ECPs yield similar results. In 1991, Schultz and Armentrout^[136] determined the dissociation enthalpy (at 298.15 K) of FeH by means of guided-ion beam mass spectrometry and reported a value of 1.63(8) eV. Using the thermal correction, derived by DeYonker and Allen^[138], the dissociation enthalpy can be converted to the dissociation energy and a value of 1.60(8) eV is obtained. The MR-DMC bond dissociation energies overestimate the experimental one by about 0.2 eV. Several studies suggest, however, that the experimental bond dissociation energies for some transition metal compounds might be in need of revision.^[113,114,119,138] The dissociation energy of metal hydrides can be derived from hydrogen abstraction reactions:

$$D_0(M-H) = D(R^+-H^-) - IP(M) - EA(H) - E_{threshold}$$

with the reaction energy $E_{\rm threshold}$ being obtained from mass spectrometric experiments. The ionization potentials (IPs) and the electron affinities (EAs) have been known accurately for many years^[114,119], so the quantity that needs revising is the heterolytic dissociation energy of the RH species, with RH corresponding to small organic compounds. Two research groups took on this task at about the same time: Cheng $et~al.^{[114]}$ revised some hydride transfer reactions by using updated Active Thermochemical Tables (ATcT)^[140] data while Fang $et~al.^{[119]}$ computed the heterolytic RH dissociation energies at the G3MP2^[141] level. The updated experimental dissociation energies for FeH are given in Tab. 6.3. The reported values are very similar and, what is more, they are in much better agreement with the MR-DMC ones. As for other theoretical approaches, DFT—using various functionals—severely overestimates the dissociation energy while the CC ones are in good agreement with the ones computed in this work. Furthermore, the focal point analysis (FPA) of DeYonker and Allen^[138] as well as the phaseless auxiliary-field QMC approach of Shee $et~al.^{[139]}$ yield dissociation energies that agree well with the MR-DMC ones.

Xu *et al.*^[113] confirmed the multi-reference character of FeH using different diagnostics. However, they obtained an accurate dissociation energy with CCSDT(2)_Q, including scalar relativistic effects and the core-valence correlation contribution, while their reported DFT dissociation energies deviate considerably from the experimental value. Nonetheless, they argued that KS DFT yields overall comparable results to CC theory

for the twenty transition metal compounds that they investigated. Finally, the breakdown of the Born-Oppenheimer approximation, which was mentioned in several studies^[129,131,132], can be refuted by the accurate MR-DMC results.

6.1.2 CoH

In the previous section, the absolute as well as bond dissociation energies of FeH were thoroughly discussed and it was established that the best results were obtained for MR-DMC using fully (Jas+MO+CI) optimized Slater-Jastrow wave functions with initial full valence CAS orbitals. This is corroborated by previous studies. [105,125] In the following sections, the evaluation will, therefore, be limited to the discussion of the dissociation energies computed for the fully optimized multi-reference guide functions, unless a novel approach was tried. The energies for CoH, as well as for the respective atomic species, are listed in appendix D.

Xu *et al.*^[113] included CoH in their database because a previous study^[142] reported large discrepancies for the dissociation energy of CoH, computed using a variety of DFT exchange-correlation functionals, compared to the experiment. This motivates the investigation of CoH with MR-DMC. Additionally, CoH is an interesting system, especially for astrophysicists, due to its expected presence in stars and the interstellar medium.^[143,144]

The electronic ground state of CoH was determined to be ${}^3\Phi^{[133]}$ and its first electronic spectrum was recorded by Heimer^[145] as early as 1937.

The potential energy curve of CoH, see appendix D, was computed at the MR-DMC level using a fixed time step of $\tau = 0.001$ a.u. with the Morse fit providing an equilibrium bond distance of 1.514 Å and a ZPE of 0.120(11) eV. The CV correlation contribution corresponds to 0.0729 eV, while the first-order SO correction of CoH, taken from Ref. 113 and estimated at the CASSCF level, amounts to -0.091 eV.

Tab. 6.4 compares the MR-DMC dissociation energy of CoH to experimentally and theoretically available data from the literature. Firstly, all of the results reported are substantially larger than the dissociation energy of Kickel and Armentrout^[146], obtained from guided-ion mass spectrometric experiments. This bond dissociation energy corresponds to a weighted average of dissociation energies, evaluated for various hy-

Tab. 6.4: Calculated and measured bond dissociation energies (in eV) for CoH. The D_0 data refers to values obtained for 0 K.

Investigators	Method	$D_{\mathbf{e}}$	D_0
This work	MR-DMC/BFD-VTZ (SO+CV)	2.31(2)	2.19(2)
Kickel and Armentrout ^[146]	Mass Spectrometry		1.95(5) ^a
Cheng et al. ^[114]	$CCSD(T)/CBS+\Delta T+\Delta Q+\Delta CV+\Delta SO^b$ Revised H abstraction reactions ^c	2.40 2.23(13)	2.11(13)
Fang <i>et al.</i> ^[119]	CCSD(T)/PW91 Revised H abstraction reactions ^c	2.32 2.19(13)	
Aoto <i>et al.</i> ^[115]	CCSD(T)(CV)/CBS+ΔDK	2.30 ^d	
Xu et al. ^[113]	CCSDT(2) _Q /apTZ-DK(3)-CV(3-DK)'e DFT/B97-1-DK DFT/M06-L-DK	2.19 2.46 2.88	
Shee <i>et al.</i> ^[139]	ph-AFQMC/CCcbs	2.39(4)	

^a Weighted average, see text.

drogen abstraction reactions (see previous section) using ethane, propane, isobutane, cyclopropane, and silane. The authors of this work argue that the presence of competition reactions would provide dissociation energies that are too low. In the same study, they determined the dissociation energy of CoH by means of the reaction of Co^+ with silane, where such competition reactions are suppressed, and reported a value of $D_0 = 2.05(4)$ eV, which is much closer to the theoretical ones. The revised dissociation energies from Cheng $et~al.^{[114]}$ and Fang $et~al.^{[119]}$ are in good agreement. However, since the uncertainties of the data are rather large, the need for accurate experimental data persists. The different CC results are spread over a sizeable range of 0.2 eV, with the dissociation energy from Aoto $et~al.^{[115]}$ being closest to the MR-DMC one from this work. DFT yields dissociation energies that are—as was the case for FeH—larger than the CC and the MR-DMC ones. Finally, the ph-AFQMC dissociation energy of Shee $et~al.^{[139]}$, extrapolated to the basis set limit based on CCSD(T) calculations from Aoto $et~al.^{[115]}$, agrees well with the one computed in this work.

^b See Table 2 in Ref. 114. Value corresponds to cal $-\Delta_{geo}$.

^c See discussion of FeH.

^d Best estimate value.

^e From Table 10 of Ref. 113.

6.2 With First-Row Elements

6.2.1 NiC

Transition metal carbides are of great interest in different areas of research, ranging from heterogeneous and homogeneous catalysis^[147–150] to astrophysics^[151]. The transition metal-carbon bond plays an important role in catalysis since it is often formed and broken during a catalytic cycle, justifying the need for highly accurate bond dissociation energies. In this work, NiC and FeC are investigated.

The $^{1}\Sigma^{+}$ ground state of NiC has been confirmed theoretically and experimentally. [151–153] The electronic valence configuration of NiC corresponds to $\delta^{4}\sigma^{2}\pi^{4}\sigma^{2}$. The equilibrium bond distance is obtained via a potential energy curve (see appendix D), computed at the MR-DMC level with a fixed time step of $\tau=0.001$ a.u., and amounts to 1.633 Å.

The bond dissociation energy of NiC was evaluated for different ansatzes. Let us start by discussing the absolute energies of NiC, see Tab. 6.5. The CAS(12,9) approach corresponds to the full valence active space which is constructed from the 4s and 3d orbitals of the nickel atom and the 2p ones of the carbon counterpart. Both, the VMC and DMC energies are substantially lower (about $0.8 E_h$) for the HF pseudopotentials from Burkatzki, Filippi, and Dolg compared to the ones for the ccECPs. For the DMC energies, the fixed-node, the ECP localization, as well as the ECP model error remain. As for the former two sources of error, they can be reduced by the use of accurate trial wave functions.^[154] The ECP model error—always present if the actual core electrons are replaced by potentials—is much harder to assess and might be the reason for the difference in the energies. Additionally, the two types of ECPs are—for their construction—fitted to different parameters which could explain the energy discrepancies. The ccECPs from Mitas and co-workers are for example fitted to excitation energies and do not take into account absolute energies. [101] The BFD ECPs, on the other hand, are constructed using absolute (valence) energies of various excited configurations.[97]

For the CAS(14,10) ansatz, the active space has been enlarged by the 2s orbital of the carbon atom. Due to the "missing" 1p orbitals, the 2s and 2p orbitals are close in energy since the 2p electrons experience less shielding from the core. The 2s electrons are therefore estimated to provide a non-negligible contribution to the correlation energy.

The enlargement of the active space yields a lower VMC energy as well as an improved nodal surface for NiC. The energies for the atomic species are listed in appendix D.

Tab. 6.5: NiC VMC and DMC energies in E_h at the Jas+MO+CI optimization level, using different ECPs and an sm666 Jastrow factor.

Ansatz	ECP	VMC energy	DMC energy
CAS(12,9)	BFD-VTZ ccECP	-175.6200(5) -174.8014(5)	-175.6912(5) -174.8775(5)
CAS(14,10)	BFD-VTZ	-175.6267(5)	-175.6960(5)

The CV correlation contribution of NiC amounts to 0.126 eV^[23], while its first-order SO correction is equal to zero due to the $^{1}\Sigma^{+}$ ground state. The ZPE is obtained from the Morse fit and corresponds to 0.0532(7) eV. The bond dissociation energies of NiC—computed for the different approaches—are displayed in Tab. 6.6, together with data from the literature. First, the comparison between the MR-DMC dissociation energies shows that, for the CAS(12,9) approach, both ECPs provide similar results, although the absolute energies deviated considerably. Going beyond the full valence active space—with the CAS(14,10) ansatz—leads only to a slight increase in the dissociation energy.

Michael D. Morse and his research group have been able, over the past years, to provide highly accurate dissociation energies for metal diatomics as well as for various transition metal dimers by means of predissociation measurements. [155–161] With this technique [161], they derive bond dissociation energies that are an order of magnitude more precise compared to the ones from established methods, such as Knudsen effusion measurements, with the uncertainty being well below the threshold of "chemical accuracy" (1 kcal/mol \approx 0.04 eV). The key of this technique lies within the high density of electronic states for open d shell comprising compounds, resulting in a rapid predissociation as soon as the ground-separated atom limit is energetically exceeded (through excitation). An upper bound for the dissociation energy can be determined from the R2PI spectrum, as a sharp drop in signal (predissociation threshold) occurs once the dissociation limit is exceeded. The predissociation threshold is, however, not only an upper limit, it was shown to also be a very accurate measure of the dissociation energy itself. [161]

Tab. 6.6 illustrates that the MR-DMC bond dissociation energies underestimate the one from Morse and co-workers^[158] by about 0.2 eV. By adding the CV correlation contribution to the dissociation energy computed with the ccECP, one obtains a value of 4.05(2) eV, which is much closer to the experimental one. However, since the ccECP al-

ready accounts for parts of the CV correlation, it remains questionable whether adding this quantity to the dissociation energy is sensible. This will be discussed in more detail below, within the framework of the bond dissociation energy of FeO. Since the ccECP accounts—in contrast to the BFD one-for the core-core correlation and both types of pseudopotentials yield similar results, this contribution can thus not explain the deviation from the experiment. The fixed-node as well as the ECP localization errors are reduced since fully optimized wave functions with large Jastrow factors are employed. It has been shown^[52,92,162] that the localization error of the pseudopotential is smaller than the fixed-node error, especially when small core ECPs are used. The model error of the pseudopotential, judged to be much smaller than 0.2 eV, cannot justify the discrepancy. It is therefore much more probable that the large deviation to the experiment can be traced back to the chosen ansatz (CAS initial wave function) not being suitable. To further investigate this and analyze which orbitals should be included (beyond full valence) in the active space, an AUTOCAS^[8,163,164] calculation, which is based on the density matrix renormalization group (DMRG), was performed in order to evaluate which orbitals are entangled. The entanglement measure is entropy-based and the threshold, indicating which orbitals should be included in the active space, is determined by means of the single-orbital entropy.^[163] The AUTOCAS calculation was performed using the ANO-RCC-VTZP^[165,166] basis set. All virtual orbitals (of an initial HF calculation) were included in the DMRG calculation. The entanglement analysis suggests an active space with seven orbitals, which is smaller than the full valence equivalent, leaving out the two δ orbitals, arising from the d_{xy} and $d_{x^2-y^2}$ atomic orbitals of Ni, respectively. This indicates that an accurate description of NiC necessitates excited configurations which include many different virtual orbitals, rather than only the ones generated from a small active space. Later in this work, in chapter 7, we will see that employing initial sCI wave functions can provide more accurate results compared to initial CAS ones.

The MR-DMC dissociation energies agree well with the MRCI ones from Lau *et al.*^[167] and from Tzeli and Mavridis^[168]. The MRCI calculation (based on CASSCF) from Borin and de Macedo^[169] provides a bond dissociation energy that is more than 1 eV below the experiment. The DFT data are spread over a very broad range and either substantially over- or underestimate the bond dissociation energy of NiC. Further research is therefore needed to develop exchange-correlation functionals that are suitable to properly describe transition metal compounds. The CC energy shows the best agreement with the experimental value of Matthew *et al.*^[158] and it is similar to the MR-DMC/ccECP one with added CV correlation (4.05(2) eV).

Tab. 6.6: Calculated and measured bond dissociation energies (in eV) for NiC. The D_0 data refers to values obtained for 0 K.

Investigators	Method	De	D_0
This work	MR-DMC/CAS(12,9)/BFD-VTZ (SO+CV)	3.96(2)	3.91(2)
This work	MR-DMC/CAS(14,10)/BFD-VTZ (SO+CV)	4.00(2)	3.95(2)
This work	MR-DMC/CAS(12,9)/ccECP-aug-cc-pVTZ (SO)	3.97(2)	3.92(2)
Matthew et al.[158]	Predissociation threshold (R2PI)		4.167(3)
Brugh and Morse ^[153]	Lack of predissociation (R2PI)		\geq 3.34
Brugh and Morse data ^[153]	Morse potential extrapolation		4.357
	DFT/BMK:DKH		5.59
Goel and Masunov ^[170]	DFT/M05:DKH		5.20
	DFT/M05-2x:DKH		2.73
Borin and de Macedo ^[169]	MRCI-CASSCF		2.98
Lau <i>et al.</i> ^[167]	MRCI+Q/cc-pV5Z-DK		3.91
Lau et at. 1-2-1	CCSDTQ(Full)/CBS-DK		4.048
Tzeli and Mavridis ^[168]	C-MRCI+DKH2+Q/C5Z 4.08 3.9		3.95

6.2.2 FeC

Similar to NiC, the electronic spectroscopy of FeC has interested researchers for many years^[171–173], with the first gas phase spectrum being reported by Balfour *et al.*^[174] in 1995.

The established electronic ground state of FeC corresponds to a $^3\Delta$ term symbol [175,176], with the configuration of the valence electrons being $\sigma^2\pi^4\delta^3\sigma^1$.

The equilibrium bond distance used for the calculations was determined by Balfour et al.^[174] via laser-induced fluorescence spectroscopy and corresponds to 1.596 Å. The CV correlation contribution and the first-order SO correction of FeC amount to 0.176 eV^[23] and -0.0206(2) eV, respectively. The latter quantity is taken from Ref. 177. The ZPE equals 0.0535 eV and is derived from the work of Aiuchi et al.^[178] The energies for FeC, as well as for the respective atomic species, are listed in appendix D.

Experimental as well as theoretical bond dissociation energies for FeC are given in Tab. 6.7. The uncertainty of the dissociation energy from Matthew *et al.*, determined via a predissociation threshold, is one order of magnitude larger compared to one of NiC, which the authors trace back to the sparsity of the FeC spectrum.^[158] The experi-

mental result $D_0 = 3.8(3)$ eV derived using data from Chang $et~al.^{[176]}$ as well as from Hettich and Freiser^[179] has a relatively large uncertainty but is in agreement with the R2PI one. The MR-DMC dissociation energy agrees well with the experimental value from Chang $et~al.^{[176]}$ However, as was the case for NiC, it is substantially lower than the dissociation energy determined by Matthew $et~al.^{[158]}$ Trying out similar approaches to NiC in order to improve the dissociation energy was dispensed with for FeC since the calculations (especially the optimizations) for this one approach already proved rather cumbersome due to the large number of CSFs. This is also the reason why the potential energy curve was not computed at the MR-DMC level of theory. The MRCI and CC bond dissociation energies agree well with the MR-DMC one, while the DFT calculations by Goel and Masunov^[170] yield dissociation energies that underestimate, both, the experimentally and theoretically available data.

Tab. 6.7: Calculated and measured bond dissociation energies (in eV) for FeC. The D_0 data refers to values obtained for 0 K.

Investigators	Method	D_{e}	D_0
This work	MR-DMC/BFD-VTZ (SO+CV)	3.81(2)	3.75(2)
Matthew <i>et al.</i> ^[158] Chang <i>et al.</i> ^[176]	Predissociation threshold (R2PI) $D_0(\text{Fe}^+\text{-C})\text{+IE}(\text{FeC})\text{-IE}(\text{Fe})^a$		3.961(19) 3.8(3)
Tzeli and Mavridis ^[180] Lau <i>et al.</i> ^[181] Tzeli and Mavridis ^[182]	MRCI CCSDTQ(Full)/CBS C-MRCI+DKH8+Q	3.87	3.705 3.778 3.81
Goel and Masunov ^[170]	DFT/M05:DKH DFT/M05-2x:DKH		3.45 2.06

^a The $D_0(\text{Fe}^+\text{-C})$ value is taken from Ref. 179

6.2.3 FeO

Iron oxides constitute highly tunable systems property-wise and are, therefore, interesting for a wide variety of applications, ranging from catalysis^[183,184], over batteries^[185–187] to photovoltaics^[188,189].

The ground state of FeO was confirmed to be $^5\Delta$ —corresponding to an electronic configuration of $\sigma^2\pi^4\sigma^2\delta^3\sigma^1\pi^2$ —by means of laser-induced fluorescence^[190] as well as

through anion-zero kinetic energy photoelectron (anion-ZEKE) spectroscopy^[191].

The equilibrium bond distance $r_{\rm e}=1.623$ Å and the ZPE of 0.0537 eV were derived from a Morse fit to an MR-DMC potential energy curve, computed for fully optimized guide functions, see Ref. 105. The first-order SO correction of FeO (-0.0558 eV), as well as the CV correlation contribution (0.126 eV), are taken from this study, which was mostly performed by this author^[105], as well. The energies for FeO, as well as for the respective atomic species, are listed in appendix D.

Tab. 6.8 summarizes theoretically and experimentally availably bond dissociation energies for FeO. The experimental data are in excellent agreement among themselves. Let us first compare the dissociation energy from this work with the MR-DMC one from Ludovicy et al.[105] Employing a ccECP provides a slightly lower dissociation energy compared to the one obtained using a BFD pseudopotential, the latter yielding an energy that agrees better with the experiment. By adding the CV correlation to the MR-DMC dissociation energy from this study, it is increased to $D_0 = 4.15(2)$ eV which agrees very well with the experiment. However, as for NiC, the question remains whether the CV correlation contribution can—in case of the ccECP—be seen as an additive quantity that can be included in the dissociation energy. It is difficult to quantify how much of the CV correlation is accounted for by the ccECP. In their work, Mitas and co-workers^[101] compare valence properties (atomic and ionic excitations) computed with their ccECPs to the ones obtained for all-electron calculations with uncorrelated cores. Finding a higher (or equal) accuracy for the properties when the ccECPs are employed, they argue that some of the core-core and core-valence correlation effects are captured. If one were to argue that most of the correlation accounted for by the ccECPs can be traced back to the core-core correlation effects, adding the CV contribution to the bond dissociation energy would be justifiable.

In their work, Krogel *et al.*^[192] employed Slater-Jastrow wave functions with LDA* orbitals (from periodic DFT calculations) and neon-core pseudopotentials. Their DMC calculations were performed within the T move approach. The DMC dissociation energy that they report slightly overestimates the experimental ones. The CC bond dissociation energy from Aoto *et al.*^[115] is in good agreement with the MR-DMC/BFD one, while it is 0.1 eV larger than the MR-DMC/ccECP counterpart. Surprisingly, the MRCI result, computed by Sakellaris *et al.*^[193], is substantially lower than the experimental one. The authors reported numerous MRCI dissociation energies with various correc-

^{*}local density approximation

tions, ranging from relativistic effects (DKH2), over core correlation effects (C) to the Davidson correction (Q). For their MRCI calculations, based on CASSCF calculations, they also varied the reference spaces, including e.g. the 4*p* orbitals for Fe. All of the dissociation energies that they computed underestimate the experiment. It should be noted, that the authors also presented bond distances for the individual approaches, all of which are smaller than the experimental one as well. As has been observed for the other transition metal dimers, DFT cannot reproduce the dissociation energy of FeO.

Tab. 6.8: Calculated and measured bond dissociation energies (in eV) for FeO. The D_0 data refers to values obtained for 0 K.

Investigators	Method	D_{e}	D_0
This work	MR-DMC/ccECP-aug-cc-pVTZ (SO)	4.08(2)	4.02(2)
Chestakov et al.[194]	Velocity map imaging		4.18(1)
Li et al. ^[195]	Collision-induced dissociation		4.18(1)
Smoes and Drowart ^[196]	Mass spectrometry		4.16(8)
Ludovicy et al.[105]	MR-DMC/BFD-VTZ(SO+CV)	4.17(2)	4.11(2)
Krogel et al. ^[192]	DMC	4.25(1)	
Aoto <i>et al.</i> ^[115]	$CCSD(T)(CV)/CBS+\Delta DK$	4.21 ^a	
Sakellaris <i>et al.</i> ^[193]	C-MRCI+DKH2+Q	3.72	
	DFT/B3LYP		3.96
Jensen <i>et al.</i> ^[137]	DFT/BP86		5.21
	DFT/PBE		5.31

^a Best estimate value.

6.3 With Second-Row Elements

6.3.1 CrS

Chromium sulfide compounds have recently gained interest, especially in electrochemistry. ^[197,198] The isovalence of transition metal sulfides to their oxide counterparts, which are known to be present e.g. in M-type stars, makes them also highly interesting for astronomers. ^[199]

In 2011, Petz and Lüchow^[121] investigated transition metal sulfides with single-reference DMC. The largest deviations were found for FeS and CrS. Since then, FeS has been successfully revisited by means of MR-DMC.^[125] In this work, CrS will, therefore, also be re-examined with MR-DMC.

The ${}^5\Pi$ ground state^[200] of CrS is described by the valence electron configuration $\sigma^2\pi^4\sigma^1\delta^2\pi^1$. The calculations for CrS were performed with the experimental bond length of 2.0781 Å, as determined by Pulliam and Ziurys.^[200] The first-order SO correction for CrS is taken from the same study^[200] and amounts to -0.0118(5) eV. The CV correlation contribution corresponds to 0.00515 eV. The ZPE—amounting to 0.02913(7) eV—is derived from the vibrational frequency reported in a very recent study^[201], the authors of which investigated CrS by means of laser-induced fluorescence spectroscopy. The energies for CrS, as well as for the respective atomic species, are listed in appendix D.

A slightly modified initial wave function compared to the usual CAS ansatz is chosen for the CrS system due to the inability to converge the MO parameters with QMC when starting from orbitals generated by a CASSCF(10,9) calculation. The active orbitals of the CAS wave function are further relaxed by performing a restricted active space selfconsistent field (RASSCF) calculation with single and double excitations into a set of virtual orbitals. The original CAS(10,9) corresponds to the RAS2, where all possible excitations are performed while a RAS3 with 11 virtual orbitals is created for the single and double excitations from the RAS2. The RAS1 remains empty. The RASSCF calculation will henceforth be referred to as RAS(10,9;2,11). This approach aims at obtaining better initial orbitals that can then be further optimized in a QMC energy minimization calculation. The CAS (=RAS2) orbitals are optimized in the partial presence of dynamic correlation through excitations to the RAS3. The RAS2 orbitals are hence expected to be closer to the converged orbitals in a full multi-reference VMC optimization. The CAS for the QMC calculations is, however, built similarly to the one of the other compounds, namely from the 4s and the 3d orbitals of chromium, and from the 3p orbitals of sulfur.

The dissociation energies of CrS for the different approaches are listed in Tab. 6.9. Similar to the other compounds, see also Refs. 125 and 105, a systematic improvement of the dissociation energy can be observed for the different methods and optimization levels. The KS nodes appear ideal since the MO optimization does not improve the dissociation energy. The ansatz with CAS orbitals yields a lower dissociation energy

compared to the one obtained with KS orbitals at the same optimization level. Relaxing the initial active orbitals through a RAS(10,9;2,11) calculation has a substantial effect on the dissociation energy. Not only are the dissociation energies significantly improved when comparing them to the ones obtained with CAS initial orbitals but, more importantly, the molecular orbital parameters could be successfully optimized with VMC. At a given optimization level, the dissociation energies for the different CAS guide functions differ by about 0.3 eV. When further optimizing the orbitals, initially taken from the RASSCF calculation, the dissociation energy can be improved by 0.05 eV. The RAS ansatz, presented here, nicely shows the potential of this approach. However, it should not be considered as a replacement for the traditional CAS approach, since the excitation into 11 orbitals is rather arbitrary and would become even more so for the computation of larger systems. What one should take away from these results is the importance of going beyond a full valence CAS approach for the generation of the initial wave functions.

Tab. 6.9: DMC dissociation energies of CrS in eV at various optimization levels, using different starting orbitals and BFD-VTZ/sm666. The energies are CV and SO corrected.

Ansatz	Orbitals	Optimization level	D_0
	HF	Jas	2.05(2)
Single det	B3LYP	Jas	2.77(2)
_	opt	Jas+MO	2.77(2)
	CAS	Jas	2.43(2) ^a
	CAS	Jas+CI	$2.70(2)^{a}$
CAS	RAS2	Jas	2.80(2)
	RAS2	Jas+CI	3.04(2)
	opt	Jas+MO+CI	$3.10(2)^{b}$

^a Taken from Ref. 105.

Tab. 6.10 yields experimental and theoretical dissociation energies for CrS. With the ansatz chosen here, the dissociation energy of CrS is improved by 0.1 eV compared to the single-determinant DMC counterpart from Petz and Lüchow^[121]. The MR-DMC dissociation energy is larger than the CCSD(T)^[202] value, but it is still smaller than the experimental D_0 of Drowart *et al.*^[203] Assessing the accuracy of the MR-DMC result proves challenging due to the large experimental error bar. Our dissociation energy is about 0.1 eV below the lower bound of Drowart and co-workers. In order to estimate

^b Taken from Ref. 23.

the accuracy of the obtained MR-DMC result, experimental data with smaller uncertainties are needed. Finally, the DFT dissociation energy is in excellent agreement with the experiment. However, due to the poor performance of DFT for all other transition metal compounds discussed in this work, this agreement should be considered with care.

Tab. 6.10: Calculated and measured bond dissociation energies (in eV) for CrS. The D_0 data refers to values obtained for 0 K.

Investigators	Method	D_0
This work	MR-DMC/BFD-VTZ (SO+CV)	3.10(2)
Drowart et al. ^[203]	Mass Spectrometry	3.36(15)
Petz and Lüchow ^[121]	DMC/PPII	2.969(9)
Bauschlicher and Maitre ^[202]	CCSD(T)	2.89
Liang and Andrews ^[204]	DFT/BPW91	3.33

6.3.2 NiSi

Doped silicon materials play an important role in modern electronic devices and the precise understanding of the transition metal-silicon bond becomes essential, especially as an ever-present goal is to reduce the device size to a minimum.^[205]

The ground state of NiSi has been established to be of $^1\Sigma^+$ symmetry. [206] The equilibrium bond distance and the ZPE are derived from the potential energy curve, recorded at MR-DMC level using a fixed time step of $\tau=0.001$ a.u., see appendix D, by means of a Morse fit and correspond to 2.051 Å and 0.0274(87) eV, respectively. The accurate computation of the potential energy curve, see next section, shows that MR-DMC is also applicable to compounds involving second-row elements, although the computational expenditure is more involved. The MR-DMC approach has also been successfully applied to FeS in a previous study. [125] The first-order SO correction of NiSi is zero due to the Σ symmetry of the ground state. The energies for NiSi, as well as for the respective atomic species, are listed in appendix D.

NiSi is valence iso-electronic to NiC. Computing the potential energy curve of NiSi proved, however, much more elaborate since silicon is a second-row element. A neon-core pseudopotential was employed for Si for all the calculations. The computation

of NiSi being considerably more expensive than the one of NiC, although the same number of electrons are involved, bears witness to the substantial effort needed for the localization of the ECP. The neon core of the Si pseudopotential means that an additional non-local channel (for the 2*p* electrons) needs to be considered in contrast to the helium-core ECP of the carbon atom.

The CV correlation contribution of NiSi, computed at the complete active space secondorder perturbation theory (CASPT2) level, amounts to 0.905 eV, which is notably large and implies that the 3s and 3p electrons probably contribute greatly to the dissociation energy. This sizable value of the correlation contribution could be attributed to the large core ECP for the Si atom: by removing the 2s and 2p electrons, only four electrons remain, implying that the core is polarizable and thus cannot be well described by a rigid, spherical pseudopotential. As we will see below, this is also mirrored by the bond dissociation energy.

Tab. 6.11: Calculated and measured bond dissociation energies (in eV) for NiSi. The D_0 data refers to values obtained for 0 K.

Investigators	Method	De	D_0
This work	MR-DMC/BFD-VTZ (SO+CV)	3.81(2)	3.78(2)
This work	MR-DMC/BFD-VTZ (SO)	2.90(2)	2.88(2)
This work	MR-DMC/ccECP-aug-cc-pVTZ (SO)	3.15(2)	3.12(2)
Sevy et al. [159]	Predissociation threshold (R2PI)		3.324(3)
Vander Auwera-Mahieu et al. ^[207]	Mass spectrometry		3.26(18)
Lindholm <i>et al.</i> ^[206]	Morse potential extrapolation ^a	3.31	
Linanoim et ul. [===]	DFT/B3P86	2.49	
Wu and Su ^[208]	DFT/B3LYP	2.33	
Shim and Gingerich ^[209]	CASSCF	2.35	
Schoendorff et al. ^[210]	CCSD(T)	1.96 ^b	
Schoendorii et al. []	$CCSD(2)_T$	3.33 ^b	

^a Obtained from dispersed fluorescence spectroscopy measurements.

Tab. 6.11 summarizes the bond dissociation energies for NiSi computed in this work, together with experimentally and theoretically available data. First of all, the MR-DMC dissociation energies are spread rather widely. Without the CV contribution, the exper-

^b all correlated value from Table 3 in Ref. 210.

imental dissociation energy of Sevy *et al.*^[159] is severely underestimated if the BFD ECP is used. Adding the core-valence correlation results in an overestimation of the experimental dissociation energy. As mentioned above, the neon-core pseudopotential, or at least the one derived from HF calculations, is probably not suitable for silicon, since it cannot accurately describe the polarization of the core, arising from the formation of a bond. With the neon-core correlation-consistent pseudopotential (ccECP), the dissociation energy is substantially improved, although is is still 0.2 eV below the experiment. One approach to further improve the results would be to employ a helium-core ECP for Si, which entails, however, a substantial increase in computational cost. An alternative involves the use of core-polarization potentials (CPPs)—which characterize core-valence correlation effects—together with pseudopotentials, as e.g. described for Si by Lee and Needs.^[211]

In a previous study^[125], the same approach (MR-DMC with the BFD ECP) was employed to FeS and an excellent dissociation energy was reported, the difference between S and Si being that the latter has only four valence electrons while the former has six. Sulfur can thus, in contrast to silicon, be accurately described by a neon-core pseudopotential, its core being less polarizable.

The bond dissociation energy from Vander Auwera-Mahieu *et al.*^[207], derived from mass spectrometry in 1969, agrees with the R2PI one, its uncertainty is, however, very large. The CASSCF and DFT dissociation energies underestimate the experimental one from Sevy *et al.* by up to 1 eV. The data of Schoendorff *et al.*^[210] shows that one needs a perturbative second-order correction to CCSD in order to reproduce the experimental dissociation energy. Finally, the bond dissociation energy of NiSi, obtained from a Morse potential extrapolation^[206], agrees well with the experiment.

6.4 Spectroscopic Constants

The potential energy curves of FeH, CoH, NiC, and NiSi were computed at the MR-DMC level—using fully optimized guide functions—and fitted to a Morse potential function^[134] from which spectroscopic constants, such as the equilibrium bond distance (minimum of the Morse curve), the harmonic frequency, as well as the anharmonicity could be deduced. The evaluation of those constants allows a further assessment of the accuracy of the employed method. Tab. 6.12 illustrates the obtained quantities and

compares them for different theoretical and experimental methods.

Tab. 6.12: Spectroscopic constants for the different transition metal compounds. The equilibrium bond distance is given in Å, the harmonic frequency ω_e and the anharmonicity $\omega_e x_e$ in cm⁻¹.

System	Investigators	Method	r_e	$\omega_{ m e}$	$\omega_{\mathrm{e}}x_{\mathrm{e}}$
	This work	MR-DMC/BFD-VTZ	1.567	1842(27)	38.9(9)
FeH	Philips et al. ^[212]	Near IR Spectrum		1826.86	31.96
геп	Dulick et al. ^[213]	MRCI-CASSCF		1831.8(19)	34.9(9)
	DeYonker and Allen ^[138]	CCSDT	1.5660	1798.8	37.8
	Jensen et al. ^[137]	DFT/B3LYP	1.57		
	This work	MR-DMC/BFD-VTZ	1.514	1932(92)	43(3)
	Beaton et al. ^[143]	Far-infrared laser magnetic resonance	1.5138		
СоН	Lipus at al. ^[214]	Laser magnetic resonance spectroscopy		1926.7487(4)	34.6
	Gordon et al. ^[215]	Near-infrared emission spectrum	1.5327	1924.5256(21)	
	Cheng et al.[114]	SFX2C-1e-CCSD(T)/aug-cc-pwCVQZ	1.502		
	This work	MR-DMC/BFD-VTZ	1.633	858(6)	5.20(5)
	Brugh and Morse ^[153]	R2PI spectroscopy	1.6273	875.155	5.38
NiC	Brewster and Ziurys ^[151]	Millimeter-wave spectrum	1.6308a		
		C-MRCI+DKH2/C5Z	1.621	916.1	
	Tzeli and Mavridis ^[168]	RCCSD(T)/5Z	1.634	851	
		CASSCF/5Z	1.658	796.4	
	This work	MR-DMC/BFD-VTZ	2.051	441(70)	2.1(5)
	Lindle along at -1 [206]	R2PI & fluorescence spectroscopy	2.0316(4)a	467.43(30)	2.046(21)
NiSi	Lindholm et al. ^[206]	DFT/B3P86	2.004	512.21	
	Wu and Su ^[208]	DFT/B3LYP	2.015	500	
	Schoendorff et al.[210]	$CCSD(2)_T$	2.059	418	

^a r_0 value.

For FeH, the MR-DMC bond distance and harmonic frequency are in excellent agreement with the theoretical and—where available—experimental results. The anharmonicity, computed in this work, agrees well with the CC one, it is, however, slightly larger than the experimental one from Philips *et al.*^[212]

The MR-DMC equilibrium bond length of CoH agrees well with the experimental value of Beaton $et\ al.^{[143]}$, while it is lower than the one obtained from near-infrared emission spectra^[215]. The CC^[114] bond distance of $r_e=1.502$ Å is 0.01 Å smaller than the one computed in this work. The harmonic frequency, deduced from the MR-DMC potential energy curve, is in good agreement with the experimental counterparts, while the anharmonicity is slightly overestimated compared to the one from laser magnetic resonance spectroscopy^[214].

All three MR-DMC quantities for NiC are in satisfying agreement with the data from Brugh and Morse^[153], measured by means of R2PI spectroscopy. The theoretically determined bond lengths and harmonic frequencies from Tzeli and Mavridis^[168], computed for various methods, are widely spread. The MR-DMC results agree best with the CC ones.

As for NiSi, the harmonic frequency and the anharmonicity at MR-DMC level show the highest uncertainties among all four compounds, which can be attributed to only five (in contrast to seven or eight) bond distances being chosen for the computation of the potential energy curve due to the enhanced expenditure of the calculations. Nonetheless, these quantities agree well with the experimental ones obtained from dispersed fluorescence measurements^[206]. The MR-DMC harmonic frequency is also in good agreement—mostly due to its large uncertainty—with the DFT and CC ones. Finally, the MR-DMC equilibrium bond length of NiSi is larger than the experimental and DFT counterparts. It agrees, however, well with the CC bond distance reported by Schoendorff *et al.*^[210]

All in all, these results show that the MR-DMC approach is able to accurately describe different properties of transition metal compounds.

6.5 Computational Approach

Some insight on the problems, more precisely on the handling of the symmetry, that arise for the computation of diatomic systems is given in appendix C. The trial wave functions were generated with the MOLPRO^[216] package. The initial wave functions were obtained from *ab initio* calculations, namely HF, KS DFT (using the B3LYP^[34–36] functional with the VWN(III)^[217] local correlation energy), and CASSCF. The active

space for the latter included the 4s and 3d orbitals of the metals and the valence p orbitals of the main group elements (1s for H). The QMC calculations were performed with the program AMOLQC^[67], developed in our group. A 69-term Jastrow correlation function (denoted as sm666 in ref. 60) with cusp-less three-particle terms was used for all the calculations.^[59] The wave function parameters—Jastrow, MO, and CI—were optimized with VMC in order to minimize the variational energy. If more than one set of parameters was optimized, the optimization was performed in an alternating way, which was found to be more effective when pseudopotentials are used.^[78] The optimized wave functions were then used as guide functions for the DMC calculations, performed for different time steps. The extrapolation to a zero time step was performed using a quadratic model.^[218]

All calculations were performed using either the ECPs of Burkatzki, Filippi, and Dolg^[97,98] with the respective triple- ζ basis sets, referred to as BFD-VTZ, or using the correlation-consistent ECPs by Mitas and co-workers^[99,100], denoted as ccECP, with the corresponding aug-cc-pVTZ basis. The non-local part of the pseudopotentials was localized in QMC on a spherical grid using the trial wave function.^[88,219] Neon-core ECPs were used for the second-row elements.

The dissociation energies were first-order spin-orbit corrected, and the core-valence correlation contribution was added. The first-order SO corrections for the atoms were derived from experimental splittings. The ones for the molecules were taken from the literature. The CV correlation contribution was estimated either by means of multi-reference second-order perturbation theory (MRMP2), as implemented in GAMESS, or with CASPT2 using MOLPRO. The core-valence basis set TK+NOSeC-V-QZP with all diffuse functions was used for these calculations. By calculating the dissociation energy with and without correlating the core electrons, one can determine the CV correlation contribution. The same active spaces as for the QMC calculations were chosen. The ZPEs of the compounds, for which a MR-DMC potential energy curve was recorded, were derived from the Morse fit. For all other compounds, the ZPEs were taken from the literature.

7 Selected Configuration Interaction

"MY METHODS ARE REALLY METHODS OF WORKING AND THINKING; THIS IS WHY THEY HAVE CREPT IN EVERYWHERE ANONYMOUSLY." – *Emmy Noether*

Parts of this chapter are published in a condensed form in Ref. 224.

Reprinted (adapted) with permission from J. Ludovicy, R. Dahl, A. Lüchow, Toward Compact Selected Configuration Interaction Wave Functions with Quantum Monte Carlo—A Case Study of C₂, J. Chem. Theory Comput. **2023**, 19, 2792-2803. Copyright 2023 American Chemical Society.

Since the beginning of modern quantum mechanics in the 1920s, the scope and performance of quantum chemistry have vastly grown. The progress in this field of research has been impressive which is in part due to—but not limited to—the always improving computational architecture. There are a plethora of quantum chemical methods, tailored to the careful description of various problems. A tradeoff has, however, always to be made between a satisfactory accuracy and an affordable computational expenditure with the accuracy having to inevitably be forfeited with increasing system size. Post-HF methods, such as CC and perturbation theory as well as DFT are powerful when it comes to characterizing systems with dynamic correlation but they often fail when the static correlation is non-negligible, e.g. for chemical reactions including bond breaking processes or for open shell systems with partially filled degenerate orbitals. Such multi-reference systems still pose a key challenge for quantum chemistry with intense research efforts striving toward finding a way to both accurately describe static and dynamic electron correlation. This problem is traditionally tackled by multi-reference methods, such as MRCI^[225,226], CASPT2^[227], or second-order n-electron valence state perturbation theory (NEVPT2)[228,229]. The last two methods employ multi-configurational zeroth-order wave functions and perform on top of that perturbation theory to correct for the dynamic electron correlation, arising from electronic motion. All of these methods have various drawbacks, ranging from relying on chemical intuition to choose the orbitals that need to be correlated to an exponential scaling with the number of electrons and the basis set size, as well as suffering from severe memory requirements. Although it has been shown in the previous chapter, that the MR-DMC approach using CASSCF initial wave functions is able to describe transition metal bonding very accurately, the pursuit of trying to investigate larger systems necessitates the move beyond CASSCF.

In order to circumvent the problems presented above, a different class of methods, namely the sCI approaches—initially pioneered about 50 years ago^[28,230,231]—has reexperienced an increased focus of research since the beginning of the 21st century due to the shift toward a more parallel programming regime. Some of the more recently developed sCI techniques include FCIQMC^[25], adaptive sampling CI (ASCI)^[26], and semi-stochastic heat-bath CI (SHCI)^[27]. The method of choice in this work is CIPSI which was pioneered by Malrieu and co-workers^[28,29] and later revived by Caffarel and co-workers^[232]. The combination of CIPSI wave functions together with the highly accurate QMC methods, more specifically DMC, has proven to be very promising for ground state as well as for excited state energetics.^[233–243] Additionally, the use of a Jastrow correlation function, responsible for the short-range dynamic electron correlation, within QMC has long been established. In related work, a transcorrelated Hamiltonian is employed in FCIQMC.^[49,50]

7.1 Statistical Analysis of CI Coefficients

The physical quantities that can be extracted from QMC calculations are necessarily subject to statistical noise due to the stochastic nature of these methods. By optimizing wave functions within the VMC framework, one question that comes to mind is how statistically accurate the optimized CI coefficients are. This issue will be addressed here.

The investigation was carried out for the $^{1}\Sigma_{g}^{+}$ ground state of C_{2} , using an equilibrium bond distance of 1.24 Å, as determined by Haghighi Mood^[78] from a potential energy curve computed at MR-DMC level. A CAS(8,8) calculation was performed with the Slater-type triple- ζ all-electron basis set TZPae^[244] by van Lenthe and Baerends. Each Slater-type basis function was expanded into 14 primitive Gaussian-type functions^[245,246] for the CASSCF calculation with MOLPRO^[216], resulting in an initial wave

function containing 168 CSFs. The true Slater basis was employed for the QMC calculations with AMOLQC^[67]. Three different Jastrow factors^[59], as described in Ref. 60, were appended to the initial CAS(8,8) wave function and the Jastrow and CI parameters were simultaneously optimized with respect to the variational energy. The absolute values of the CI coefficients are averaged over five calculations with varying seeds. The data is listed in full in appendix E.

In Figs. 7.1 (CSFs 1 to 25) and 7.2 (CSFs 84 to 168), the absolute values of the CI coefficients are shown for optimized Slater-Jastrow wave functions with different Jastrow factors, together with the CAS(8,8) counterpart. Only the conclusions relevant to the investigation here will be discussed since a more detailed analysis of the impact of the Jastrow correlation function on the CI coefficients is conducted below, in section 7.3.5. The CI coefficients are sorted such that the CSFs are identical for each index, see the caption of the figures.

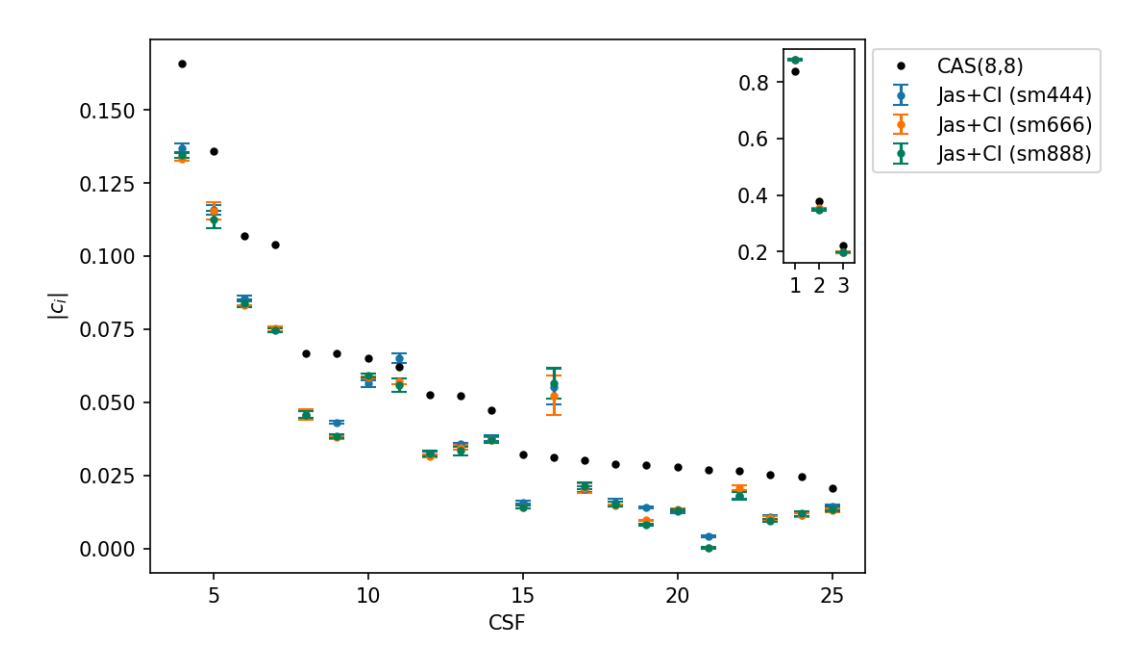


Fig. 7.1: Absolute values of the CSF coefficients for different wave functions with and without Jastrow factor. The first three coefficients are depicted in the sub-plot. The original CAS coefficients (black) are sorted from largest to smallest. For the Slater-Jastrow wave functions, the coefficients are sorted such that the CSFs are identical for each index, i.e. *x*-coordinate. The CSFs are normalized for each approach.

First of all, both figures reveal that the coefficients of the Slater-Jastrow wave functions are overall mostly lowered by the optimization which shows that the electron correlation is accounted for by the Jastrow factor rather than by the expansions themselves. Additionally, one can roughly observe that, for the individual CSFs, the coefficients are

smaller the larger the Jastrow factor is, the difference being greatest when moving from the sm444 to the sm666 Jastrow. Unsurprisingly, the CI coefficients of the first 25 CSFs can be determined very accurately up to the third (sometimes fourth) decimal place, see also Tab. 7.1.

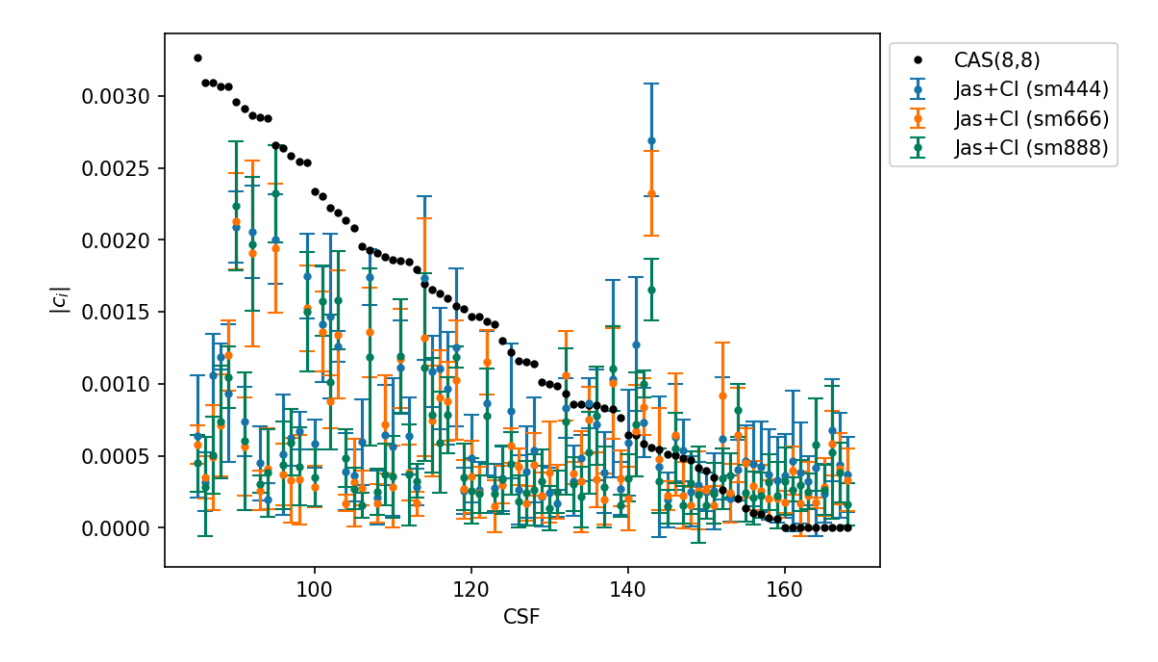


Fig. 7.2: Absolute values of the CSF coefficients for different wave functions with and without Jastrow factor. The original CAS coefficients (black) are sorted from largest to smallest. For the Slater-Jastrow wave functions, the coefficients are sorted such that the CSFs are identical for each index, i.e. *x*-coordinate. The CSFs are normalized for each approach.

For the last 84 CSFs, the picture is quite different. Although the CI coefficients of the VMC optimized wave functions are smaller than the ones of the CAS(8,8) wave function, at least until about CSF 130, they are identical—within the statistical uncertainty—for all three Jastrow factors. For approximatively the last 25 CSFs, the CI coefficients are equivalent, irrespective of the chosen approach. What is more important, however, is the fact the statistical errors of the coefficients are mostly of the same order of magnitude as their value, rendering the meaningfulness of their optimization with QMC questionable.

These findings are corroborated by Tab. 7.1, where the CI coefficients of the first ten and last five CSFs are listed, together with their respective relative errors. The sorting of the entries is equal to the one of Figs. 7.1 and 7.2. Tab. 7.1 illustrates that the absolute errors of the CI coefficients are roughly of the same order of magnitude for all (depicted) CSFs, while the relative errors tell a completely different story. From approximately CSF 60 onwards, see appendix E, the relative errors are predominately—for all three Jastrow

factors—two-digit (sometimes even three-digit), which implies that the CI coefficients, obtained from the VMC optimizations, are to some extent statistically not significant.

Tab. 7.1: Absolute values of the first ten and last five CI coefficients of Slater-Jastrow wave functions, optimized for different Jastrow factors. The relative errors of the coefficients are given as well. The Jastrow and CI parameters were simultaneously optimized with respect to the variational energy. The coefficients are sorted such that the CSFs are identical for each row. The value in parentheses indicates one standard deviation.

	sm444		sm666		sm888
$ c_i $	Relative Error [%]	$ c_i $	Relative Error [%]	$ c_i $	Relative Error [%]
0.878(2)	0.2	0.8789(9)	0.1	0.881(1)	0.1
0.350(3)	0.9	0.353(3)	0.9	0.347(3)	0.9
0.196(1)	0.6	0.197(2)	1.2	0.1972(8)	0.4
0.137(2)	1.3	0.1332(5)	0.4	0.134(1)	0.8
0.116(2)	1.4	0.116(3)	2.5	0.113(3)	2.7
0.086(1)	1.3	0.083(2)	0.2	0.084(1)	1.5
0.075(1)	1.3	0.0753(8)	1.1	0.0747(5)	0.7
0.046(1)	2.4	0.046(2)	3.9	0.046(1)	2.3
0.0432(5)	1.2	0.0381(5)	1.4	0.0385(6)	1.5
0.056(1)	2.0	0.0586(4)	0.6	0.0593(5)	0.9
:	:	:	:	:	:
0.0004(5)	114.3	0.00017(4)	21.9	0.0006(3)	55.3
0.0002(2)	85.4	0.0003(2)	71.5	0.0003(2)	67.0
0.0007(4)	52.6	0.0006(2)	38.2	0.0005(5)	87.5
0.0004(4)	93.9	0.0004(2)	60.0	0.0004(1)	53.6
0.0004(3)	70.4	0.0003(2)	65.4	0.0002(2)	88.5

One question that remains is whether it is possible to dispense with the CI optimization with VMC, if one were to reduce the CSF coefficients by a certain factor. This is, in the following, exemplarily tested for an sm444 Slater-Jastrow wave function. The coefficient ratio, obtained by dividing the absolute value of the optimized CI coefficient by the CAS(8,8) counterpart, can serve as an estimate for the multiplication factor. To make this ansatz—if successful—feasible for practical applications, the factor that is eventually used corresponds to the mean of the coefficient ratios, starting with the second CSF since the coefficient of the first one is always increased by the addition of a Jastrow factor. The ratios could not be determined for the CSFs that have a coefficient

of zero in the original CAS(8,8) wave function. The ratios of these eight CSFs were not considered for the averaging. A multiplication factor of 0.74 is obtained. For the first CSF, the ratio amounts to 1.05. The original CAS(8,8) coefficients are multiplied by the respective factors (0.74 for CSFs 2 to 168, and 1.05 for CSF 1), an sm444 Jastrow factor is added and optimized with VMC. The resulting VMC and DMC energies, see *Jas-all* (*altered coefficients*), are listed in Tab. 7.2. For the *Jas* entries, the wave function comprises the original CAS(8,8) coefficients. The DMC calculations are performed using a time step of $\tau = 0.001$ a.u. The remaining entries will be discussed below.

Tab. 7.2: VMC and DMC energies in E_h for C_2 Slater-Jastrow wave functions at different optimization levels. An sm444 Jastrow factor was used.

Optimization level	VMC energy	DMC energy
Jas+CI	-75.8567(3)	-75.9090(3)
Jas	-75.8452(3)	-75.9062(3)
Jas-all (altered coefficients) ^a	-75.8519(3)	-75.9065(3)
Jas+CI-0.03 (altered coefficients) ^{a,b}	-75.8550(3)	-75.9079(3)
Jas+CI-0.02 (altered coefficients) ^{a,c}	-75.8560(3)	-75.9083(3)

^a See text for details.

Within the VMC framework, one can see that the wave function, for which all coefficients have been altered manually (Jas-all), provides an energy that is much closer in value to the Jas+CI energy than to the Jas one which makes the approach look promising. For the much more accurate DMC technique, the picture, unfortunately, looks quite different. DMC allows for a direct assessment of the nodal surface quality of a wave function. Tab. 7.2 shows that, in contrast to VMC, by altering all the coefficients manually, one obtains a DMC energy that is similar to the one of the CAS(8,8) guide function. By optimizing the CI coefficients together with the Jastrow factor, thereby introducing the dynamic electron correlation into the nodes, the DMC energy is lowered by 3 m E_h . The nodes of a wave function being primarily determined by the CI coefficients, the poor nodal surface quality of the manually altered wave function can be attributed to the importance (magnitude of the coefficients) of the individual configu-

^b Jas+CI optimization of an initial CAS(8,8) wave function containing only CSFs with coefficients greater than 0.03). The coefficients of the remaining CSFs are multiplied by 0.74.

^c Jas+CI optimization of an initial CAS(8,8) wave function containing only CSFs with coefficients greater than 0.02. The coefficients of the remaining CSFs are multiplied by 0.74.

rations not being reduced in an equal measure, with some configurations even gaining in importance, when a Jastrow factor is introduced, see Figs. 7.1 and 7.2. Since we are usually interested in the much more accurate DMC energies, we advise against altering all coefficients manually.

To not completely abandon the approach yet, we constructed two more wave functions by truncating the initial CAS(8,8) counterpart at cut-off values—corresponding to the absolute value of the CI coefficients—of 0.02 (25 CSFs) and 0.03 (17 CSFs), respectively. For both wave functions, the Jastrow and CI parameters were simultaneously optimized with VMC. The remaining CSFs—143 for the 0.02 threshold, 151 for the 0.03 counterpart—were added to the optimized wave functions and their coefficients were multiplied by 0.74, as discussed above. Finally, the Jastrow factors of these two wave functions were re-optimized. With this approach, we aim at finding out whether it is sensible to only optimize some of the CI coefficients with QMC, thereby reducing the computation effort. And indeed, the results look promising. For the Jas+CI-0.03 wave function, a substantial lowering of both, the VMC and DMC energies, compared to the Jas-all counterpart, can be observed. As for the Jas+CI-0.02 wave function, which comprises 25 VMC optimized CI coefficients, the VMC and DMC energies are close in value to Jas+CI ones. This is remarkable since it shows that one can obtain a similar VMC energy, but more importantly, a similar nodal surface quality by optimizing only a fraction of the CI coefficients (25 vs 168). These results show that it is possible to forgo the optimization of the CI coefficients. However, the procedure adopted here is tailored to C_2 . In order to make this approach applicable in practice, further research is needed to determine a multiplication factor that is valid for various systems and to identify a universal coefficient threshold, below which the CI coefficients can be manually altered in a reliable way.

Out of interest, the averaged coefficient ratios for the sm666 and the sm888 Jastrow factors were computed as well and amount to 0.63 and 0.60, respectively. The ratio for the first CSF (1.05) is the same for all three Jastrow correlation functions. The ratios becoming smaller for larger Jastrow factors hints at the correlation being increasingly captured by the Jastrows rather than by the configurations.

7.2 Using the Linear Optimization Method

Later in this thesis, see 7.3, we will confirm the importance of the Jastrow correlation function when it comes to choosing configurations. The assumption that the Jastrow factor will influence the configuration selection is, however, rather intuitive. Our first attempt of an sCI scheme in the presence of a Jastrow factor is based on the linear optimization method, as described by Toulouse and Umrigar^[66]. In order to assess the energetic contribution of a given determinant to the current wave function, one can compute the second-order perturbative change in energy (see Eq. (4.1))—an approach that originates from the CIPSI method. The physical quantities, needed for the computation of the energy contribution, can be obtained as the matrix elements of the Hamiltonian within the framework of the linear optimization method, applied to the optimization of the CI coefficients. The linear method works within the basis spanned by the current wave function and its first derivatives with respect to the wave function parameters. For the CI parameters, this means that one obtains the individual CSFs as derivatives. In their work, Toulouse and Umrigar^[66] present expressions for the elements of the non-symmetric Hamilton matrix in the form of \bar{H}_{i0} , \bar{H}_{0i} , and \bar{H}_{ij} (Eqs. 54b, 54c, and 54d, respectively, in Ref. 66). The energy contribution $\delta e_i^{(2)}$ of CSF i can be obtained from these expressions as follows:

$$\delta e_i^{(2)} = \frac{-\bar{H}_{i0} \cdot \bar{H}_{0i}}{\bar{H}_{ii} - \bar{H}_{00}},\tag{7.1}$$

with $\bar{H}_{00} = \langle E_{\rm L}({\bf R}) \rangle$. Eq. (7.1) illustrates that only the first column, the first row, as well as the diagonal elements, of the Hamilton matrix are needed. Since the linear optimization method is implemented in AMOLQC^[67], this sCI approach in the presence of a Jastrow factor can be tested with minor additional effort.

The ansatz was tested for the ${}^{1}\Sigma_{g}^{+}$ ground state of C_{2} , using the experimental equilibrium bond distance of 1.243 Å from Huber and Herzberg^[247]. A CAS(8,8) initial wave function was employed. The procedure for the generation of the Slater-Jastrow wave function was identical to the one described in the previous section, except that only the Jastrow parameters were optimized with VMC. An sm444 Jastrow factor was used. For the calculation of the $\delta e_{i}^{(2)}$, the coefficient of the first CSF was set to one, while all remaining coefficients were set to zero. This approach allows for an assessment of the energetic contribution of each CSF to the Slater-Jastrow wave function comprising only

the HF determinant and should be considered as an attempted proof of concept.

The absolute values of the quantities of Eq. (7.1) were averaged over five calculations using different seeds and a sample size of 128,000,000. The results are shown (for the first ten CSFs) in Tab. 7.3. The remaining data is listed in appendix E. The \bar{H}_{00} quantity corresponds to -75.7403(2) $E_{\rm h}$.

Tab. 7.3: Absolute values of the first ten (i = 1, ..., 10) Hamilton matrix elements together with the energy contributions $\delta e_i^{(2)}$. The quantities are given in $E_{\rm h}$. The value in parentheses indicates one standard deviation.

i	$\bar{H}_{0i} \times 10^3$	$\bar{H}_{i0} \times 10^3$	$ $ $ar{H}_{ii}$	$\delta e_i^{(2)} \times 10^4$
1	113.2(2)	112.5(2)	72.2(2)	36(2)
2	137.66(8)	137.2(2)	63.0(3)	14.8(4)
3	84.36(9)	84.1(1)	48.1(2)	2.56(2)
4	61.0(2)	60.9(3)	75.0(3)	51(14)
5	9.88(9)	10.0(2)	73.6(3)	0.46(5)
6	28.38(8)	28.3(2)	46.17(3)	0.272(2)
7	22.5(3)	22.3(3)	71.4(4)	1.16(9)
8	6.0(2)	6.2(2)	72.12(8)	0.104(5)
9	73.7(3)	73.7(2)	65.6(4)	5.3(2)
10	59.0(2)	59.01(6)	68.6(2)	4.9(1)

First of all, Tab. 7.3 shows the asymmetry of the Hamilton matrix since the \bar{H}_{0i} and the \bar{H}_{i0} are not identical. They are, however, close in value. Overall, the energy contributions $\delta e_i^{(2)}$ are comparatively small, ranging from 10^{-3} to 10^{-10} . The CSFs being sorted, for the initial CAS(8,8) wave function, from largest to smallest with respect to the absolute value of their coefficients, the energetic contributions become—as expected smaller the further one moves down the table. The decrease is, however, not monotonic (in contrast to the CI coefficients), which hints at the Jastrow correlation function influencing the importance of the individual CSFs in terms of their energy contribution to the Slater-Jastrow wave function. The small magnitude of the energy contributions (except for a few) can be traced back to the off-diagonal matrix elements of the Hamiltonian (\bar{H}_{0i} and \bar{H}_{i0}). Although they are larger in value (between 10^{-1} to 10^{-5}) than the $\delta e_i^{(2)}$, they enter, see Eq. (7.1), as a product in the numerator, explaining the scale of the energy contribution results. The $\delta e_i^{(2)}$ values being that small, especially for the larger index CSFs, it is, unfortunately, not obvious which CSFs should be included in the wave function for this first sCI iteration, except for the first, second, and fourth entries, which provide substantial energy contributions of the order of several mE_h . All three CSFs correspond to double or mixed double excitations, known to yield large contributions to the HF determinant. By setting, exemplarily, a threshold of $0.1 \text{ m}E_h$ for the selection, merely 11 CSFs would be chosen.

Additionally, the proposed ansatz faces various challenges. First, the sampling of $|\Psi|^2$ might not provide a sufficiently accurate sample for the computation of the matrix elements comprising the individual CSFs. This issue primarily affects the \bar{H}_{ii} values, as well as the off-diagonal entries \bar{H}_{0i} and \bar{H}_{i0} . The large uncertainties observed in the \bar{H}_{ii} energies, particularly in comparison to the highly accurate \bar{H}_{00} value, suggest that the strong zero-variance principle of the linear method may no longer hold. One way to circumvent this is to re-weight the sample used for the computation of the individual contributions by a factor of $|\Psi_i|^2/|\Psi|^2$. Another potential improvement lies in calculating the denominator using correlated sampling, which yields energy differences with smaller statistical uncertainties compared to the individual energies themselves. The use of a symmetric Hamilton matrix instead does not alter the picture, which is not surprising since, even for the non-symmetric counterpart, the values were rather similar.

The prospect of a more promising approach for a Jas-sCI scheme based on correlated sampling, as described by Per and co-workers^[248], see section 7.4, combined with the aforementioned assertions led us to discontinue further pursuit of this ansatz for an sCI scheme in the presence of the Jastrow factor.

7.3 CIPSI-Jastrow Wave Functions

Parts of the following sections are published in a condensed form in Ref. 224.

Reprinted (adapted) with permission from J. Ludovicy, R. Dahl, A. Lüchow, Toward Compact Selected Configuration Interaction Wave Functions with Quantum Monte Carlo—A Case Study of C₂, J. Chem. Theory Comput. **2023**, 19, 2792-2803. Copyright 2023 American Chemical Society.

In this part of the work, the $^{1}\Sigma_{g}^{+}$ ground state of C_{2} is investigated with truncated CIPSI-Jastrow wave functions. The computational procedure is described in detail in section 7.3.9. This molecule is well suited for this kind of analysis because it has only a small number of electrons and displays multi-reference character at the ground state level. For this reason, C_{2} is a popular benchmark system that has already been

thoroughly investigated in the literature, both theoretically and experimentally. [249–260] Two studies that have performed similar investigations to the ones discussed here are highlighted in the following. Firstly, Clay and Morales [255] have investigated C_2 in the equilibrium and a stretched geometry with sCI-Jastrow wave functions with the CSFs being generated using different approaches, not, however, the CIPSI scheme. They also discussed the orbital set choice and found that both the CSF selection scheme and the choice of initial orbitals have a severe impact on the FN-DMC energy. Secondly, Giner *et al.* [235] studied CIPSI-Jastrow wave functions, re-optimized—Jastrow, MOs, and determinant coefficients—with VMC, of various first-row atoms. They described the importance of re-optimizing the CI coefficients when a Jastrow factor is used and argued that the MO optimization has only a minor influence on the DMC energies (except for the Be atom). They did not, however, extend their investigation to molecules and, more importantly, to the computation of energy differences. Umrigar *et al.* [71] showed the importance of re-optimizing the molecular orbital parameters in the presence of a Jastrow factor for Si₂ and C₂ with CASSCF initial wave functions.

7.3.1 Truncated CIPSI-Jastrow Wave Functions

Post-Hartree-Fock methods aim at incorporating electron correlation in the wave function, which can be achieved in myriad ways. Within—amongst others—the CIPSI approach, this is traditionally realized through a linear combination of SDs, which includes the static as well as the dynamic electron correlation. Another way, which yields much more compact wave functions, is to capture the dynamic correlation by adding a Jastrow factor to the wave function. With this correlation function, the need for lengthy determinant expansions vanishes, because in order to capture the short-range dynamic correlation, excitations in higher-lying orbitals are necessary. This is demonstrated by Fig. 7.3, where the truncated CIPSI wave functions are compared to Jastrow-optimized ones.

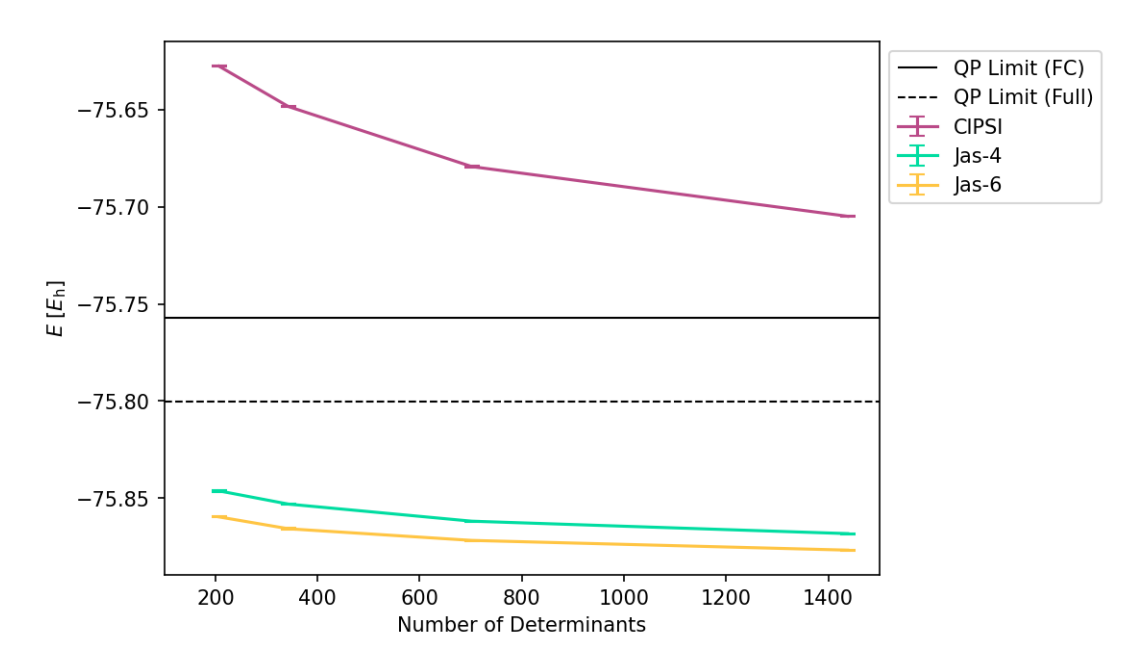


Fig. 7.3: VMC energies of truncated CIPSI wave functions with and without Jastrow factor as a function of the number of determinants. The QP Limit (FC) corresponds to the estimated frozen core FCI limit $E + E_{PT2}$ in the given basis. The QP Limit (Full) includes the correlation of the 1s orbitals, see text. The data points are connected as guidance for the eyes.

The energies of the truncated CIPSI wave functions (pink data) converge monotonically toward the FCI estimate (solid line in Fig. 7.3) for the given basis set. By including a Jastrow correlation function, the energy is substantially lowered by about $0.2\ E_h$ for each threshold, respectively. The CIPSI wave function contains 1, 985, 516 determinants. The QP (QUANTUM PACKAGE) Limit (FC) energy originates from a frozen core CIPSI calculation. Since the QMC calculations with a Jastrow factor correlate all electrons, the estimated CIPSI FCI limit, correlating all electrons, is calculated with QUANTUM PACKAGE as well (dashed line in Fig. 7.3). Note that the CIPSI-Jastrow VMC energies are substantially lower than this limit, already for 200 determinants. The higher-order Jastrow factor provides lower energies due to more ample flexibility in the wave function.

The accuracy of VMC being limited by the wave function form and flexibility^[11], we intend to investigate how the CIPSI-Jastrow wave functions perform within the more accurate DMC framework. This method allows—after a zero time step extrapolation—to assess the quality of the nodal hypersurface of a given wave function, the accuracy being determined by the fixed-node error. This will be discussed below, see section 7.3.3.

7.3.2 Comparison of Determinant and CSF Expansions

Although QUANTUM PACKAGE^[261] employs spin-adapted wave functions, we opted for the use of CSFs in this work for two different reasons. Firstly, by cutting off the CIPSI wave function, it can no longer be ensured that the truncated expansion is an eigenfunction of the \hat{S}^2 operator and secondly, by constructing CSFs from determinants, the length of the expansion can be substantially reduced—see Tab. 7.4—which leads to computationally less demanding optimizations with VMC. For the CSFs, the thresholds in Tab. 7.4 correspond to the determinant cutoffs. The CSFs are generated for all the determinants that are above the respective thresholds. As for the missing determinants, needed to complete the CSFs: their coefficients are obtained from the original CIPSI wave function. The last column in Tab. 7.4 gives the number of determinants if the CSFs are re-expanded into the SD basis.

Threshold	# Dets	# CSFs	# Dets (re-expanded)
0.0100	207	85	337
0.0075	343	138	575
0.0050	702	266	1090
0.0025	1438	528	2242

Tab. 7.4: Number of determinants and CSFs for the different thresholds.

In Fig. 7.4, the VMC energies of SD and CSF expansions are compared for different sets of optimized parameters. First of all, one can see that with every additional set of parameters that are optimized, a significant decrease in energy can be observed for each threshold, regardless of the choice of expansion. Furthermore, the VMC energies decrease monotonically as a function of the expansion length, which is inherent since the wave functions have higher flexibility due to more variational parameters being included. The CIPSI-Jastrow wave functions with CSFs yield lower VMC energies compared to the ones using SDs for all thresholds, irrespective of the optimization level. After expanding the CSFs back to determinants—see last column in Tab. 7.4—the wave functions contain more determinants than the original ones. Shorter CSF expansions leading to lower energies, hence, usually implies computationally more demanding calculations. The optimization of the CI coefficients—usually a very time-consuming part of the VMC calculations—remains, nonetheless, cheaper for CSF wave functions. The Jastrow correlation function having a non-zero overlap with the determinant ex-

pansion, it is essential to re-optimize the expansion coefficients (as well as the MO parameters). This is corroborated by various other studies as well. [105,235,251,253,262] Note, that the Jas+CI curves are much steeper than the ones for the fully optimized wave functions, which seem to be close to convergence already.

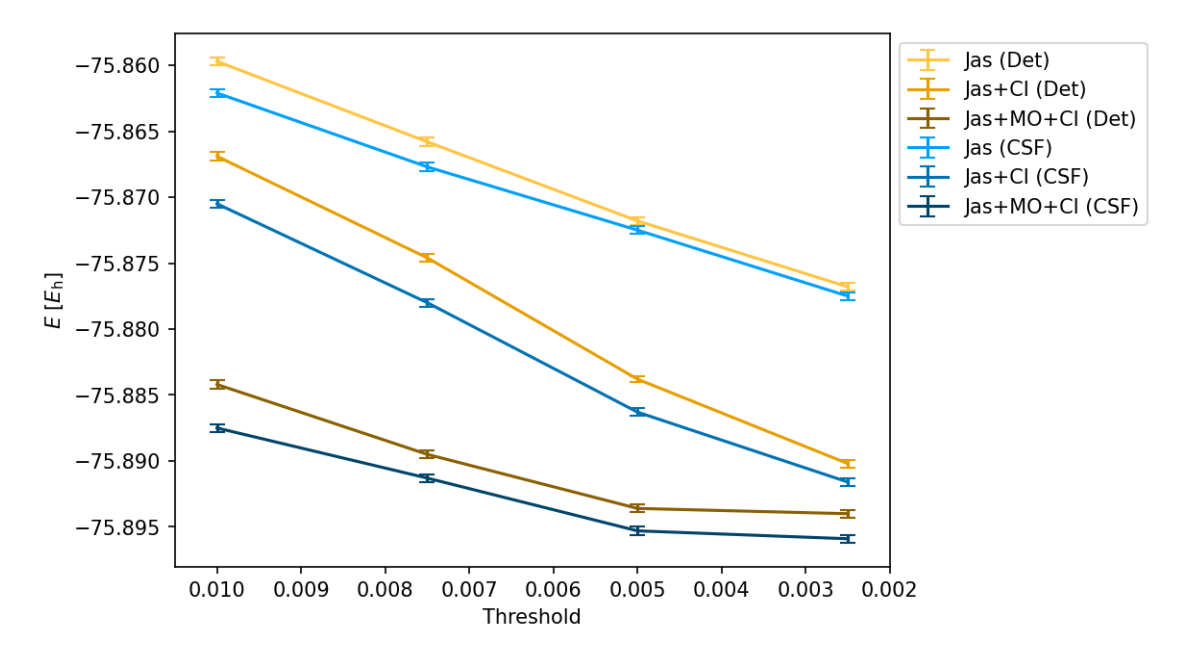


Fig. 7.4: VMC energies of determinant and CSF CIPSI-Jastrow wave functions at various optimization levels computed for different thresholds. An sm666 Jastrow factor was used. The data points are connected as guidance for the eyes.

Since the DMC energies will be discussed in more detail in the next section, within the framework of different Jastrow factors, it is dispensed, here, with an exhaustive discussion. The DMC energies can be found in appendix E. In summary, the CSF-based wave functions are slightly favored compared to the SD-based ones in terms of nodal surface quality.

7.3.3 Influence of Different Jastrow Factors

Having established the importance of using a Jastrow correlation function, that explicitly handles electron correlation, the impact of the size of the Jastrow factor on the wave function optimization with VMC as well as on the quality of the nodal surface, studied with DMC, is to be investigated here. Fig. 7.5 introduces the VMC energies for two Jastrow factors and different optimization levels. The Jastrow factors are denoted Jas-4 (for sm444) and Jas-6 (for sm666), respectively, throughout this study.

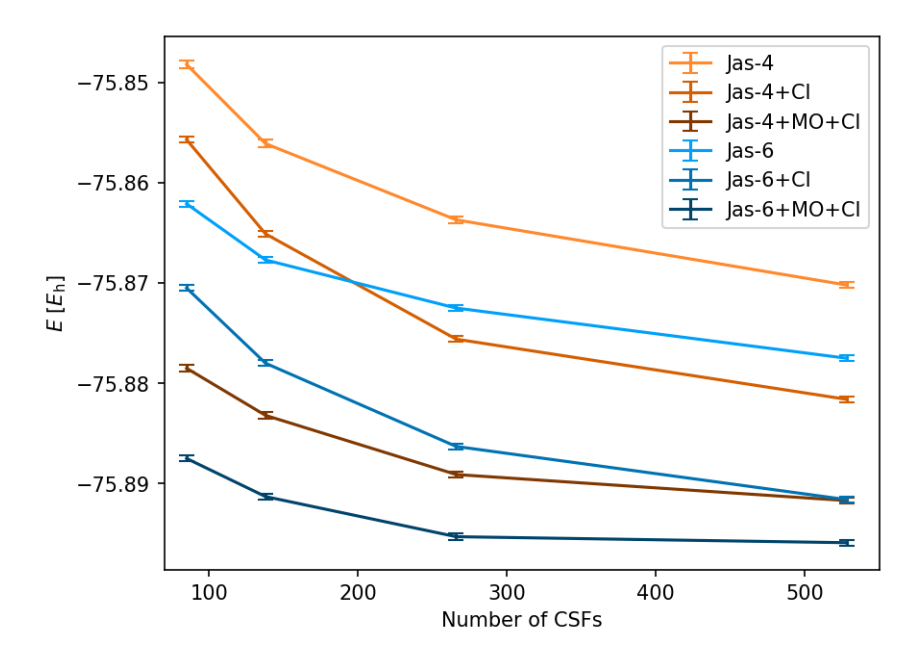


Fig. 7.5: VMC energies of truncated CIPSI-Jastrow wave functions at various optimization levels as a function of the number of CSFs. The order of the Jastrow factor is given by Jas-X. The data points are connected as guidance for the eyes.

For the fully optimized wave functions, the energies appear converged, while for the Jas and Jas+CI optimization levels, it is anticipated that lower energies are obtained for larger expansions. Furthermore, the larger Jastrow factor (Jas-6) provides lower VMC energies for each optimization level, which is expected, since a higher amount of variational parameters goes hand in hand with a more flexible wave function. The decrease in energy is largest when moving from the Jas to the Jas+CI optimization level, which also yields the steepest energy curves. Giner $et\ al.^{[235]}$ investigated CIPSI-Jastrow wave functions for several atoms using HF initial orbitals and they found no significant improvement of their VMC energies by also optimizing the molecular orbitals. For C_2 , this is clearly not the case. By also including the orbital optimization, the VMC energies are lowered by 5 to more than 15 m $E_{\rm h}$, depending on the cutoff value.

In Fig. 7.6, the DMC energies of the optimized CIPSI-Jastrow wave functions are compared to the DMC energies obtained with the truncated CIPSI wave functions. In the DMC—in contrast to the VMC—framework, one does not necessarily observe a systematic lowering of the energy with an increasing expansion size. This has been reported by various studies. [263–265] DMC provides the exact ground state energy of a system with the nodes of the trial wave function as a boundary condition. There is no guarantee that this energy is approached monotonically with growing expansion size. Fig. 7.6 demonstrates, however, that the DMC energies reported here, and throughout

this study, decrease monotonically within the statistical uncertainty with increasing expansion size—this is also the case for the CIPSI nodes—if the CI (and MO) parameters are re-optimized in the presence of the Jastrow factor. This has already been observed in a study by Giner *et al.*^[235] Additionally, for each threshold, the CIPSI nodes yield significantly higher energies than the nodes obtained by re-optimizing the CIPSI-Jastrow wave functions. To ensure, however, a fair comparison between the CIPSI method—unfolding its true potential only when using large expansions—and the CIPSI-Jastrow procedure, the two approaches are compared in the next section. As for the different optimization levels, the larger Jas-6 factor is superior for the Jas+CI optimization for the smaller cutoff values. By also including the MO optimization, both Jastrow factors provide similar energies for each threshold.

Although the VMC energies of the fully optimized wave functions appeared converged for the larger expansions—see Fig. 7.5—the DMC results show that the nodal surfaces are clearly not converged. Note that, although the VMC energies of the Jas-4+MO+CI and the Jas-6+CI wave functions with the smallest cutoff coincide, see Fig. 7.5, the nodal surface of the former wave function is much better. Thus, the performance of a given approach within VMC cannot necessarily be translated to DMC.

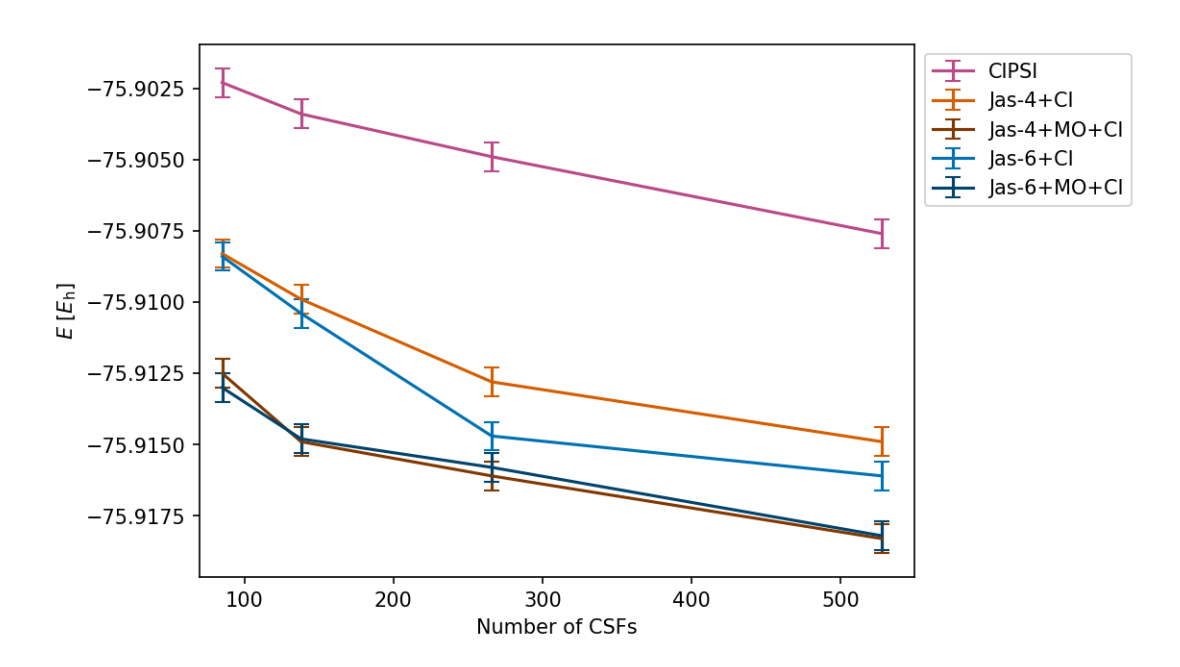


Fig. 7.6: DMC energies of truncated CIPSI wave functions at various optimization levels as a function of the number of CSFs. The order of the Jastrow factor—if used—is given by Jas-X. The data points are connected as guidance for the eyes.

7.3.4 Comparison to the Literature

Now, various methods are to be weighed against one another in order to evaluate the potential of the CIPSI-Jastrow ansatz. In Fig. 7.7, the absolute energies of C₂ are compared for different methods. The J-VBSCF* DMC energy is taken from Ref. 253. The DMC/CAS(8,8) and the MRCI(Q) energies originate from the works of Barnett *et al.* [266] and Peterson et al. [267], respectively. The DMC/CAS(8,8) (Jas+MO+CI) energy was computed in this work. The DMC/CIPSI value is obtained from Ref. 236, with the CIPSI wave function comprising 173,553 SDs. Toulouse and Umrigar^[66] have extrapolated their C₂ DMC energies—obtained for several truncated wave functions—to the limit that all CSFs (of the considered CI space) are included in the wave function. The extrapolated value corresponds to the DMC/RAS one in Fig. 7.7. This procedure, adopted in several other works^[71,255] as well, makes use of the fact that the original wave function is normalized to one. By plotting the DMC energies of the fully optimized truncated CIPSI-Jastrow wave functions with respect to the sum of the squares of the CI coefficients, one can extrapolate the DMC energy to one using a linear fit, see Fig. 7.8. Five truncated CIPSI-Jastrow wave functions were used for the extrapolation. The additional DMC energy (computed for the discussion of the bond dissociation energy, see below) of the fully optimized wave function using a cutoff value of 0.0010 (1766 CSFs) corresponds to -75.9197(5) E_h . The energy is not displayed in Fig. 7.7 for clarity reasons. The extrapolated DMC energy for the CIPSI-Jastrow approach is also given in Fig. 7.7. The estimated exact value originates from Bytautas and Ruedenberg^[250] and is derived from Table X in Ref. 250 by adding the core correlations amount to the nonrelativistic valence-correlated energy.

When studying Fig. 7.7, several observations can be made. First, the DMC/CIPSI (no Jas) energy from Caffarel and co-workers^[236] is about 10 to 15 m $E_{\rm h}$ lower than the ones computed for the truncated CIPSI wave functions (pink data, no Jas), which emphasizes that by truncating CIPSI expansions and dispensing with a Jastrow factor, one loses a substantial amount of the correlation energy. Remarkably, the DMC energy of the fully optimized CIPSI-Jastrow wave function with the largest threshold (85 CSFs, dark blue) is lower than the DMC/CAS(8,8) (Jas+MO+CI) one which contains 168 CSFs. This corroborates the fact that excitations beyond the full valence CAS are important, which has been shown in other studies as well.^[71,239] In addition, the energy of the largest CIPSI-Jastrow wave function at the Jas+CI optimization level (528 CSFs, blue)

^{*}valence bond self-consistent field

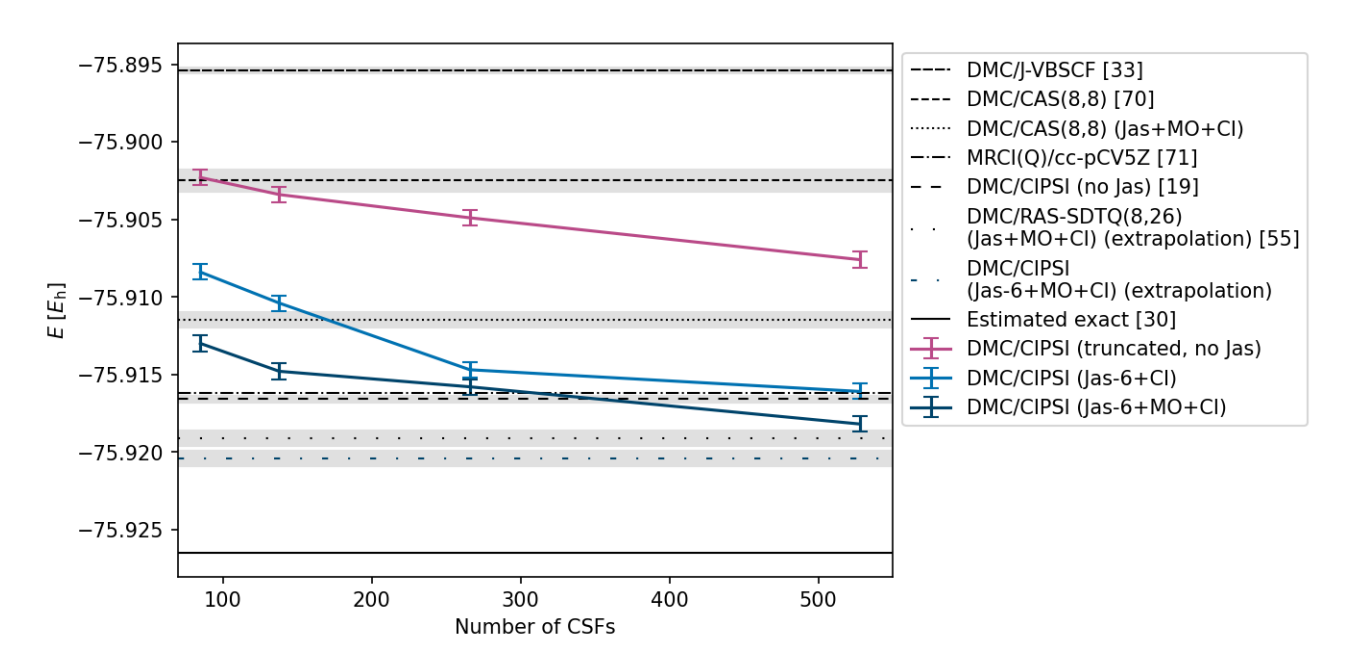


Fig. 7.7: Comparison of CIPSI-Jastrow-DMC energies, computed in this work (pink and blue data), with different methods and ansatzes from the literature. The data without indicated references was computed in this work. See text for references. Error bars are indicated in grey. The data points are connected as guidance for the eyes.

already equals the DMC/CIPSI energy of Caffarel and co-workers with 173,553 determinants. Furthermore, the fully optimized CIPSI-Jastrow wave function with the largest expansion (528 CSFs, dark blue) provides a DMC energy that is considerably lower than both the MRCI(Q) and the DMC/CIPSI data and that is close to the extrapolated DMC/RAS energy from Toulouse and Umrigar. The DMC energy obtained for the fully optimized wave function with a threshold of 0.0010 (see above) is slightly lower than the extrapolated DMC/RAS one, which corresponds to -75.9191(5) $E_{\rm h}$. The extrapolated DMC/CIPSI-Jas-6+MO+CI energy amounts to -75.9204(5) $E_{\rm h}$ which is about 1 m $E_{\rm h}$ lower than the one from the DMC/RAS ansatz. These findings illustrate that the CIPSI-Jastrow-DMC approach is promising since it allows for accurate energies using very compact wave functions.

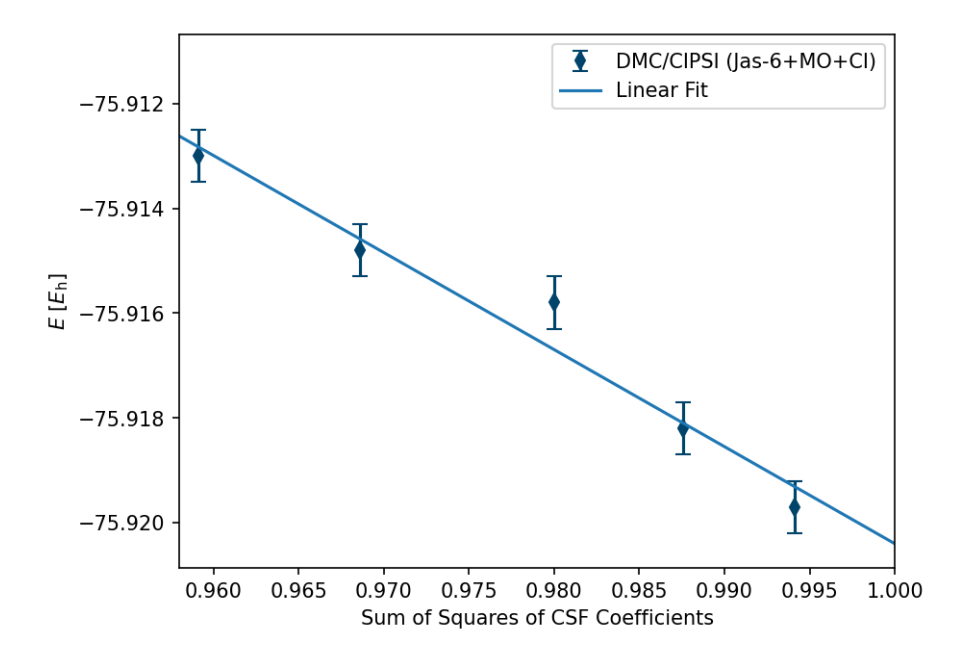


Fig. 7.8: Time step extrapolated DMC energies of fully optimized truncated CIPSI-Jastrow wave functions as a function of the sum of the squares of the CI coefficients, together with the linear fit. An sm666 Jastrow factor was used.

7.3.5 CI Coefficients

Having seen in the previous parts of this study that re-optimizing the CI coefficients in the presence of a Jastrow correlation function has a considerable impact on both the VMC and DMC energies, it is worth taking a look at how the coefficients are altered by the optimization. The investigation is done exemplarily for the smallest wave function. After the CI optimization, the sum of the squares of the CI coefficients is re-normalized to one (ignoring the Jastrow factor). The results are presented in Fig. 7.9.

The absolute values of the CI coefficients are diminished—starting from the fifth one—if a Jastrow factor is included in the wave function, see the left graph. This nicely corroborates the effect of the Jastrow factor, namely that it—rather than the expansion—accounts for the short-range dynamic electron correlation. The CI expansion being normalized, the CI coefficients—and thus the weights—of the first few CSFs are necessarily increased by adding a Jastrow factor. The decrease of the absolute value of the CI coefficients is even more distinct for the fully optimized wave function which shows that the MO optimization has a major impact on the CI coefficients and hence on the nodal surface. The right graph in Fig. 7.9 illustrates how the coefficients are altered by the optimization for each CSF. For the Jas+CI optimization, the coefficients are much closer

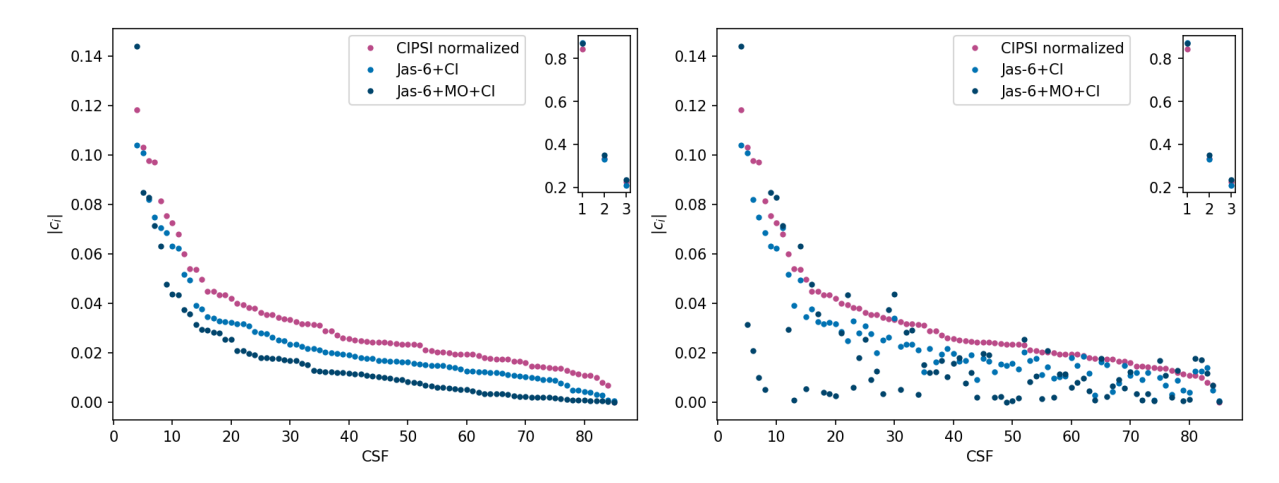


Fig. 7.9: Absolute values of the CSF coefficients for CIPSI wave functions with and without Jastrow factor truncated at a threshold of 0.0100. The first three coefficients are depicted in the sub-plots. Left: all coefficients are sorted from largest to smallest. Right: the original CIPSI coefficients (pink) are sorted from largest to smallest. For the CIPSI-Jastrow wave functions, the coefficients are sorted such that the CSFs are identical for each index, i.e. *x*-coordinate. The CSFs are normalized for each approach.

in value to the original CIPSI coefficients than for the full optimization. Additionally, the trend for the Jas-6+CI coefficient decrease is similar—with minor fluctuations—to the one for the normalized CIPSI coefficients. Considering, now, also the optimization of the MOs, the picture changes drastically, especially for the lower index CSFs, which have—with a few exceptions—significantly smaller coefficients after the full wave function optimization. On the other hand, the coefficients of several CSFs are increased by the Jas+MO+CI optimization. This shows that the selection of the CSFs is influenced by the optimization which emphasizes that choosing configurations in the presence of a Jastrow correlation function is important.

In order to investigate this in more depth, we decided to closer analyze the CSFs, whose coefficients are drastically altered by the full optimization of the wave function, by looking at which excitations are favored or, contrarily, less likely. We focused on the first 30 CSFs (of the fully optimized wave function) for the analysis of the excitations, the coefficient changes being most prominent for those configurations. Fig. 7.10 comprises the orbitals from which the excitations take place, while Fig. 7.11 shows the excited orbitals.

First of all, no significant qualitative change—except for a few exceptions, see below—can be observed between the HF and the optimized orbitals. Starting with the CSFs that gain in importance by the optimization: all possible combinations—preserving the symmetry—of $\pi \to \pi^*$ excitations from $1b_{2u}$ and $1b_{3u}$ to $1b_{3g}$ and $1b_{2g}$ constitute the

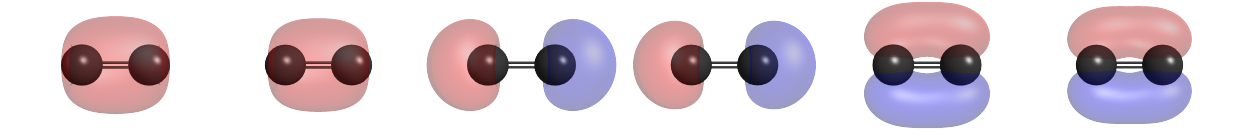


Fig. 7.10: The orbital on the left is always the HF orbital, while the one on the right corresponds to the optimized (Jas-6+MO+CI) VMC orbital. Left: $2a_g$, middle: $2b_{1u}$, right: $1b_{2u}$. The orbitals are ordered—from left to right—according to increasing energy eigenvalue. The molecule is displayed in the yz-plane with the z-axis being aligned with the CC bonding axis. Orbital $1b_{3u}$ (not shown) is degenerate to orbital $1b_{2u}$ and oriented along the xz-plane. These four orbitals—together with two σ orbitals, built from the respective carbon 1s orbitals—are doubly occupied in the HF determinant.

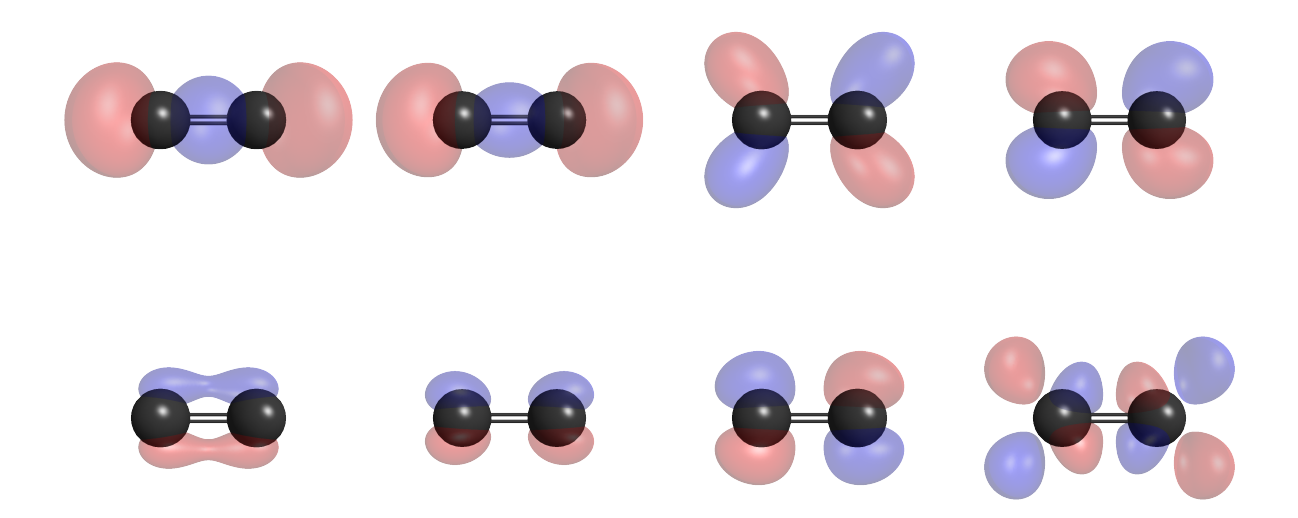


Fig. 7.11: The orbital on the left is always the HF orbital, while the one on the right corresponds to the optimized (Jas-6+MO+CI) VMC orbital. **First row** - Left: $3a_g$, right: $1b_{3g}$ (with degenerate $1b_{2g}$ orbital along xz-plane, not shown). **Second row** - Left: $2b_{2u}$ (with degenerate $2b_{3u}$, not shown), right: $2b_{3g}$ (with degenerate $2b_{2g}$, not shown). The orbitals are ordered—from left to right—according to increasing energy eigenvalue. The molecule is displayed in the yz-plane with the z-axis being aligned with the CC bonding axis.

most important ones. In addition, $\sigma^*(2b_{1u}) \to \sigma(3a_g)$ and $\sigma^*(2b_{1u}) \to \pi^*(1b_{3g}, 1b_{2g})$ excitations are favored. Finally, different combinations of $\sigma(2a_g) \to \pi(2b_{2u}, 2b_{3u})$, $\sigma(2a_g) \to \sigma(3a_g)$, and $\pi(1b_{2u}, 1b_{3u}) \to \pi(2b_{2u}, 2b_{3u})$ excitations are more important in the fully optimized wave function than in the original CIPSI one. All of the discussed excitations correspond to either double (favored) or quadruple excitations. Considering, now, the CSFs with smaller coefficients for the optimized wave function than for the original CIPSI expansion, the $\sigma \to \sigma$ excitation from $2a_g$ to $3a_g$ is strongly disfavored. Furthermore, CSFs with excitations from the $2b_{1u}$, $1b_{2u}$, and $1b_{3u}$ orbitals to the

 $3a_g$, $2b_{3g}$, and $2b_{2g}$ orbitals lose in importance. Finally, mixed double excitations from e.g. $1b_{2u}$ to $1b_{3g}$ and $2b_{3g}$ are considered less favorable. The VMC optimized $2b_{3g}$ (and $2b_{2g}$) orbitals are qualitatively very different from the HF orbitals, see Fig. 7.11. One can observe a significant contribution from the d_{xz} and d_{yz} orbitals of both carbon atoms to the π^* orbitals, which is judged to be the reason why the coefficients of the CSFs that include these orbitals are considerably reduced by the optimization. Generally, one can see that the anti-bonding character, see e.g. orbital $1b_{3g}$, seems to be increased by the optimization while the bonding one, see e.g. orbitals $3a_g$ and $2b_{2u}$, slightly decreases, which is rather surprising. All in all, it can be seen that the simultaneous optimization of all wave function parameters significantly changes the CI picture. One can, however, based solely on the excitations, not identify a systematic explanation for this change in CI coefficients.

7.3.6 Bond Dissociation Energy

So far, it has been demonstrated that the CIPSI-Jastrow ansatz is able to provide accurate absolute energies for C_2 . As chemists, we are, however, primarily interested in computing molecular properties of a given system, which is why the focus will now be put on how well the CIPSI-Jastrow-DMC method performs for the electronic dissociation energy D_e of C_2 . The CIPSI method, usually including several hundred thousand up to more than a million determinants, depending on the system at hand, is quasi-size consistent. A difficulty that arises for the truncated CIPSI-Jastrow approach is that it probably suffers from size inconsistency since the chosen cutoffs are rather aggressive. In order to assess this, different truncation schemes for the carbon atom wave function were analyzed. The results are listed in Tab. 7.5. The VMC and DMC energies for the carbon atom can be found in appendix E. The dissociation energies are first-order spinorbit (SO) corrected, the correction (for the carbon atom) being determined from experimental splittings and amounting to -0.003669 eV.[135] Firstly, it should be noted that the best estimate computed in this work is 6.39(2) eV. This value should thus be used as a reference for the discussion of the truncation schemes. An additional (smaller) threshold was added for the computation of the dissociation energy in order to assess whether a convergence can be observed. For the first scheme, the same coefficient threshold for the C atom wave function as for the dimer was employed. Apart from the smallest cutoff, the dissociation energies (first D_e column) are not very accurate. This is not surprising, since by choosing equal thresholds, a much better description of the atom, compared to the molecule, is achieved, which is mirrored by the dissociation energy being severely underestimated. In the second truncation scheme, the cutoff value for the carbon atom wave function corresponds to the square root of the respective threshold for C₂. The dissociation energies are—apart from the smallest threshold overestimated by more than 0.1 eV, hinting at a poor description of the carbon atom, corroborated by the rather aggressive truncation thresholds for the respective carbon wave functions. Note that the first three dissociation energies are identical because the same C wave functions were employed. In the last ansatz, the sum of the CSF weights (squares of the CI coefficients) after the truncation was determined. The carbon atom wave functions were truncated such that the normalization was as close as possible to the one of C_2 . For this scheme, a nice convergence of the dissociation energy can be observed. This approach is superior since a similar amount of correlation is recovered for both, the atom and the molecule. It should be noted that, for the smallest C_2 cutoff, the dissociation energies for all three truncation schemes are in good agreement with each other. In order to assess whether this is based on the expansions being large enough to both accurately describe the atom and the molecule or whether this is a mere coincidence, the dissociation energies should be evaluated for an even smaller C₂ threshold and the respective carbon thresholds. In a next step, the best estimate of the dissociation energy from this study is compared to data from the literature, see Tab. 7.6. The ZPE, necessary for D_0 , is taken from Ref. 268 and amounts to 0.1146 eV.

Tab. 7.5: Computed DMC bond dissociation energies of C₂ in eV at the Jas-6+MO+CI optimization level with different truncation schemes for the carbon atom wave functions. The number of CSFs for the different wave functions is given as well. The dissociation energies are first-order SO corrected, see text for details.

Thres C ₂	Thres C ^a	#CSFs	$D_{\rm e}$	Thres C ^b	#CSFs	De	Thres C ^c	#CSFs	De
0.0100	0.0100	40	6.16(2)	0.1000	2	6.52(2) ^d	0.1000	2	6.52(2) ^d
0.0075	0.0075	46	6.18(2)	0.0870	2	$6.52(2)^{d}$	$0.0550^{\rm e}$	5	6.68(2)
0.0050	0.0050	55	6.20(2)	0.0710	2	$6.52(2)^{d}$	0.0380	13	6.37(2)
0.0025	0.0025	94	6.21(2)	$0.0500^{\rm e}$	5	6.67(2)	0.0340	19	6.40(2)
0.0010	0.0010	186	6.35(2)	0.0320	20	6.38(2)	0.0230	26	6.39(2)

^a Same threshold for C and C_2 .

There are myriad values in the literature for the bond dissociation energy of C_2 . In this study, only the more recent and highly accurate experimental as well as theoretical

^b C threshold corresponds to square root of C₂ threshold.

^c Sums of squared CI coefficients of the C wave functions were chosen such that they are as close as possible to the sums of squared CI coefficients of the C₂ wave functions.

^d Same C atom wave functions.

^e Same C atom wave functions.

data are considered. The dissociation energy from Borsovsky et al. [260] is, to the best of my knowledge, the best experimental estimate currently available. Tab. 7.6 shows that the dissociation energy from this work, fits well into the range of recent experimental estimates and that it is in agreement with (most) theoretical values. The i-FCIQMC approach underestimates the experimental dissociation energy. The procedure for the computation of the DMC/CIPSI-Jastrow (this work) and the DMC/CAS(8,8) values is the same, apart from the choice of expansion. By employing a CIPSI initial expansion in contrast to a CASSCF wave function—the bond dissociation energy of C₂ could be improved. What is more, the dissociation energy computed in this work agrees well with the CASPT2 and the DMC/CAS(8,18) data. Toulouse and Umrigar^[251] report a DMC dissociation energy of 6.482(3) eV, obtained using a full valence CAS approach with a fully optimized wave function, including the optimization of the basis function exponents. This bond dissociation energy overestimates the theoretical and experimental ones. Finally, the CC value from Karton, keeping in mind the computational expenditure needed for these calculations, shows an excellent agreement with the experiment.

Tab. 7.6: Calculated or measured bond dissociation energies of C_2 in eV, with and without ZPE. The D_0 data refers to values obtained for 0 K. The horizontal line in the middle of the table separates the theoretical data from the one relying on experimental results.

Investigators	Method	$D_{\rm e}$	D_0
This work	DMC/CIPSI(Jas-6+MO+CI)/TZPae	6.39(2)	6.28(2)
Karton ^[258]	CCSDTQ567/CBS	, ,	6.248
Haghighi Mood ^[78]	DMC/CAS(8,8)(Jas+MO+CI)/TZPae	6.433(16)	6.315(16)
Umrigar <i>et al.</i> ^[71]	DMC/CAS(8,18)(Jas+MO+CI)/BFD-V5Z	6.36(1)	, ,
Toulouse and Umrigar ^[251]	DMC/CAS(8,8)/CVB1 full optimization ^a	6.482(3)	
Cleland <i>et al.</i> ^[269]	i -FCIQMC/VQZ+ $\Delta E_{\rm F12}^{\rm ccsd(T)}$	6.296(9)	
Hermann <i>et al</i> . ^[257]	CASPT2-F12/cc-pVTZ-F12	6.370	6.257
Ruscic ^[270]	exp (ATcT)		6.245(3)
Borsovszky et al. ^[260]	exp (VMI and MPI)		6.2476(3)
Urdahl <i>et al.</i> ^[249]	exp (LIF)		6.30(2)
Visser <i>et al.</i> ^[259]	exp (TC-RFWM)/icMRCI+Q/cc-pCVQZ-F12	6.36(2)	6.25(2)
Bytautas and Ruedenberg ^[250]	exp (from ATcT, atomic ionization energies)	6.44(2) ^b	6.30(2)

^a Optimization of the Jastrow, CSF, orbital, and basis exponent parameters.

b Non-relativistic estimate. Corresponds to the sum of nonrelativistic valence-correlated and core correlations values, see Table X of Ref. 250. Relativistic estimate ($D_0 + ZPE$) corresponds to 6.42(2) eV.

7.3.7 Choice of Initial Orbitals

So far, all of the results that have been presented were obtained using HF orbitals. Various studies have shown that the use of KS orbitals is favorable in combination with quantum Monte Carlo. [66,120,125,248,271,272] Several studies [240,241,243], making use of the CIPSI-Jastrow approach, employ CASSCF or even natural orbitals to construct the CIPSI expansions. In this part of the study, the performance of different sets of initial orbitals with respect to the DMC energies of C_2 , see Fig. 7.14, is analyzed. The QMC calculations for this part of the work were conducted in the SD basis. Since only trends are discussed, the results are judged to be alike for the CSF basis.

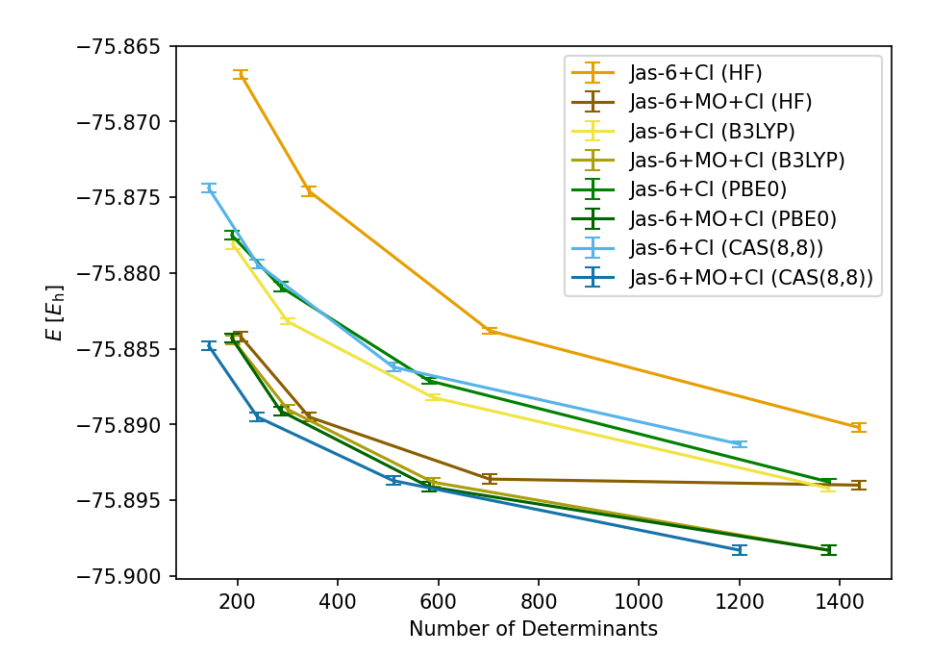


Fig. 7.12: VMC energies of truncated CIPSI-Jastrow wave functions as a function of the number of determinants for different sets of initial orbitals. An sm666 Jastrow factor was used. The data points are connected as guidance for the eyes.

The VMC energies of the Jas+CI and the fully optimized CIPSI-Jastrow wave functions using different initial orbitals are shown in Fig. 7.12. The HF orbitals provide the highest VMC energies in every case. At the Jas+CI level, the B3LYP KS orbitals are slightly favored while for the full optimization, the VMC energies are similar (except for HF), irrespective of the initial orbital choice.

In 2019, Per and co-workers argued that an accurate density is important in order to obtain good nodal surfaces.^[273] They found that the PBE0 (followed by the B3LYP) functional provided the best results for the systems that they investigated. Comparing the DMC energies of C₂ using initial PBE0 and B3LYP KS orbitals, respectively, it was

found that B3LYP provided superior results, see Fig. 7.13. This is also the case for the VMC energies, see Tab. E.6 in the appendix.

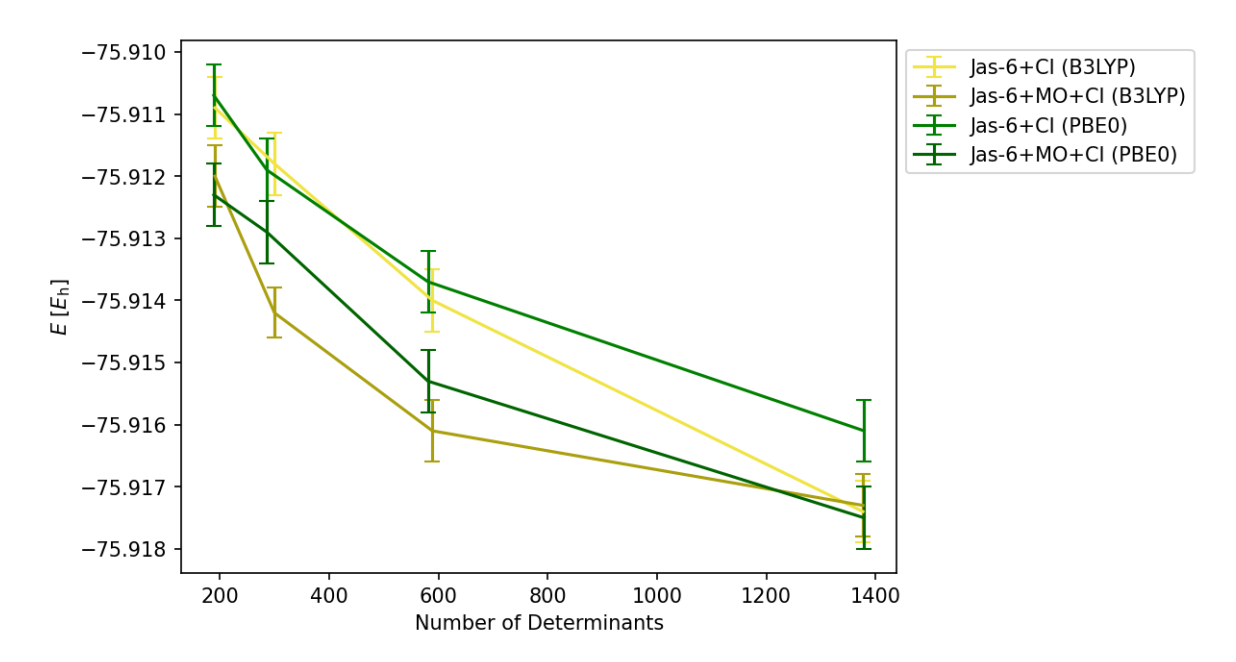


Fig. 7.13: DMC energies of truncated CIPSI-Jastrow wave functions as a function of the number of determinants for different sets of initial orbitals. An sm666 Jastrow factor was used. The data points are connected as guidance for the eyes.

The PBE0 results are not shown for the discussion of the DMC energies, see Fig. 7.14, for clarity reasons. Several observations can be made regarding Fig. 7.14. Firstly, for a given cutoff value, the size of the expansion is reduced—compared to HF—when using KS orbitals. This is even more prominent when CASSCF orbitals are employed. By plotting the absolute value of the CI coefficients as a function of the determinant indices, see Fig. 7.15, one observes a steeper descent of the CIPSI coefficients when using CASSCF orbitals than for the HF and B3LYP counterparts. This indicates that some correlation is—compared to HF—already included in the orbitals, the expansion, therefore, being shorter for a given threshold. For wave functions constructed from the same determinants, assuming that the optimization works well, the choice of initial orbitals would make no difference to the final VMC and DMC energies. The differing number of determinants for a given cutoff in Fig. 7.14 thus implies that different determinants are chosen, depending on the choice of initial orbitals. Secondly, at the Jas+CI optimization level, the expansions using B3LYP KS orbitals yield overall lower DMC energies than the wave functions computed with the CASSCF counterparts. Remarkably, for the largest expansion using KS orbitals, the energy is not improved by optimizing the MO parameters. For larger systems, therefore, it seems promising to omit the costly MO optimization when using KS orbitals. The fully optimized CIPSI-Jastrow approach with CASSCF orbitals provides the lowest energies for each threshold. This procedure has, however, the disadvantage of needing to choose an active space for the generation of the orbitals, which stands in the way of the CIPSI-Jastrow-DMC method becoming a black box approach. It should be noted that, ideally, one would employ orbitals that are optimized within the sCI framework, which has been studied by Yao and Umrigar.^[274]

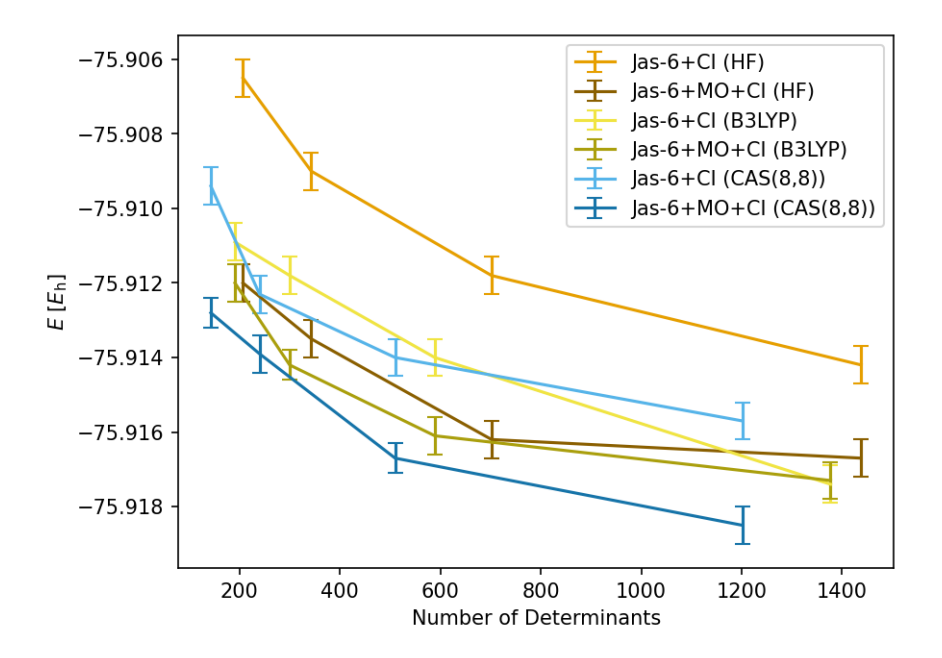


Fig. 7.14: DMC energies of truncated CIPSI-Jastrow wave functions as a function of the number of determinants for different sets of initial orbitals. For each plot, the data points correspond to the $|c_i|$ cutoff values of 0.0100, 0.0075, 0.0050, and 0.0025. An sm666 Jastrow factor was used. The data points are connected as guidance for the eyes.

Clay and Morales^[255] investigated C_2 in both the equilibrium and a stretched geometry with QMC using multi-Slater-Jastrow wave functions. They argued that using orbital sets that already take into account electronic correlation for the generation of the configurations is important, especially because one observes a faster convergence with the number of included CSFs. This significance of the initial orbital choice is nicely corroborated by the findings of this study. Cuzzocrea *et al.*^[242] recently published excitation energies for cyanine dyes using CIPSI-Jastrow wave functions. They found that the use of different initial orbitals has no significant impact on the excitation energies. The arguments that have been made above are only valid for the absolute energies of C_2 . Whether the choice of initial orbitals has an impact on the dissociation energy of C_2 necessitates further investigation.

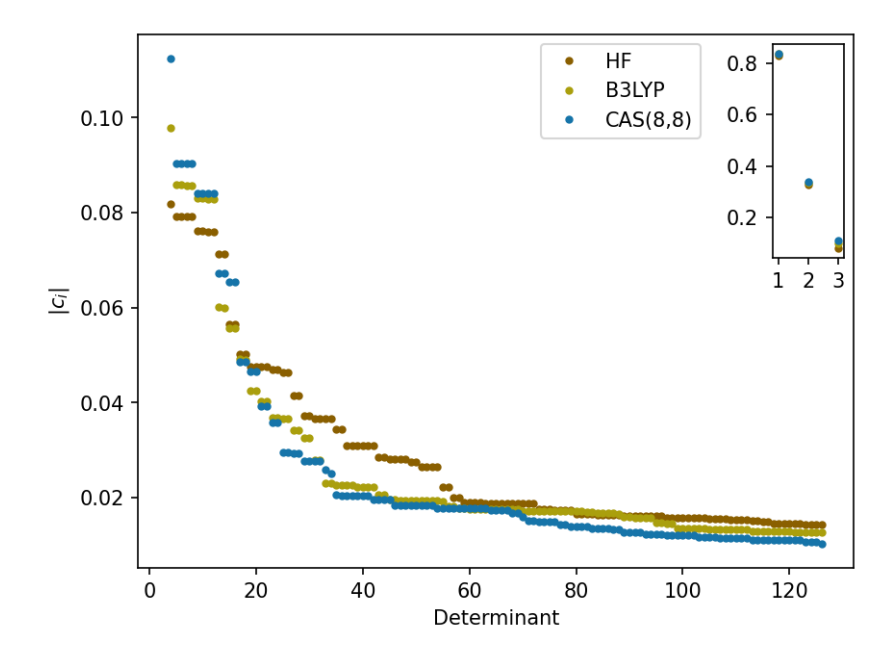


Fig. 7.15: Absolute values of the determinant coefficients for CIPSI-Jastrow wave functions truncated at a threshold of 0.0025. The first three coefficients are depicted in the sub-plot. The coefficients are sorted from largest to smallest. The plot only includes the first 125 determinants, for clarity reasons.

7.3.8 Selected CI in the Presence of a Jastrow Factor

One goal of this study is to provide an approach that allows for the generation of compact sCI wave functions. Having established the validity of the CIPSI-Jastrow-DMC procedure above, the importance of moving beyond the original CIPSI selection will be demonstrated in this part. Since the CI picture is substantially altered when simultaneously optimizing all the wave function parameters (see discussion of the CI coefficients), the selection of the CSFs in the presence of a Jastrow factor is judged to be of great importance. Before discussing this in more detail, however, let us first compare the full valence CAS and the CIPSI expansions, see Tab. 7.7. The CAS(8,8) wave function contains 168 CSFs, so, in order to compare both ansatzes, the CIPSI expansion is truncated, after sorting with respect to $|c_i|$, at 168 CSFs. Tab. 7.7 demonstrates that, irrespective of the optimization level, CIPSI is superior—at least for C₂—to CAS in terms of energy. Additionally, the fully optimized CIPSI-Jastrow wave function has a better nodal surface, demonstrated by the considerably lower DMC energy. These findings are not surprising, since CAS is known to include various CSFs that do not significantly contribute to the correlation energy. CIPSI, on the other hand, chooses configurations based on their energy contribution. This was already shown by Dash et al. in their work on 1,3-trans-butadiene. [275] The comparison between CIPSI and CAS justifies the transition from CAS initial wave functions—used in several previous studies of our group^[78,105,125]—to CIPSI expansions, leaving behind the limitations of CASSCF and paving the way toward the investigation of larger systems.

Tab. 7.7: VMC and DMC energies in E_h for different wave function ansatzes. The CAS(8,8) wave function contains 168 CSFs. The CIPSI expansion was truncated at 168 CSFs.

	CAS(8,8)	CIPSI
E	-75.6381 a	-75.6751(4) ^b
E_{VMC} (Jas-6)	-75.8594(3)	-75.8707(3)
E_{VMC} (Jas-6+CI)	-75.8696(3)	-75.8820(2)
E_{VMC} (Jas-6+MO+CI)	-75.8792(3)	-75.8937(3)
$E_{\rm DMC}$ (Jas-6+MO+CI)	-75.9115(5)	-75.9151(5)

^a CASSCF energy.

Let us, now, move on to the discussion of the sCI scheme in the presence of a Jastrow correlation function (Jas-sCI). In this part, the selection of the CSFs is discussed—more precisely, different selection schemes will be compared by discussing the effects of the Jastrow factor and the molecular orbital. All the energies, portrayed in Tabs. 7.8, 7.9, and 7.10, are obtained for wave functions with 168 CSFs. While sCI usually refers to iterative selection schemes, in this study, only one CI selection step is presented which may, in subsequent work, be the basis for a full iterative Jastrow-sCI algorithm.

First of all, the effect of adding a Jastrow factor and the choice of MOs are put in contrast. Tab. 7.8 reveals that the nodal surface is improved—for the same expansion size—by using orbitals from a correlated (here CASSCF) calculation as opposed to using HF orbitals in the CIPSI calculation. The effect is, however, much smaller compared to the approach of adding a Jastrow correlation function to the CIPSI HF wave function and optimizing the Jastrow and CI parameters. It should be mentioned that the CIPSI/HF and CIPSI/CAS DMC energies were calculated with an optimized Jastrow factor in order to increase the efficiency of the calculations. Note, however, that the Jastrow factor does not change the nodes of the wave functions and thus the DMC energies.

In the next step, the CSFs are selected in the presence of the Jastrow factor, see Tab. 7.9. For the Jas-sCI entries, we started with larger expansions (*Initial cutoff*) at the Jas-6+CI *Initial opt level*, truncated the wave functions (after the optimization and sorting) to 168 CSFs, and subsequently re-optimized the Jastrow and CI parameters. The HF orbitals remain unaltered for this Jas-sCI procedure in order to limit the evaluation to the impact of the Jastrow factor. For the smaller initial wave function (0.0050), a lower VMC energy

^b Calculated with VMC.

Tab. 7.8: DMC energies in *E*_h for different wave function ansatzes. The expansions were truncated at 168 CSFs. The CIPSI entries correspond to pure CIPSI wave functions. For the CIPSI-Jas wave function, the Jastrow and CI parameters were optimized. The initial orbitals—used for the CIPSI calculation—are either HF or CASSCF orbitals.

	E_{DMC}
CIPSI/HF CIPSI/CAS	-75.9047(5) -75.9061(5)
CIPSI-Jas/HF (Jas-6+CI)	-75.9121(5)

is obtained in the Jas-sCI scheme while the DMC energy is similar to the DMC CIPSI-Jas one. As for the larger initial expansion, a decrease in energy is observed for both the VMC and DMC energies compared to the CIPSI selection. This shows that one can get lower energies (VMC and DMC) with the same expansion length if the CSFs are chosen in the presence of a Jastrow correlation function. Since the optimization of the molecular orbitals was dispensed with, these findings show that the selection is altered when a Jastrow factor is present, justifying the need for a Jas-sCI scheme.

Tab. 7.9: VMC and DMC energies in *E*_h for different wave function ansatzes. The expansions were truncated at 168 CSFs. For the CIPSI-Jas wave function, the Jastrow and CI parameters were optimized. For the Jas-sCI entries, the CIPSI wave functions for different thresholds (see *Initial cutoff*) were truncated (to 168 CSFs) and the Jastrow and CI parameters were re-optimized. The initial orbitals—used for the CIPSI calculation—are Hartree-Fock orbitals.

	Initial cutoff (# CSFs)	Initial opt level	E _{VMC} (Jas-6+CI)	E _{DMC} (Jas-6+CI)
CIPSI-Jas/HF			-75.8820(2)	-75.9121(5)
Jas-sCI/HF	0.0050 (266) 0.0025 (528)	Jas-6+CI Jas-6+CI	-75.8842(2) -75.8849(3)	-75.9127(5) -75.9145(5)

Lastly, the optimization of the MOs was also included in the Jas-sCI scheme in order to evaluate the impact of improved orbitals on the selection, see Tab. 7.10. Again, for the Jas-sCI entries, we started with larger expansions (*Initial cutoff*) at different optimization levels (*Initial opt level*), truncated the wave functions (after the optimization and sorting) to 168 CSFs, and subsequently re-optimized the Jastrow, MO, and CI parameters. Let us start by discussing the results for the smaller initial wave function (0.0050). Firstly, the fully optimized initial wave function provides lower VMC and DMC energies than the CIPSI selection. For the Jas-6+CI initial wave function, no significant improvement (for VMC and DMC) is observed. More importantly, though, is the finding that when the CSFs are selected using improved orbitals, both lower VMC and DMC energies—compared to the Jas-6+CI initial optimization level—are obtained. This shows that the orbitals influence the selection of the CSFs. One last comparison

for this smaller initial wave function will be made. The DMC energy for the fully optimized CIPSI-Jastrow wave function, truncated at a threshold of 0.0050 (266 CSFs) is equal to -75.9158(5) $E_{\rm h}$. Comparing this energy to the ones from Tab. 7.10 (third and fourth row), one can see, firstly, that, for the (0.0050, Jas-6+CI) initial wave function, the same—within the statistical error—DMC energy can be obtained with a more compact wave function (168 vs 266 CSFs). Secondly, and more importantly, a lower DMC energy is attained (for a smaller expansion size) if one starts with a fully optimized wave function (0.0050, Jas-6+MO+CI). Note, however, that the DMC energy of -75.9158(5) $E_{\rm h}$ is not significantly better than the CIPSI-Jas (168 CSFs, Jas-6+MO+CI) DMC energy of -75.9151(5) $E_{\rm h}$ although it contains more CSFs.

For the larger initial expansion (0.0025) at the Jas-6+CI *Initial opt level*, a Jas-sCI DMC energy of -75.9161(5), that is lower than the DMC CIPSI-Jas energy (-75.9151(5)), but that is similar to the one of the initially fully optimized Jas-sCI wave function (0.0025, Jas-6+MO+CI) (-75.9162(5)), is obtained. This result shows that it might not be necessary to make the CSF selection with improved orbitals, since the MO optimization after the final Jas-sCI iteration might be able to compensate for the effect of improved initial orbitals. This implies that it might be possible to design an iterative Jas-sCI algorithm without needing to (costly) optimize the MOs at each iteration for the selection of the CSFs.

Tab. 7.10: VMC and DMC energies in E_h for different wave function ansatzes. The expansions were truncated at 168 CSFs. For the CIPSI-Jas wave function, the Jastrow, MO, and CI parameters were optimized. For the Jas-sCI entries, the CIPSI wave functions for different thresholds (see *Initial cutoff*) as well as different optimization levels (see *Initial opt level*) were truncated (to 168 CSFs) and fully re-optimized. The initial orbitals—used for the CIPSI calculation—are Hartree-Fock orbitals.

	Initial cutoff (# CSFs)	Initial opt level	E _{VMC} (Jas-6+MO+CI)	E _{DMC} (Jas-6+MO+CI)
CIPSI-Jas/HF			-75.8937(3)	-75.9151(5)
Jas-sCI/HF	0.0050 (266)	Jas-6+CI Jas-6+MO+CI	-75.8941(3) -75.8951(3)	-75.9154(5) -75.9165(5)
Jas-sCI/HF	0.0025 (528)	Jas-6+CI Jas-6+MO+CI	-75.8941(3) -75.8946(3)	-75.9161(5) -75.9162(5)

Having observed an improvement in the energy for some Jas-sCI approaches, the respective wave functions are to be investigated in more detail, trying to gain more insight into how the selections are different from one another. The CIPSI and the (0.0050, Jas-6+MO+CI) Jas-sCI selections differ by 36 of the total 168 CSFs. When analyzing the occupation of these CSFs, no systematic preference can be deduced. For the Jas-sCI se-

lection, configurations that include excitations e.g. out of orbital $2a_g$ are removed while CSFs with excitations into orbitals $1b_{3g}$ and $1b_{2g}$ (primarily from $1b_{2u}$ and $1b_{3u}$) are introduced into the wave function. The orbitals are illustrated in Figs. 7.10 and 7.11.

Tailoring CIPSI expansions has been successfully done in various studies^[235,239–243], corroborating the promising nature of the CIPSI-Jastrow approach. In these studies, it was yet never tried to go beyond the CIPSI selection. The findings of this study emphasize, however, the importance of choosing the expansion in the presence of the Jastrow factor, which is why, in a next step, further investigations, see 7.4, are based on expanding (small) VMC optimized wave functions by generating new CSFs rather than reducing the size of existing expansions.

7.3.9 Computational Approach

Some insight on the problems, more precisely on the handling of the symmetry, that arise for the computation of diatomic systems is given in appendix C. The CIPSI calculations were performed using the QUANTUM PACKAGE^[261] software which works in the basis of SDs. The use of CSFs is judged preferable because firstly, they have the advantage of being eigenfunctions of the \hat{S}^2 operator and secondly, the smaller expansions allow for less expensive CI coefficient optimizations with VMC. The spatial symmetries are included as well in the construction of the CSFs. It should be noted, however, that QUANTUM PACKAGE works with spin-adapted wave functions which are obtained by adding all missing determinants—needed to have eigenfunctions of \hat{S}^2 —to the internal space. Since QUANTUM PACKAGE does not handle symmetry, which is necessary for the generation of CSFs with spatial symmetry, the HF orbitals were generated with GAMESS^[221] in D_{2h} . The 1s orbitals were kept frozen for the CIPSI calculations. The experimentally derived equilibrium distance of 1.243 Å from Huber and Herzberg^[247] was used. All calculations were performed using the Slater-type triple- ζ all-electron basis set TZPae^[244] by van Lenthe and Baerends. Each Slater-type basis function was expanded into 14 primitive Gaussian-type functions^[245,246] for the GAMESS and QUAN-TUM PACKAGE^[261] calculations. The CIPSI wave function was truncated at different thresholds, namely 0.0100, 0.0075, 0.0050, and 0.0025 (additional cutoff of 0.0010 for the dissociation energy). The thresholds correspond to the absolute value of the CI coefficients. The QMC calculations were performed within the Slater basis using the electronic structure program AMOLQC.^[67] Two different Jastrow factors—denoted sm444 and sm666 in Ref. 60—with cusp-less three-particle terms were chosen for the calculations.^[59] The Jastrow factors are denoted Jas-4 and Jas-6, respectively, throughout this study.

The Jastrow, MO, and CI parameters were partially and fully optimized within the VMC framework using the linear^[70] or the stabilized Newton^[74] method as described in Ref. 66. For the optimization of the molecular orbitals, the following rotations were considered: doubly to partially occupied, doubly occupied to virtual, partially occupied to virtual, as well as partially to partially occupied. Partially occupied refers to orbitals that are occupied only in some of the CSFs (cf. active orbitals in CASSCF).

DMC calculations were performed with four different time steps ($\tau = 0.001, 0.002, 0.005, 0.007$ a.u.) for each wave function and the energies were extrapolated to a zero time step. The extrapolation was performed using a quadratic model.^[218] The SDs were converted to CSFs for each threshold and the calculations were repeated.

The bond dissociation energy of C_2 was calculated for each cutoff at DMC level, using the fully optimized guide functions for C and C_2 , respectively. The dissociation energies were first-order spin-orbit corrected. The first-order SO correction for the carbon atom was derived from experimental splittings.^[135] C_2 being a closed-shell system, its first-order SO correction is equal to zero.

For the evaluation of the orbital choice, different sets of initial orbitals are compared, namely Kohn-Sham (using the PBE0^[37,38] and the B3LYP^[34–36], with the VWN(III)^[217] local correlation energy, functionals) and CAS(8,8) orbitals. The computational procedure is identical to the one described for the HF orbitals.

7.4 Jastrow-sCI Scheme

In this final part, an sCI scheme that selects the CSFs based on their energetic contribution to the wave function in the presence of a Jastrow correlation function is introduced.

In 2017, Per and Cleland^[248] presented an energy-based truncation scheme for the use in QMC. In their work, the authors focused on truncating large CI expansions and testing—very successfully so—the truncation method for a variety of small systems within the DMC framework. Our objective is to use the same truncation scheme as

a basis for an sCI scheme in the presence of the Jastrow factor. We aim, however, at extending—rather than reducing—the CI expansions.

In order to determine the energy contribution of the CSF Φ_I , the following wave function—with Ψ_0 as the initial wave function—is defined:

$$\Psi_I = \Psi_0 - c_I \Phi_I. \tag{7.2}$$

In the sCI scheme presented in section 7.2, the second-order perturbative energy was computed exclusively using the given CSF. The advantage of employing the wave function form presented in Eq. (7.2) for the evaluation of the energetic contribution lies within Ψ_0 and Ψ_I being very similar, they only differ by a single CSF. This enables a very accurate determination of the energy contribution through correlated sampling using QMC.

The energy of the initial wave function E_0 as well as the one of Ψ_I , denoted as E_I , are determined—using a sample of size N—as follows:

$$E_0 = \frac{1}{N} \sum_{i}^{N} \frac{\hat{H} \Psi_0(\mathbf{x}_i)}{\Psi_0(\mathbf{x}_i)}$$
 (7.3)

$$E_I = \frac{1}{N} \sum_{i}^{N} \frac{|\Psi_I(\mathbf{x}_i)|^2}{|\Psi_0(\mathbf{x}_i)|^2} \frac{\hat{H}\Psi_I(\mathbf{x}_i)}{\Psi_I(\mathbf{x}_i)}.$$
 (7.4)

Finally, the energy contribution of the *I*-th CSF can be evaluated:

$$\delta e_I = E_0 - E_I. \tag{7.5}$$

The algorithm, adopted for the Jas-sCI scheme, can be outlined as follows:

- 1. Start with a determinant or a set of determinants.
- 2. Generate all possible single and double excitations, abiding by the symmetry requirements of the considered state.

- 3. Convert the determinants to CSFs (to avoid spin contamination).
- 4. Optimize the Jastrow and CI parameters with VMC.
- 5. Determine the energy contributions according to Eq. (7.5).
- 6. Retain the CSFs with an energy contribution larger than a certain threshold.
- 7. Re-expand the CSFs into determinants.
- 8. Go back to 2. and repeat until the stop criterion is reached.

The Jas-sCI scheme is tested for the $^{1}\Sigma_{g}^{+}$ ground state of C_{2} , using the experimental equilibrium bond distance of 1.243 Å from Huber and Herzberg^[247]. The starting wave function is the HF determinant, computed using the Slater-type triple- ζ all-electron basis set TZPae^[244] by van Lenthe and Baerends. Each Slater-type basis function was expanded into 14 primitive Gaussian-type functions^[245,246] for the HF calculation with MOLPRO^[216]. The Slater basis was used for the QMC calculations. An sm666 Jastrow factor, see earlier, was employed. The core orbitals were excluded for the generation of the excited determinants.

In the first sCI iteration, ten virtual orbitals (up to orbital 16) were used for the excitations, resulting in a wave function with 86 CSFs. The energy contribution threshold for the second iteration was set to 1 m $E_{\rm h}$, yielding a wave function containing 61 CSFs (246 determinants). To maintain computational feasibility, only determinants with coefficients greater than 0.05 in absolute value (14 out of the 246) were considered for generating the single and double excitations. Five additional virtual orbitals (up to orbital 21) were included for the excitations. Following the basis transformation, the resulting wave function comprised 1765 CSFs. The energy threshold for the third iteration was kept at 1 m $E_{\rm h}$, resulting in a wave function with 471 CSFs (3080 determinants). The same threshold (0.05) for the generation of the excited determinants was upheld for the excitations, while five additional orbitals were included (up to orbital 26). The final wave function comprised 3450 CSFs.

Tab. 7.11 compares the Jas-sCI VMC energies with the CIPSI-Jastrow counterparts for different expansion sizes. The latter results are taken from section 7.3. First, it is important to note that the proposed Jas-sCI scheme, in contrast to the CIPSI approach, is designed to undergo only very few iterations due to the computational expenses associ-

ated with the QMC optimizations. Three iterations are considered sufficient as they—in theory—already incorporate six-fold excitations. The energy of a CIPSI-Jastrow wave function with 85 CSFs is about 15 m $E_{\rm h}$ lower than the one obtained for the first Jas-sCI iteration, despite both wave functions having similar expansion sizes. This discrepancy is expected since the CSFs in CIPSI are chosen based on their energetic contributions, whereas the first Jas-sCI step only includes singly and doubly excited determinants. In the second iteration, a decrease in energy compared to the first iteration is observed. However, the number of CSFs increases significantly and what is more, a CIPSI-Jastrow wave function with only 266 CSFs provides a lower VMC energy. The difference in energy can be attributed to the occupancy of the virtual orbitals. In the Jas-sCI wave function, orbital 21 constitutes the highest occupied orbital, whereas in the CIPSI-Jastrow counterpart, orbital 33 is already occupied.

Tab. 7.11: VMC energies in E_h for different wave function ansatzes. The Jastrow and CI parameters were optimized. An sm666 Jastrow factor was used.

Ansatz	# CSFs	E _{VMC}	# CSFs	$E_{ m VMC}$
CIPSI-Jas	85	-75.8705(3)	266	-75.8863(3)
Jas-sCI	Iteı	ration 1	Iteı	ration 2
	86	-75.8568(2) ^a	1765	-75.8795(2)

^a Only single and double excitations out of the HF determinant.

Let us, now, delve into the discussion of the two sCI schemes within the much more accurate DMC framework. Tab. 7.12 presents the DMC energies for Jas-sCI and CIPSI-Jastrow with different expansion sizes. As anticipated, when comparing the first Jas-sCI iteration with the smallest CIPSI-Jastrow wave function, it is expected that the latter would yield a superior nodal surface. This outcome aligns with the explanations provided during the discussion of the VMC energies. Moving on to the second iteration, the DMC energy computed using the Jas-sCI scheme—now also energy-based—is approximately $2 \text{ m}E_{\text{h}}$ higher than the CIPSI-Jastrow counterpart, despite the latter having a considerably smaller expansion size. This observation is consistent with the VMC results, indicating that excitations into higher-lying orbitals are important for achieving accurate nodal surfaces.

We decided to dispense with the optimization of the final wave function (third iteration) since it includes 3450 CSFs. The exponential growth in the number of CSFs constitutes a major challenge and renders the presented Jas-sCI scheme impracticable. The aim would be to design an algorithm that scales linearly or maybe quadratically with the

Tab. 7.12: DMC energies in E_h for different wave function ansatzes. The Jastrow and CI parameters were optimized. A time step of $\tau = 0.001$ a.u. was used.

Ansatz	# CSFs	$E_{\rm DMC}$	# CSFs	E_{DMC}
CIPSI-Jas	85	-75.9081(3)	266	-75.9145(3)
Jas-sCI	Ite	ration 1	Iteı	ration 2
Juo 001	86	-75.9026(3)	1765	-75.9121(3)

number of CSFs. And although it was shown that the Jas-sCI scheme—in principle works, the results, particularly when compared with the CIPSI selection of the CSFs, are in need of improvement. The sheer amount of excited determinants, generated already in the second iteration step for a small number of selector determinants, leads to computationally expensive CI optimizations with QMC for wave functions that contain a lot of configurational "deadwood" [24], referring to CSFs that will ultimately be discarded in the sCI process. A significant issue arises from the fact that these generated determinants lack coefficients, making it impossible to perform a pre-selection. Consequently, energy contributions must be computed for numerous (unimportant) CSFs, resulting in computationally intensive calculations since the sample has to be re-evaluated for each energy contribution. Additionally, in order to keep the problem size at bay, the number of virtual orbitals used for the excitations needs to be restricted, leading to the omission of important excitations into higher-lying orbitals, as described earlier. One potential solution to address these challenges is to employ the CIPSI determinants instead of considering all possible singly and doubly excited determinants for the Jas-sCI scheme. For example, in the case of C₂, the CIPSI wave function contains in the given basis—roughly two million determinants. One could thus adapt the algorithm to select determinants from this pool, which would correspond to a pre-selection of the determinants based on their energetic contributions. This could potentially enhance the efficiency of the Jas-sCI scheme and one would not have to dispense with the effect of the Jastrow factor on the configuration selection. Finally, one could make use of the results presented in section 7.1 and only optimize parts of the CI coefficients while scaling the remaining ones with a pre-determined factor, thereby reducing the computational cost of the optimization steps.

8 Conclusion

"Adventure is out there." – *Up*

This thesis is dedicated to the investigation of systems characterized by strong multireference character. The goal is to evaluate how to best—in terms of method optimization, but also method development—capture both, the static and dynamic electron correlation, an endeavor that has engaged scientists since the early days of quantum mechanics. Quantum Monte Carlo (QMC) techniques, specifically variational Monte Carlo (VMC) and diffusion Monte Carlo (DMC), are employed as the methods of choice in this work.

In the first part of the thesis, an exhaustive study of transition metal dimers, including hydrogen, first-row, and second-row elements, is conducted, with a particular emphasis on the electronic dissociation energy. Slater-Jastrow wave functions are constructed based on initial full valence complete active space (CAS) wave functions, whereas HF and KS determinants are utilized for the single-reference approaches. Partial or full optimization of the Jastrow, orbital, and CI parameters is carried out to minimize the variational energy, followed by DMC calculations. The results reveal that while the single-reference approaches yield poor outcomes, the accuracy of both absolute and dissociation energies in MR-DMC is improved by incorporating more sets of parameters in the VMC optimization. The key factor contributing to this improvement is the optimization of molecular orbitals (MOs) in the presence of the Jastrow factor. Additionally, a comparison is made between two different types of ECPs, which generally result in similar dissociation energies. Overall, the MR-DMC dissociation energies exhibit good agreement with highly accurate experimental data for the majority of the systems investigated. Furthermore, it is found that MR-DMC mostly outperforms CC and DFT in terms of accuracy. A further assessment of the MR-DMC approach is accomplished by evaluating spectroscopic constants extracted from Morse fits to the MR-DMC potential energy curves. The MR-DMC constants agree well with experimental

and theoretical data. These findings collectively demonstrate the ability of MR-DMC to provide accurate dissociation energies and other properties of transition metal compounds using compact wave functions.

The second part of the thesis focuses on evaluating existing and developing new selected configuration interaction (sCI) approaches. Specifically, the C₂ molecule is investigated in its ${}^{1}\Sigma_{\sigma}^{+}$ ground state. First, the circumstances under which the optimization of the CI coefficients with QMC can be avoided are discussed. In addition, an sCI approach incorporating the Jastrow factor based on the linear optimization method is explored. The ansatz presents, however, several challenges. Furthermore, a rigorous analysis of C₂ is conducted using VMC-optimized truncated CIPSI-Jastrow wave functions, where the truncation is based on the absolute value of the CI coefficients. The inclusion of the Jastrow correlation function results in lower VMC and DMC energies compared to pure CIPSI expansions, demonstrating the legitimacy of using the Jastrow factor to account for short-range dynamic electron correlation. Accurate absolute and dissociation energies are obtained using the CIPSI-Jastrow-DMC approach. The study reveals significant changes in the CI picture in the presence of the Jastrow factor. The impact of the choice of initial orbitals, ranging from HF to KS and CASSCF, on the VMC and DMC energies is also discussed. It is found that the CASSCF orbitals are favored. The key finding of the study is, however, that by selecting CSFs in the presence of the Jastrow correlation function, lower energies can be achieved with the same expansion size compared to the CIPSI selection. Finally, a new Jastrow-sCI scheme, utilizing an energy contribution criterion, is proposed and its effectiveness is evaluated for C_2 . The main difficulty of the approach lies in dealing with the substantial number of excited determinants, generated in each iteration step. Different strategies to improve the scheme are discussed.

Bibliography

- [1] D. P. Tew, W. Klopper, T. Helgaker, *Journal of Computational Chemistry* **2007**, 28, 1307–1320.
- [2] W. Heitler, F. London, Zeitschrift für Physik 1927, 44, 455–472.
- [3] E. A. Hylleraas, Zeitschrift für Physik **1929**, 54, 347–366.
- [4] D. R. Hartree, W. Hartree, B. Swirles, *Philosophical Transaction of the Royal Society of London. Series A. Mathematical and Physical Sciences* **1939**, 238, 229–247.
- [5] K. D. Vogiatzis, D. Ma, J. Olsen, L. Gagliardi, W. A. D. Jong, *The Journal of Chemical Physics* **2017**, 147, 184111.
- [6] D. S. Levine, D. Hait, N. M. Tubman, S. Lehtola, K. B. Whaley, M. Head-Gordon, *Journal of Chemical Theory and Computation* **2020**, *16*, 2340–2354.
- [7] E. Ramos-Cordoba, P. Salvador, E. Matito, *Physical Chemistry Chemical Physics* **2016**, *18*, 24015–24023.
- [8] C. J. Stein, V. V. Burg, M. Reiher, *Journal of Chemical Theory and Computation* **2016**, 12, 3764–3773.
- [9] C. L. Benavides-Riveros, N. N. Lathiotakis, M. A. Marques, *Physical Chemistry Chemical Physics* **2017**, *19*, 12655–12664.
- [10] A. Lüchow, WIREs Computational Molecular Science 2011, 1, 388–402.
- [11] B. M. Austin, D. Y. Zubarev, W. A. Lester, Chemical Reviews 2012, 112, 263–288.
- [12] M. Born, Zeitschrift für Physik **1926**, 38, 803–827.

- [13] E. Schrödinger, *Physical Review* **1926**, 28, 1049–1070.
- [14] L. Piela, *Ideas of Quantum Chemistry 2nd ed.*, Elsevier, **2014**.
- [15] M. Born, R. Oppenheimer, Annalen der Physik 1927, 389, 457–484.
- [16] D. R. Hartree, *Mathematical Proceedings of the Cambridge Philosophical Society* **1928**, 24, 89–110.
- [17] V. Fock, Zeitschrift für Physik **1930**, 61, 126–148.
- [18] C. C. J. Roothaan, Reviews of Modern Physics 1951, 23, 69–89.
- [19] G. G. Hall, Proceedings of the Royal Society of London. Series A. Mathematical and Physical Sciences **1951**, 205, 541–552.
- [20] R. McWeeny, Proceedings of the Royal Society of London. Series A. Mathematical and Physical Sciences **1955**, 232, 114–135.
- [21] T. Helgaker, P. Jørgensen, J. Olsen, *Molecular Electronic-Structure Theory*, John Wiley & Sons Ltd, **2000**.
- [22] B. Roos, P. R. Taylor, P. E. M. Siegbahn, *Chemical Physics* **1980**, 48, 157–173.
- [23] J. Ludovicy, Master's thesis, RWTH Aachen University, 2018.
- [24] J. Ivanic, K. Ruedenberg, Theoretical Chemistry Accounts 2001, 106, 339–351.
- [25] G. H. Booth, A. J. W. Thom, A. Alavi, *The Journal of Chemical Physics* **2009**, 131, 054106.
- [26] N. M. Tubman, J. Lee, T. Y. Takeshita, M. Head-Gordon, K. B. Whaley, *The Journal of Chemical Physics* **2016**, *145*, 044112.
- [27] A. A. Holmes, N. M. Tubman, C. J. Umrigar, Journal of Chemical Theory and Computation 2016, 12, 3674–3680.
- [28] B. Huron, J.-P. Malrieu, P. Rancurel, *The Journal of Chemical Physics* **1973**, *58*, 5745–5759.

- [29] S. Evangelisti, J.-P. Daudey, J.-P. Malrieu, Chemical Physics 1983, 75, 91–102.
- [30] P. S. Epstein, *Physical Review* **1926**, 28, 695–710.
- [31] R. K. Nesbet, *Proceedings of the Royal Society of London. Series A. Mathematical and Physical Sciences* **1955**, 230, 312–321.
- [32] P. Hohenberg, W. Kohn, *Physical Review B* **1964**, 136, B864–B871.
- [33] W. Kohn, L. J. Sham, Physical Review 1965, 140, A1133-A1138.
- [34] A. D. Becke, *Physical Review A* **1988**, *38*, 3098–3100.
- [35] C. Lee, W. Yang, R. G. Parr, *Physical Review B* **1988**, *37*, 785–789.
- [36] A. Becke, The Journal of Chemical Physics 1993, 98, 5648–5652.
- [37] J. P. Perdew, K. Burke, M. Ernzerhof, *Physical Review Letters* **1996**, 77, 3865–3868.
- [38] C. Adamo, V. Barone, The Journal of Chemical Physics 1999, 110, 6158–6170.
- [39] D. C. Clary, N. C. Handy, *Physical Review A* **1976**, 14, 1607–1613.
- [40] T. Kato, Communications on Pure and Applied Mathematics 1957, 10, 151–177.
- [41] L. Kong, F. A. Bischoff, E. F. Valeev, Chemical Reviews 2012, 112, 75–107.
- [42] W. Kutzelnigg, W. Klopper, The Journal of Chemical Physics 1991, 94, 1985–2001.
- [43] H. Fliegl, W. Klopper, C. Hättig, The Journal of Chemical Physics 2005, 122, 084107.
- [44] H. Fliegl, C. Hättig, W. Klopper, *International Journal of Quantum Chemistry* **2006**, 106, 2306–2317.
- [45] T. B. Adler, G. Knizia, H. J. Werner, The Journal of Chemical Physics 2007, 127, 221106.
- [46] R. J. Gdanitz, Chemical Physics Letters **1993**, 210, 253–260.
- [47] R. J. Gdanitz, Chemical Physics Letters **1998**, 283, 253–261.

- [48] S. Ten-no, Chemical Physics Letters 2007, 447, 175–179.
- [49] H. Luo, A. Alavi, Journal of Chemical Theory and Computation 2018, 14, 1403–1411.
- [50] A. J. Cohen, H. Luo, K. Guther, W. Dobrautz, D. P. Tew, A. Alavi, *The Journal of Chemical Physics* **2019**, *151*, 8–13.
- [51] B. L. Hammond, J. W. A. Lester, P. J. Reynolds, *Monte Carlo methods in ab initio quantum chemistry*, World Scientific, **1994**.
- [52] W. M. C. Foulkes, L. Mitas, R. J. Needs, G. Rajagopal, *Reviews of Modern Physics* **2001**, 73, 33–83.
- [53] N. Metropolis, A. W. Rosenbluth, M. N. Rosenbluth, A. H. Teller, E. Teller, *The Journal of Chemical Physics* **1953**, *21*, 1087–1092.
- [54] W. K. Hastings, Biometrika 1970, 57, 97–109.
- [55] C. J. Umrigar, M. P. Nightingale, K. J. Runge, *The Journal of Chemical Physics* **1993**, 99, 2865–2890.
- [56] R. Jastrow, *Physical Review* **1955**, *98*, 1479–1484.
- [57] C. J. Huang, C. J. Umrigar, M. P. Nightingale, *The Journal of Chemical Physics* **1997**, 107, 3007–3013.
- [58] S. F. Boys, N. C. Handy, *Proceedings of the Royal Society A* **1969**, 310, 63–78.
- [59] A. D. Güçlü, G. S. Jeon, C. J. Umrigar, J. K. Jain, *Physical Review B* **2005**, 72, 1–6.
- [60] A. Lüchow, A. Sturm, C. Schulte, K. Haghighi Mood, *The Journal of Chemical Physics* **2015**, *142*, 084111.
- [61] K. E. Schmidt, J. W. Moskowitz, *The Journal of Chemical Physics* **1990**, 93, 4172–4178.
- [62] M. Kotani, A. Amemiya, E. Ishiguro, T. Kimura, *Tables of Molecular Integrals*, Maruzen Co., **1963**.
- [63] R. Pauncz, Spin Eigenfunctions: Construction and Use, Springer, 1979.

- [64] J. H. V. Vleck, A. Sherman, Reviews of Modern Physics 1935, 7, 167–228.
- [65] P. J. Reynolds, D. M. Ceperley, B. J. Alder, W. A. Lester, *The Journal of Chemical Physics* **1982**, *77*, 5593–5603.
- [66] J. Toulouse, C. J. Umrigar, The Journal of Chemical Physics 2007, 126, 084102.
- [67] A. Lüchow, S. Manten, C. Diedrich, A. Bande, T. C. Scott, A. Schwarz, R. Berner, R. Petz, A. Sturm, M. Hermsen, K. Haghighi Mood, C. Schulte, L. Reuter, M. A. Heuer, J. Ludovicy, *Amolgc v7.1.0 ed.*, **2021**.
- [68] J. E. Dennis, D. M. Gay, R. E. Welsch, ACM Transactions on Mathematical Software 1981, 7, 369–383.
- [69] A. Cuzzocrea, A. Scemama, W. J. Briels, S. Moroni, C. Filippi, *Journal of Chemical Theory and Computation* **2020**, *16*, 4203–4212.
- [70] M. P. Nightingale, V. Melik-Alaverdian, Physical Review Letters 2001, 87, 043401.
- [71] C. J. Umrigar, J. Toulouse, C. Filippi, S. Sorella, R. G. Hennig, *Physical Review Letters* **2007**, *98*, 110201.
- [72] L. Zhao, E. Neuscamman, Journal of Chemical Theory and Computation 2017, 13, 2604–2611.
- [73] X. Lin, H. Zhang, A. M. Rappe, *The Journal of Chemical Physics* **2000**, 112, 2650–2654.
- [74] C. J. Umrigar, C. Filippi, *Physical Review Letters* **2005**, 94, 150201.
- [75] S. Sorella, *Physical Review B* **2005**, 71, 241103.
- [76] A. Scemama, C. Filippi, *Physical Review B* **2006**, 73, 241101.
- [77] S. Sorella, *Physical Review B* **2001**, *64*, 024512.
- [78] K. Haghighi Mood, Ph.D. thesis, RWTH Aachen University, 2018.
- [79] A. Lüchow, J. B. Anderson, Annual review of Physical Chemistry 2000, 51, 501–526.

- [80] H. F. Trotter, Proceedings of the American Mathematical Society 1959, 10, 545–551.
- [81] M. Suzuki, Communications in Mathematical Physics 1976, 51, 183–190.
- [82] R. Assaraf, M. Caffarel, A. Khelif, Physical Review E 2000, 61, 4566–4575.
- [83] J. A. Pople, Reviews of Modern Physics 1999, 71, 1267–1274.
- [84] D. M. Ceperley, Journal of Statistical Physics 1986, 43, 815–826.
- [85] W. J. Stevens, M. Krauss, H. Basch, P. G. Jasien, *Canadian Journal of Chemistry* **1992**, 70, 612–630.
- [86] W. J. Stevens, H. Basch, M. Krauss, *The Journal of Chemical Physics* **1984**, *81*, 6026–6033.
- [87] M. Dolg, U. Wedig, H. Stoll, H. Preuss, The Journal of Chemical Physics 1987, 86, 866–872.
- [88] W. M. C. Foulkes, L. Mitas, R. J. Needs, G. Rajagopal, *The Journal of Chemical Physics* **1991**, *95*, 3467–3475.
- [89] V. I. Lebedev, USSR Computational Mathematics and Mathematical Physics 1975, 15, 44–51.
- [90] V. I. Lebedev, USSR Computational Mathematics and Mathematical Physics **1976**, 16, 10–24.
- [91] B. L. Hammond, P. J. Reynolds, W. A. Lester, *The Journal of Chemical Physics* **1987**, 87, 1130–1136.
- [92] L. Mitas, *Physical Review A* **1994**, 49, 4411–4414.
- [93] H.-J. Flad, M. Dolg, The Journal of Chemical Physics 1997, 107, 7951–7959.
- [94] R. J. Needs, M. D. Towler, N. D. Drummond, P. L. Ríos, *Journal of Physics: Condensed Matter* **2010**, 22, 023201.
- [95] M. Casula, *Physical Review B* **2006**, 74, 161102.

- [96] M. Casula, S. Moroni, S. Sorella, C. Filippi, *The Journal of Chemical Physics* **2010**, 132, 154113.
- [97] M. Burkatzki, C. Filippi, M. Dolg, The Journal of Chemical Physics 2007, 126, 234105.
- [98] M. Burkatzki, C. Filippi, M. Dolg, The Journal of Chemical Physics 2008, 129, 164115.
- [99] M. C. Bennett, G. Wang, A. Annaberdiyev, C. A. Melton, L. Shulenburger, L. Mitas, *The Journal of Chemical Physics* **2018**, 149, 104108.
- [100] A. Annaberdiyev, G. Wang, C. A. Melton, M. C. Bennett, L. Shulenburger, L. Mitas, *The Journal of Chemical Physics* **2018**, *149*, 134108.
- [101] M. C. Bennett, C. A. Melton, A. Annaberdiyev, G. Wang, L. Shulenburger, L. Mitas, *The Journal of Chemical Physics* **2017**, *147*, 224106.
- [102] G. B. Bachelet, D. M. Ceperley, M. G. B. Chiocchetti, *Physical Review Letters* **1989**, 62, 2088–2091.
- [103] W. M. C. Foulkes, M. Schluter, Physical Review B 1990, 42, 11505–11529.
- [104] M. C. Bennett, F. A. Reboredo, L. Mitas, J. T. Krogel, *Journal of Chemical Theory and Computation* **2022**, *18*, 828–839.
- [105] J. Ludovicy, K. Haghighi Mood, A. Lüchow, *Journal of Chemical Theory and Computation* **2019**, *15*, 5221–5229.
- [106] E. I. Stiefel in *Transition Metal Sulfur Chemistry*, Vol. 653, E. I. Stiefel, K. Matsumoto (Eds.), American Chemical Society, **1996**, pp. 2–38.
- [107] S. Xiao, X. Li, W. Sun, B. Guan, Y. Wang, Chemical Engineering Journal 2016, 306, 251–259.
- [108] E. L. Kunkes, F. Studt, F. Abild-Pedersen, R. Schlögl, M. Behrens, *Journal of Catalysis* **2015**, 328, 43–48.
- [109] H. Eshghi, M. Rahimizadeh, S. Saberi, *Catalysis Communications* **2008**, 9, 2460–2466.

- [110] C. Angeli, R. Cimiraglia, Molecular Physics 2011, 109, 1503–1509.
- [111] W. Jiang, N. J. Deyonker, A. K. Wilson, *Journal of Chemical Theory and Computation* **2012**, *8*, 460–468.
- [112] W. Zhang, D. G. Truhlar, M. Tang, Journal of Chemical Theory and Computation 2013, 9, 3965–3977.
- [113] X. Xu, W. Zhang, M. Tang, D. G. Truhlar, Journal of Chemical Theory and Computation 2015, 11, 2036–2052.
- [114] L. Cheng, J. Gauss, B. Ruscic, P. B. Armentrout, J. F. Stanton, *Journal of Chemical Theory and Computation* **2017**, *13*, 1044–1056.
- [115] Y. A. Aoto, A. P. D. L. Batista, A. Köhn, A. G. D. Oliveira-Filho, *Journal of Chemical Theory and Computation* **2017**, *13*, 5291–5316.
- [116] Y. Zhao, D. G. Truhlar, The Journal of Chemical Physics 2006, 125, 194101.
- [117] M. Fuchs, Y.-M. Niquet, X. Gonze, K. Burke, *The Journal of Chemical Physics* **2005**, 122, 094116.
- [118] M. Musia, A. Perera, R. J. Bartlett, The Journal of Chemical Physics 2011, 134, 114108.
- [119] Z. Fang, M. Vasiliu, K. A. Peterson, D. A. Dixon, Journal of Chemical Theory and Computation 2017, 13, 1057–1066.
- [120] L. K. Wagner, L. Mitas, The Journal of Chemical Physics 2007, 126, 034105.
- [121] R. Petz, A. Lüchow, ChemPhysChem 2011, 12, 2031–2034.
- [122] C. Diedrich, A. Lüchow, S. Grimme, *The Journal of Chemical Physics* **2005**, 122, 021101.
- [123] L. Horváthová, M. Dubecký, L. Mitas, I. Štich, *Journal of Chemical Theory and Computation* **2013**, 9, 390–400.
- [124] K. Doblhoff-Dier, J. Meyer, P. E. Hoggan, G. J. Kroes, L. K. Wagner, *Journal of Chemical Theory and Computation* **2016**, 12, 2583–2597.

- [125] K. Haghighi Mood, A. Lüchow, *The Journal of Physical Chemistry A* **2017**, 121, 6165–6171.
- [126] J. H. Walker, T. E. Walker, H. P. Kelly, The Journal of Chemical Physics 1972, 57, 2080–2086.
- [127] P. K. Carroll, P. McCormack, The Astrophysical Journal 1972, 177, L33–L36.
- [128] R. R. Smith, *Proceedings of the Royal Society of London. A. Mathematical and Physical Sciences* **1973**, 332, 113–127.
- [129] J. J. Harrison, J. M. Brown, The Astrophysical Journal 2008, 686, 1426–1431.
- [130] R. J. Hargreaves, K. H. Hinkle, C. W. Bauschlicher, S. Wende, A. Seifahrt, P. F. Bernath, *The Astronomical Journal* **2010**, *140*, 919–924.
- [131] J. M. Brown, H. Körsgen, S. P. Beaton, K. M. Evenson, *The Journal of Chemical Physics* **2006**, 124, 234309.
- [132] D. Shulyak, A. Reiners, S. Wende, O. Kochukhov, N. Piskunov, A. Seifahrt, *Astronomy & Astrophysics* **2010**, 523, A37.
- [133] S. P. Beaton, K. M. Evenson, T. Nelis, J. M. Brown, *The Journal of Chemical Physics* **1988**, *89*, 4446–4448.
- [134] P. M. Morse, *Physical Review* **1929**, 34, 57–64.
- [135] A. Kramida, Y. Ralchenko, J. Reader, and NIST ASD Team, NIST Atomic Spectra Database (ver. 5.9), [Online]. Available: https://dx.doi.org/10.18434/T4W30F [2022, October 5]. National Institute of Standards and Technology, Gaithersburg, MD, 2021.
- [136] R. H. Schultz, P. B. Armentrout, *The Journal of Chemical Physics* **1991**, 94, 2262–2268.
- [137] K. P. Jensen, B. O. Roos, U. Ryde, The Journal of Chemical Physics 2007, 126, 014103.
- [138] N. J. DeYonker, W. D. Allen, The Journal of Chemical Physics **2012**, 137, 234303.

- [139] J. Shee, B. Rudshteyn, E. J. Arthur, S. Zhang, D. R. Reichman, R. A. Friesner, *Journal of Chemical Theory and Computation* **2019**, *15*, 2346–2358.
- [140] B. Ruscic, R. E. Pinzon, M. L. Morton, G. V. Laszevski, S. J. Bittner, S. G. Nijsure, K. A. Amin, M. Minkoff, A. F. Wagner, *The Journal of Physical Chemistry A* 2004, 108, 9979–9997.
- [141] L. A. Curtiss, P. C. Redfern, K. Raghavachari, V. Rassolov, J. A. Pople, *The Journal of Chemical Physics* **1999**, *110*, 4703–4709.
- [142] R. Peverati, Y. Zhao, D. G. Truhlar, *The Journal of Physical Chemistry Letters* **2011**, 2, 1991–1997.
- [143] S. Beaton, K. Evenson, J. Brown, *Journal of Molecular Spectroscopy* **1994**, *164*, 395–415.
- [144] M. Barnes, A. Merer, G. Metha, Journal of Molecular Spectroscopy 1995, 173, 100–112.
- [145] A. Heimer, Zeitschrift für Physik 1937, 104, 448–457.
- [146] B. L. Kickel, P. B. Armentrout, Journal of the American Chemical Society 1995, 117, 764–773.
- [147] W. Keim, Angewandte Chemie International Edition in English 1990, 29, 235–244.
- [148] K. Tamao, K. Sumitani, M. Kumada, Journal of the American Chemical Society 1972, 94, 4374–4376.
- [149] B. M. Rosen, K. W. Quasdorf, D. A. Wilson, N. Zhang, A. M. Resmerita, N. K. Garg, V. Percec, *Chemical Reviews* **2011**, *111*, 1346–1416.
- [150] Z. Zuo, D. T. Ahneman, L. Chu, J. A. Terrett, A. G. Doyle, D. W. C. Macmillan, *Science* **2014**, *345*, 437–440.
- [151] M. A. Brewster, L. M. Ziurys, *The Astrophysical Journal* **2001**, 559, L163–L166.
- [152] I. Shim, K. A. Gingerich, *Chemical Physics Letters* **1999**, 303, 87–95.

- [153] D. J. Brugh, M. D. Morse, The Journal of Chemical Physics 2002, 117, 10703–10714.
- [154] H.-J. Flad, A. Savin, M. Schultheiss, A. Nicklass, H. Preuss, *Chemical Physics Letters* **1994**, 222, 274–280.
- [155] E. M. Spain, M. D. Morse, The Journal of Physical Chemistry 1992, 96, 2479–2486.
- [156] E. L. Johnson, Q. C. Davis, M. D. Morse, *The Journal of Chemical Physics* **2016**, 144, 234306.
- [157] A. Sevy, R. F. Huffaker, M. D. Morse, *The Journal of Physical Chemistry A* **2017**, 121, 9446–9457.
- [158] D. J. Matthew, E. Tieu, M. D. Morse, The Journal of Chemical Physics 2017, 146, 144310.
- [159] A. Sevy, E. Tieu, M. D. Morse, The Journal of Chemical Physics 2018, 149, 174307.
- [160] D. M. Merriles, E. Tieu, M. D. Morse, The Journal of Chemical Physics 2019, 151, 044302.
- [161] M. D. Morse, Accounts of Chemical Research **2019**, 51, 119–126.
- [162] J. Kolorenč, L. Mitas, Reports on Progress in Physics **2011**, 74, 026502.
- [163] C. J. Stein, M. Reiher, *Journal of Chemical Theory and Computation* **2016**, *12*, 1760–1771.
- [164] C. J. Stein, M. Reiher, *Molecular Physics* **2017**, *115*, 2110–2119.
- [165] B. O. Roos, R. Lindh, P. Malmqvist, V. Veryazov, P.-O. Widmark, *The Journal of Physical Chemistry A* **2004**, *108*, 2851–2858.
- [166] B. O. Roos, R. Lindh, P. Malmqvist, V. Veryazov, P.-O. Widmark, *The Journal of Physical Chemistry A* **2005**, *109*, 6575–6579.
- [167] K. C. Lau, Y. C. Chang, X. Shi, C. Y. Ng, The Journal of Chemical Physics 2010, 133, 114304.
- [168] D. Tzeli, A. Mavridis, *The Journal of Chemical Physics* **2007**, 126, 194304.

- [169] A. C. Borin, L. G. M. de Macedo, Chemical Physics Letters 2004, 383, 53–58.
- [170] S. Goel, A. E. Masunov, *International Journal of Quantum Chemistry* **2011**, 111, 4276–4287.
- [171] M. D. Allen, T. C. Pesch, L. M. Ziurys, *The Astrophysical Journal* **1996**, 472, L57–L60.
- [172] K. Aiuchi, K. Shibuya, Journal of Molecular Spectroscopy 2001, 209, 92–104.
- [173] M. Fujitake, A. Toba, M. Mori, F. Miyazawa, N. Ohashi, K. Aiuchi, K. Shibuya, *Journal of Molecular Spectroscopy* **2001**, 208, 253–270.
- [174] W. J. Balfour, J. Cao, C. V. Prasad, C. X. Qian, *The Journal of Chemical Physics* **1995**, 103, 4046–4051.
- [175] D. J. Brugh, M. D. Morse, The Journal of Chemical Physics 1997, 107, 9772–9782.
- [176] Y.-C. Chang, C.-S. Lam, B. Reed, K.-C. Lau, H. T. Liou, C. Y. Ng, *The Journal of Physical Chemistry A* **2009**, *113*, 4242–4248.
- [177] P. M. Sheridan, L. M. Ziurys, T. Hirano, *The Astrophysical Journal* **2003**, 593, L141–L144.
- [178] K. Aiuchi, K. Tsuji, K. Shibuya, Chemical Physics Letters 1999, 309, 229–233.
- [179] R. L. Hettich, B. S. Freiser, *Journal of the American Chemical Society* **1986**, 108, 2537–2540.
- [180] D. Tzeli, A. Mavridis, The Journal of Chemical Physics 2002, 116, 4901–4921.
- [181] K.-C. Lau, Y.-C. Chang, C.-S. Lam, C. Y. Ng, The Journal of Physical Chemistry A **2009**, 113, 14321–14328.
- [182] D. Tzeli, A. Mavridis, The Journal of Chemical Physics **2010**, 132, 194312.
- [183] Y. Wang, H. Arandiyan, J. Scott, A. Bagheri, H. Dai, R. Amal, *Journal of Materials Chemistry A* **2017**, *5*, 8825–8846.
- [184] Y. Liu, W. Wang, X. Xu, J. P. M. Veder, Z. Shao, *Journal of Materials Chemistry A* **2019**, 7, 7280–7300.

- [185] M. S. Whittingham, Chemical Reviews 2004, 104, 4271–4301.
- [186] H. B. Wu, J. S. Chen, H. H. Hng, X. W. Lou, Nanoscale 2012, 4, 2526–2542.
- [187] M. Zheng, H. Tang, L. Li, Q. Hu, L. Zhang, H. Xue, H. Pang, *Advanced Science* **2018**, *5*, 1700592.
- [188] S. Rühle, A. Y. Anderson, H. N. Barad, B. Kupfer, Y. Bouhadana, E. Rosh-Hodesh, A. Zaban, *The Journal of Physical Chemistry Letters* **2012**, *3*, 3755–3764.
- [189] I. Concina, Z. H. Ibupoto, A. Vomiero, *Advanced Energy Materials* **2017**, 7, 1700706.
- [190] A.-C. Cheung, N. Lee, A. Lyyra, A. Merer, A. Taylor, *Journal of Molecular Spectroscopy* **1982**, *95*, 213–225.
- [191] G. Drechsler, U. Boesl, C. Bäßmann, E. W. Schlag, *The Journal of Chemical Physics* 1997, 107, 2284–2291.
- [192] J. T. Krogel, J. A. Santana, F. A. Reboredo, *Physical Review B* **2016**, 93, 075143.
- [193] C. N. Sakellaris, E. Miliordos, A. Mavridis, *The Journal of Chemical Physics* **2011**, 134, 234308.
- [194] D. A. Chestakov, D. H. Parker, A. V. Baklanov, *The Journal of Chemical Physics* **2005**, 122, 084302.
- [195] M. Li, S.-R. Liu, P. B. Armentrout, The Journal of Chemical Physics 2009, 131, 144310.
- [196] S. Smoes, J. Drowart in *Modern High Temperature Science*, J. L. Margrave (Ed.), Humana Press, **1984**, pp. 31–52.
- [197] Z. Shadike, Y.-N. Zhou, L.-L. Chen, Q. Wu, J.-L. Yue, N. Zhang, X.-Q. Yang, L. Gu, X.-S. Liu, S.-Q. Shi, Z.-W. Fu, *Nature Communications* **2017**, *8*, 566.
- [198] L. Blanc, C. J. Bartel, H. Kim, Y. Tian, H. Kim, A. Miura, G. Ceder, L. F. Nazar, ACS Materials Letters 2021, 3, 1213–1220.
- [199] Q. Shi, Q. Ran, W. Tam, J.-H. Leung, A.-C. Cheung, *Chemical Physics Letters* **2001**, 339, 154–160.

- [200] R. L. Pulliam, L. M. Ziurys, The Journal of Chemical Physics 2010, 133, 174313.
- [201] L. Zhang, Y. Yu, R. Cheng, J. Yang, Spectroscopy Letters 2022, 55, 302–309.
- [202] C. W. Bauschlicher, P. Maitre, Theoretica Chimica Acta 1995, 90, 189–203.
- [203] J. Drowart, A. Pattoret, S. Smoes, *Proceedings of the British Ceramic Society* **1967**, 8, 67–89.
- [204] B. Liang, L. Andrews, The Journal of Physical Chemistry A 2002, 106, 6945–6951.
- [205] K. D. D. Gunaratne, C. Berkdemir, C. L. Harmon, A. W. Castleman, *Physical Chemistry Chemical Physics* **2013**, *15*, 6068–6079.
- [206] N. F. Lindholm, D. J. Brugh, G. K. Rothschopf, S. M. Sickafoose, M. D. Morse, *The Journal of Chemical Physics* **2003**, *118*, 2190–2196.
- [207] A. Vander Auwera-Mahieu, N. S. McIntyre, J. Drowart, *Chemical Physics Letters* **1969**, *4*, 198–200.
- [208] Z. J. Wu, Z. M. Su, The Journal of Chemical Physics **2006**, 124, 184306.
- [209] I. Shim, K. A. Gingerich, *Zeitschrift für Physik D Atoms, Molecules and Clusters* **1990**, *16*, 141–148.
- [210] G. Schoendorff, A. R. Morris, E. D. Hu, A. K. Wilson, *The Journal of Physical Chemistry A* **2015**, *119*, 9630–9635.
- [211] Y. Lee, R. J. Needs, *Physical Review B* **2003**, 67, 035121.
- [212] J. G. Phillips, S. P. Davis, B. Lindgren, W. J. Balfour, *Astrophysical Journal Supplement Series* **1987**, *65*, 721–778.
- [213] M. Dulick, J. C. W. Bauschlicher, A. Burrows, C. M. Sharp, R. S. Ram, P. Bernath, *The Astrophysical Journal* **2003**, *594*, 651–663.
- [214] K. Lipus, T. Nelis, E. Bachem, W. Urban, Molecular Physics 1989, 68, 1171–1177.
- [215] I. E. Gordon, R. J. L. Roy, P. F. Bernath, *Journal of Molecular Spectroscopy* **2006**, 237, 11–18.

- [216] H.-J. Werner, P. J. Knowles, G. Knizia, F. R. Manby, M. Schütz, P. Celani, T. Korona, R. Lindh, A. Mitrushenkov, G. Rauhut, K. R. Shamasundar, T. B. Adler, R. D. Amos, A. Bernhardsson, A. Berning, D. L. Cooper, M. J. O. Deegan, , A. J. Dobbyn, F. Eckert, E. Goll, C. Hampel, A. Hesselmann, G. Hetzer, T. Hrenar, G. Jansen, C. Köoppl, Y. Liu, A. W. Lloyd, R. A. Mata, A. J. May, S. J. McNicholas, W. Meyer, M. E. Mura, A. Nicklass, D. P. O'Neill, P. Palmieri, D. Peng, K. Pflüger, R. Pitzer, M. Reiher, T. Shiozaki, H. Stoll, A. J. Stone, R. Tarroni, T. Thorsteinsson, M. Wang, MOLPRO, version 2015.1, a package of ab initio programs.
- [217] S. H. Vosko, L. Wilk, M. Nusair, Canadian Journal of Physics 1980, 58, 1200–1211.
- [218] A. Lüchow, J. B. Anderson, *The Journal of Chemical Physics* **1996**, 105, 7573–7578.
- [219] S. Fahy, X. W. Wang, S. G. Louie, Physical Review B 1990, 42, 3503–3522.
- [220] H. Nakano, The Journal of Chemical Physics 1993, 99, 7983–7992.
- [221] M. W. Schmidt, K. K. Baldridge, J. A. Boatz, S. T. Elbert, M. S. Gordon, J. H. Jensen, S. Koseki, N. Matsunaga, K. A. Nguyen, S. Su, T. L. Windus, M. Dupuis, J. A. Montgomery, *Journal of Computational Chemistry* 1993, 14, 1347–1363.
- [222] T. Koga, H. Tatewaki, H. Matsuyama, Y. Satoh, *Theoretical Chemistry Accounts* 1999, 102, 105–111.
- [223] T. Noro, M. Sekiya, T. Koga, H. Matsuyama, *Theoretical Chemistry Accounts* **2000**, 104, 146–152.
- [224] J. Ludovicy, R. Dahl, A. Lüchow, Journal of Chemical Theory and Computation 2023, 19, 2792–2803.
- [225] R. J. Buenker, S. D. Peyerimhoff, W. Butscher, Molecular Physics 1978, 35, 771–791.
- [226] H. J. Werner, P. J. Knowles, *The Journal of Chemical Physics* **1988**, *89*, 5803–5814.
- [227] K. Andersson, P. Malmqvist, B. O. Roos, A. J. Sadlej, K. Wolinski, *The Journal of Physical Chemistry* **1990**, *94*, 5483–5488.
- [228] C. Angeli, R. Cimiraglia, S. Evangelisti, T. Leininger, J.-P. Malrieu, *The Journal of Chemical Physics* **2001**, *114*, 10252–10264.

- [229] C. Angeli, R. Cimiraglia, J.-P. Malrieu, Chemical Physics Letters 2001, 350, 297–305.
- [230] C. F. Bender, E. R. Davidson, *The Journal of Chemical Physics* **1968**, 49, 4219–4221.
- [231] R. J. Buenker, S. D. Peyerimhoff, Theoretica chimica acta 1974, 35, 33–58.
- [232] E. Giner, A. Scemama, M. Caffarel, Canadian Journal of Chemistry 2013, 91, 879–885.
- [233] A. Scemama, T. Applencourt, E. Giner, M. Caffarel, *The Journal of Chemical Physics* **2014**, *141*, 244110.
- [234] E. Giner, A. Scemama, M. Caffarel, The Journal of Chemical Physics 2015, 142, 044115.
- [235] E. Giner, R. Assaraf, J. Toulouse, Molecular Physics 2016, 114, 910–920.
- [236] M. Caffarel, T. Applencourt, E. Giner, A. Scemama, ACS Symposium Series 2016, 1234, 15–46.
- [237] A. Scemama, Y. Garniron, M. Caffarel, P.-F. Loos, *Journal of Chemical Theory and Computation* **2018**, *14*, 1395–1402.
- [238] P.-F. Loos, A. Scemama, A. Blondel, Y. Garniron, M. Caffarel, D. Jacquemin, *Journal of Chemical Theory and Computation* **2018**, *14*, 4360–4379.
- [239] S. D. Pineda Flores, E. Neuscamman, *The Journal of Physical Chemistry A* **2019**, 123, 1487–1497.
- [240] M. Dash, J. Feldt, S. Moroni, A. Scemama, C. Filippi, *Journal of Chemical Theory and Computation* **2019**, *15*, 4896–4906.
- [241] M. Dash, S. Moroni, C. Filippi, A. Scemama, *Journal of Chemical Theory and Computation* **2021**, *17*, 3426–3434.
- [242] A. Cuzzocrea, S. Moroni, A. Scemama, C. Filippi, *Journal of Chemical Theory and Computation* **2022**, *18*, 1089–1095.
- [243] S. Shepard, R. L. Panadés—Barrueta, S. Moroni, A. Scemama, C. Filippi, *Journal of Theoretical and Computational Chemistry* **2022**, *18*, 6722–6731.

- [244] E. van Lenthe, E. J. Baerends, *Journal of Computational Chemistry* **2003**, 24, 1142–1156.
- [245] K. O-ohata, H. Taketa, S. Huzinaga, *Journal of the Physical Society of Japan* **1966**, 21, 2306–2313.
- [246] G. A. Petersson, S. Zhong, J. A. Montgomery, M. J. Frisch, *The Journal of Chemical Physics* **2003**, *118*, 1101–1109.
- [247] K. P. Huber, G. Herzberg, *Molecular Spectra and Molecular Structure. IV. Constants of Diatomic Molecules*, Van Nostrand Reinhold Company, **1979**.
- [248] M. C. Per, D. M. Cleland, The Journal of Chemical Physics 2017, 146, 164101.
- [249] R. S. Urdahl, Y. Bao, W. M. Jackson, Chemical Physics Letters 1991, 178, 425–428.
- [250] L. Bytautas, K. Ruedenberg, The Journal of Chemical Physics 2005, 122, 154110.
- [251] J. Toulouse, C. J. Umrigar, The Journal of Chemical Physics 2008, 128, 174101.
- [252] G. H. Booth, D. Cleland, A. J. Thom, A. Alavi, *The Journal of Chemical Physics* **2011**, 135, 084104.
- [253] B. Braïda, J. Toulouse, M. Caffarel, C. J. Umrigar, *The Journal of Chemical Physics* **2011**, *134*, 084108.
- [254] T. P. Kelly, A. Perera, R. J. Bartlett, J. C. Greer, *The Journal of Chemical Physics* **2014**, 140, 084114.
- [255] R. C. Clay, M. A. Morales, The Journal of Chemical Physics 2015, 142, 234103.
- [256] W. Zou, D. Cremer, Chemistry A European Journal 2016, 22, 4087–4099.
- [257] M. Hermann, G. Frenking, *Chemistry A European Journal* **2016**, 22, 4100–4108.
- [258] A. Karton, Chemical Physics Letters **2019**, 737, 136810.
- [259] B. Visser, M. Beck, P. Bornhauser, G. Knopp, J. A. van Bokhoven, P. Radi, C. Gourlaouen, R. Marquardt, *Molecular Physics* **2019**, *117*, 1645–1652.

- [260] J. Borsovszky, K. Nauta, J. Jiang, C. S. Hansen, L. K. McKemmish, R. W. Field, J. F. Stanton, S. H. Kable, T. W. Schmidt, *Proceedings of the National Academy of Sciences of the United States of America* **2021**, *118*, 1–7.
- [261] Y. Garniron, T. Applencourt, K. Gasperich, A. Benali, A. Ferté, J. Paquier, B. Pradines, R. Assaraf, P. Reinhardt, J. Toulouse, P. Barbaresco, N. Renon, G. David, J.-P. Malrieu, M. Véril, M. Caffarel, P.-F. Loos, E. Giner, A. Scemama, *Journal of Chemical Theory and Computation* 2019, 15, 3591–3609.
- [262] A. Ammar, E. Giner, A. Scemama, *Journal of Chemical Theory and Computation* **2022**, *18*, 5325–5336.
- [263] R. Berner, A. Lüchow, The Journal of Physical Chemistry A 2010, 114, 13222–13227.
- [264] A. Lüchow, R. F. Fink, The Journal of Chemical Physics 2000, 113, 8457–8463.
- [265] H.-J. Flad, M. Caffarel, A. Savin in *Recent Advances in Quantum Monte Carlo Methods*, W. A. Lester (Ed.), World Scientific Publishing Co Pte Ltd, **1997**, pp. 73–98.
- [266] R. N. Barnett, Z. Sun, W. A. Lester, *The Journal of Chemical Physics* **2001**, 114, 2013–2021.
- [267] K. A. Peterson, A. K. Wilson, D. E. Woon, T. H. Dunning, *Theoretical Chemistry Accounts* **1997**, 97, 251–259.
- [268] K. K. Irikura, Journal of Physical and Chemical Reference Data 2007, 36, 389–397.
- [269] D. Cleland, G. H. Booth, C. Overy, A. Alavi, *Journal of Chemical Theory and Computation* **2012**, *8*, 4138–4152.
- [270] B. Ruscic, The Journal of Physical Chemistry A **2015**, 119, 7810–7837.
- [271] L. Wagner, L. Mitas, Chemical Physics Letters 2003, 370, 412–417.
- [272] D. M. Cleland, M. C. Per, The Journal of Chemical Physics 2016, 144, 124108.
- [273] M. C. Per, E. K. Fletcher, D. M. Cleland, *The Journal of Chemical Physics* **2019**, 150, 184101.

- [274] Y. Yao, C. J. Umrigar, Journal of Chemical Theory and Computation 2021, 17, 4183–4194.
- [275] M. Dash, S. Moroni, A. Scemama, C. Filippi, *Journal of Chemical Theory and Computation* **2018**, *14*, 4176–4182.
- [276] C. Zitlau, Master's thesis, RWTH Aachen University, 2017.

Acronyms

CAS complete active space

CASPT2 complete active space second-order perturbation

theory

CASSCF complete active space self-consistent field

CBS complete basis set coupled cluster

ccECP correlation-consistent effective core potential

CCSD coupled cluster singles doubles

CCSD(T) coupled cluster singles doubles perturbative triples

CI configuration interaction

CIPSI configuration interaction using a perturbative se-

lection made iteratively

CISD configuration interaction singles doubles

CSF configuration state function

CV core-valence

DFT density functional theory**DMC** diffusion Monte Carlo

ECP effective core potential

FCI full configuration interaction

FCIQMC full configuration interaction quantum Monte

Carlo

FN-DMC fixed-node diffusion Monte Carlo

GTO Gaussian-type orbital

HF Hartree-Fock

KS Kohn-Sham

MCSCF multi-configuration self-consistent field

MO molecular orbital

MP2 Møller-Plesset second-order perturbation theory

MRCC multi-reference coupled cluster

MRCI multi-reference configuration interaction MR-DMC multi-reference diffusion Monte Carlo

MRMP2 multi-reference second-order perturbation theory

QMC quantum Monte Carlo

RAS restricted active space

RASSCF restricted active space self-consistent field

SCF self-consistent field

sCI selected configuration interaction

SD Slater determinant

SO spin-orbit

STO Slater-type orbital

VMC variational Monte Carlo

ZPE zero-point energy

Appendix A

CIPSI Algorithm

0. Start with a determinant or a set of determinants, defining a subspace S_0 :

$$|\Psi_0^{(0)}\rangle = \sum_{i \in S_0} c_i^{(0)} |D_i\rangle \text{ with } E_0^{(0)}.$$

- 1. Collect determinants $|\alpha\rangle$ connected by \hat{H} to $|\Psi_0^{(n)}\rangle$ (double excitations).
- 2. Calculate the second-order perturbative change in energy $\delta e_{\alpha}^{(2)}$:

$$\delta e_{\alpha}^{(2)} = \frac{\langle \Psi_0^{(n)} | \hat{H} | \alpha \rangle^2}{E_0^{(n)} - \langle \alpha | \hat{H} | \alpha \rangle}.$$

3. Add determinant(s) with largest $|\delta e|$ to the reference subspace:

$$S_n \to S_{n+1} = S_n \cup \{|\alpha\rangle\}.$$

4. Diagonalize \hat{H} within S_{n+1} to obtain the ground state wave function and energy:

$$|\Psi_0^{(n+1)}\rangle = \sum_{i \in S_{n+1}} c_i^{(n+1)} |D_i\rangle \text{ with } E_0^{(n+1)}.$$

5. Go back to 1. and repeat until stop criterion is reached.

Appendix B

Integral Form of the Schrödinger Equation

The derivation is performed using the notation of Hammond, Lester, and Reynolds.^[51] The formal solution of the time-independent Schrödinger equation can be obtained as

$$|\Psi_0\rangle = E_0 \hat{H}^{-1} |\Psi\rangle. \tag{B.1}$$

The operator \hat{H}^{-1} (inverse of the Hamiltonian) is an integral operator. By inserting a complete set of position states $\int |\mathbf{R}\rangle \langle \mathbf{R}| \, d\mathbf{R}$ into Eq. (B.1) and multiplying (from the left) by the position state $\langle \mathbf{R}'|$, one obtains:

$$\langle \mathbf{R}' | \Psi_0 \rangle = E_0 \int \langle \mathbf{R}' | \hat{H}^{-1} | \mathbf{R} \rangle \langle \mathbf{R} | \Psi_0 \rangle d\mathbf{R}.$$
 (B.2)

Using the following definition of the Green's function

$$G(\mathbf{R}',\mathbf{R}) \equiv \langle \mathbf{R}' | \hat{H}^{-1} | \mathbf{R} \rangle, \tag{B.3}$$

Eq. (B.2) can be rewritten as follows:

$$\Psi_0(\mathbf{R}') = E_0 \int G(\mathbf{R}', \mathbf{R}) \Psi_0(\mathbf{R}) d\mathbf{R}.$$
 (B.4)

By applying the inverse of an operator succeeded by the operator itself on a state, the state remains unchanged:

$$\hat{H}(\hat{H}^{-1})\Psi_0 = \Psi_0. \tag{B.5}$$

Combining Eqs. (B.1) and (B.4), one can—using Eq. (B.5)—write

$$\Psi_0(\mathbf{R}') = \hat{H}(\mathbf{R}')\hat{H}^{-1}\Psi_0(\mathbf{R}') = \int \hat{H}(\mathbf{R}')G(\mathbf{R}',\mathbf{R})\Psi_0(\mathbf{R})d\mathbf{R}.$$
 (B.6)

From this equation follows

$$\hat{H}(\mathbf{R}')G(\mathbf{R}',\mathbf{R}) = \delta(\mathbf{R} - \mathbf{R}'). \tag{B.7}$$

Inserting Eq. (B.7) into Eq. (B.4) yields the Schrödinger equation in its original form. In the Monte Carlo formalism, the Green's function $G(\mathbf{R}', \mathbf{R})$ is interpreted as a transition probability, describing the probability of moving from \mathbf{R} to \mathbf{R}' . In its original (differential) form, the Schrödinger equation only includes information for a given position (e.g. \mathbf{R}), while in its integral form, see Eq. (B.4), the wave function at a given point necessitates knowledge of all other positions as well.

Appendix C

Symmetry of Diatomic Molecules

Computing high symmetry molecules is a cumbersome endeavor. The strategies and challenges of the computation of diatomics will be briefly propounded here. In this work, both homo- and heteronuclear dimers, belonging to the $D_{\infty h}$ and $C_{\infty v}$ symmetry groups, respectively, are investigated. They need to be computed in lower order symmetry groups, giving rise to various problems. In this thesis, the homonuclear dimers are computed in D_{2h} while the C_{2v} point group is used for the heteronuclear counterparts. Tab. C.1 displays the resolution of different electronic states into a lower order symmetry. It becomes clear that one cannot distinguish e.g. between a Π and a Φ state in C_{2v} . Additionally, the Σ^+ and Δ states can be described by symmetry A_1 . Similarly, for homonuclear molecules, the Π_g and Φ_g electronic states cannot be discerned, while e.g. Π_g and Π_u states do not share the same symmetries.

Tab. C.1: Examples of true linear symmetry states and their lower order counterparts (used for calculations). The *z* axis is chosen as the intermolecular axis.

$C_{\infty v}$ Symmetry	C _{2v} Symmetry	$D_{\infty h}$ Symmetry	D _{2h} Symmetry
Σ^+	A_1	Σ_g^+	A_g
П	$B_1 + B_2$	$egin{array}{c} \Pi_g \ \Pi_u \end{array}$	$B_{2g} + B_{3g} B_{2u} + B_{3u}$
Δ	$A_1 + A_2$	Δ_g	$A_g + B_{1g}$
Φ	$B_1 + B_2$	Φ_g	$B_{2g}+B_{3g}$

Let us now investigate the behavior of the atomic orbitals (basis functions) for the individual symmetries, focusing, for the sake of simplicity, on s, p, and d orbitals. This is done exemplarily for the $C_{\infty v}$ and C_{2v} state symmetries. Note that in actual calculations, basis sets including f and g functions are necessary in order to accurately describe

transition metal compounds, which further complicates the situation. In Tab. C.2, the classification of the spherical harmonics is given for the $C_{\infty v}$ and C_{2v} groups, respectively.

Tab. C.2: Irreducible representations of the C_{2v} group and the respective spherical harmonics, transforming according to the different representations. The $C_{\infty v}$ orbital symmetries are given in parentheses. The z axis is chosen as the intermolecular axis.

C _{2v} Symmetry	Spherical Harmonics						
$ \begin{array}{c} a_1 \\ b_1 \\ b_2 \\ a_2 \end{array} $	$ \begin{vmatrix} s(\sigma) \\ p_x(\pi) \\ p_y(\pi) \\ d_{xy}(\delta) \end{vmatrix} $	$p_z(\sigma) \\ d_{xz}(\pi) \\ d_{yz}(\pi)$	$d_{z^2}(\sigma)$	$d_{x^2-y^2}(\delta)$			

For a wave function that adheres to the true $C_{\infty v}$ symmetry of the molecule, a mixing between different symmetry orbitals would not occur. However, the σ and the δ (only $d_{x^2-y^2}$) orbitals transform in C_{2v} according to a_1 , allowing them to mix in the calculation. In order to preserve the true symmetry of the molecule, the orbital mixing and rotating should thus be restricted. Additionally, degenerate orbitals belonging to different representations, such as the π orbitals in b_1 and b_2 as well as the δ orbitals in a_1 and a_2 , should be treated as equivalent. In practice, if one wants to perform a CASSCF calculation on a Δ (Π) state in C_{2v} , the A_1 and A_2 (B_1 and B_2) state symmetries should be optimized simultaneously (see Tab. C.1), which corresponds to a pseudo-state-averaged calculation. Note that the resulting wave function will only describe one of the two (degenerate) states.

Appendix D

Transition Metal Compounds

VMC and DMC Energies

Tab. D.1: Ground states, ECPs, DMC energies in E_h , and first-order SO corrections in E_h for the different atomic species. The wave functions were fully optimized (Jas+MO+CI) within VMC (Jas+MO for the single configuration wave functions). An sm666 Jastrow factor was used.

Element	Ground State	ECP	Ansatz	Energy	SO correction
Fe	⁵ D	BFD-VTZ ccECP-VTZ	CAS(8,6)	-123.8126(4) ^a -123.3233(5)	-0.00184
Со	⁴ F	BFD-VTZ	CAS(9,6)	-145.7192(4)	-0.00361
Ni	^{3}F	BFD-VTZ ccECP-VTZ	CAS(10,6)	-170.1212(5) ^b -169.3161(5)	-0.00443
Cr	$^{7}\mathrm{S}$	BFD-VTZ	CAS(6,6)	-86.9010(4) ^c	n/a
Н	^{2}S	/	/	-0.5000	n/a
С	³ P	BFD-VTZ BFD-VTZ ccECP-VTZ	CAS(2,3) CAS(4,4) CAS(2,3)	-5.4244(3) ^b -5.4278(2) -5.4108(3)	-0.000135
0	³ P	ccECP-VTZ	CAS(4,3)	-15.8709(5)	-0.000355
Si	³ P	BFD-VTZ ccECP-VTZ	CAS(2,3)	-3.7674(3) -3.7596(4)	-0.000682
S	³ P	BFD-VTZ	CAS(4,3)	-10.1314(1) ^a	-0.000892

^a Taken from Ref. 125.

^b Taken from Ref. 23.

^c Taken from Ref. 276.

Tab. D.2: VMC and DMC energies in E_h , number of CSFs, ECPs, and first-order SO corrections in E_h for different transition metal dimers. The wave functions were fully optimized (Jas+MO+CI) within VMC. An sm666 Jastrow factor was used.

System	# CSFs	ECP	Ansatz	VMC	DMC	SO correction
FeH	30	ccECP-VTZ	CAS(9,7)	-123.8342(5)	-123.8932(5)	-0.0018
СоН	40	BFD-VTZ	CAS(10,7)	-146.2455(5)	-146.3018(5)	-0.0034
NiC	445 851 445	BFD-VTZ BFD-VTZ ccECP-VTZ	CAS(12,9) CAS(14,10) CAS(12,9)	-175.6200(5) -175.6267(5) -174.8014(5)	-175.6912(5) -175.6960(5) -174.8775(5)	n/a
FeC	1384	BFD-VTZ	CAS(10,9)	-129.3082(5)	-129.3717(5)	-0.000755(6)
FeO	145	ccECP-VTZ	CAS(12,9)	-139.2582(5)	-139.3441(5)	-0.00205
NiSi	473	BFD-VTZ ccECP-VTZ	CAS(12,9)	-173.9293(5) -173.1267(5)	-174.0004(5) -173.1965(5)	n/a

Tab. D.3: CrS VMC and DMC energies in E_h at various optimization levels, using different starting orbitals and BFD-VTZ/sm666.

Ansatz	Orbitals	# CSFs	Optimization level	VMC energy	DMC energy	SO correction
	HF		Jas	-97.0284(2)	-97.1041(5)	
Single det	B3LYP	1	Jas	-97.0543(2)	-97.1304(5)	
	opt		Jas+MO	-97.0570(2)	-97.1306(5)	-0.000434(19)
	RAS2		Jas	-97.0655(2)	-97.1318(5)	0.000101(1))
CAS	RAS2	670	Jas+CI	-97.0778(2)	-97.1406(5)	
	opt		Jas+MO+CI	-97.0822(3) ^a	-97.1426(4) ^a	

^a Taken from Ref. 23.

Potential Energy Curves

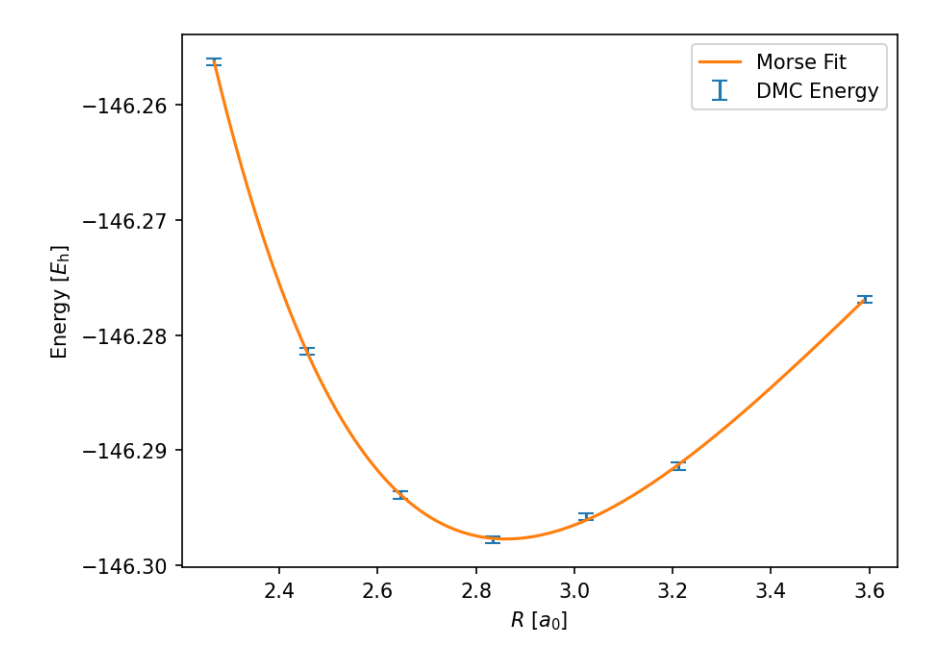


Fig. D.1: CoH MR-DMC potential energy curve at the Jas+MO+CI optimization level with the corresponding Morse fit. A time step of $\tau=0.001$ was employed for each data point. An sm666 Jastrow factor was used.

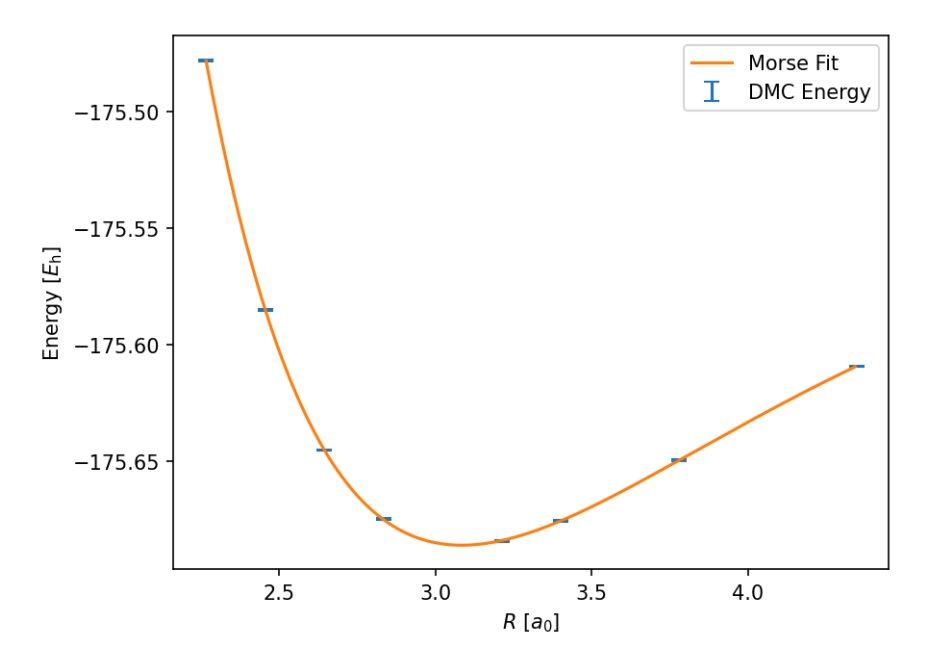


Fig. D.2: NiC MR-DMC potential energy curve at the Jas+MO+CI optimization level with the corresponding Morse fit. A time step of $\tau=0.001$ was employed for each data point. An sm666 Jastrow factor was used.

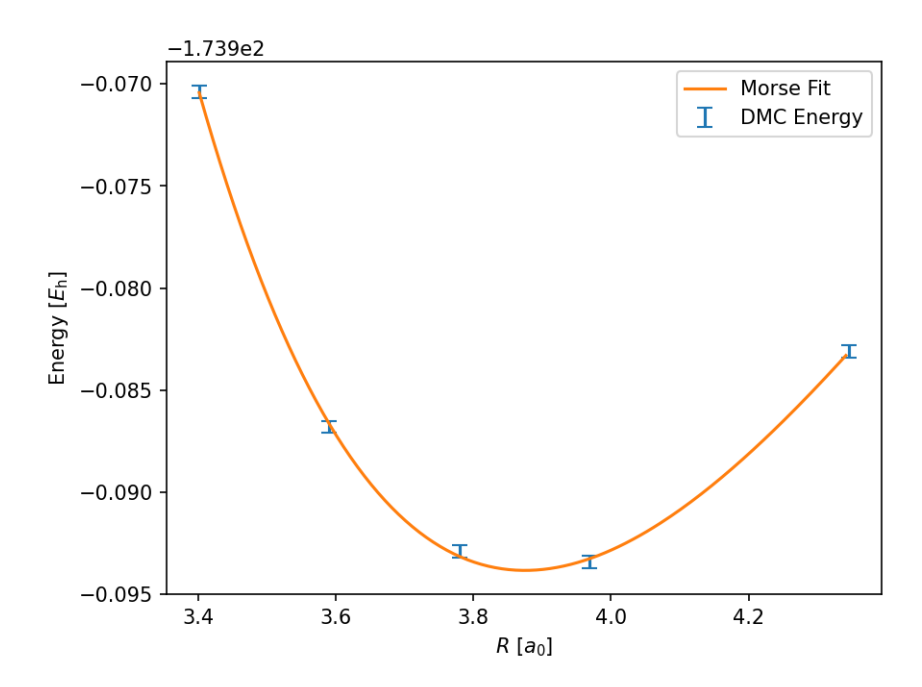


Fig. D.3: NiSi MR-DMC potential energy curve at the Jas+MO+CI optimization level with the corresponding Morse fit. A time step of $\tau=0.001$ was employed for each data point. An sm666 Jastrow factor was used.

Appendix E

Selected Configuration Interaction

Statistical Analysis of CI Coefficients

Tab. E.1: Absolute values of the CI coefficients for different wave functions with and without Jastrow factor. The *Error* columns correspond to one standard deviation. If a Jastrow factor was used, the Jastrow and CI parameters were simultaneously optimized with respect to the variational energy. The coefficients of the CAS(8,8) column are sorted from largest to smallest. For the remaining columns, the coefficients (and errors) are sorted such that the CSFs are identical for each index. The CSFs are normalized for each approach.

CAS(8,8)	sm4	144	sm6	566	sm8	388
$ c_i $	$ c_i $	Error	$ c_i $	Error	$ c_i $	Error
8.377E-01	8.781E-01	1.64E-03	8.789E-01	8.75E-04	8.812E-01	1.21E-03
3.779E-01	3.504E-01	3.06E-03	3.528E-01	3.00E-03	3.468E-01	3.24E-03
2.195E-01	1.960E-01	1.12E-03	1.970E-01	2.37E-03	1.972E-01	7.69E-04
1.659E-01	1.370E-01	1.75E-03	1.332E-01	5.14E-04	1.346E-01	1.09E-03
1.359E-01	1.160E-01	1.62E-03	1.156E-01	2.92E-03	1.127E-01	3.01E-03
1.071E-01	8.558E-02	1.11E-03	8.316E-02	2.01E-04	8.403E-02	1.30E-03
1.041E-01	7.494E-02	9.60E-04	7.528E-02	8.21E-04	7.469E-02	5.29E-04
6.685E-02	4.583E-02	1.10E-03	4.591E-02	1.80E-03	4.589E-02	1.04E-03
6.684E-02	4.320E-02	5.16E-04	3.808E-02	5.36E-04	3.854E-02	5.86E-04
6.503E-02	5.646E-02	1.15E-03	5.859E-02	3.53E-04	5.927E-02	5.42E-04
6.233E-02	6.514E-02	1.64E-03	5.716E-02	1.02E-03	5.610E-02	2.28E-03
5.267E-02	3.269E-02	4.11E-04	3.172E-02	4.36E-04	3.265E-02	9.59E-04
5.226E-02	3.588E-02	4.34E-04	3.472E-02	9.60E-04	3.350E-02	1.46E-03
4.729E-02	3.780E-02	8.99E-04	3.725E-02	1.09E-03	3.733E-02	1.04E-03
3.215E-02	1.586E-02	4.74E-04	1.426E-02	4.12E-04	1.421E-02	5.10E-04
3.129E-02	5.536E-02	6.04E-03	5.237E-02	6.74E-03	5.665E-02	5.30E-03
3.036E-02	2.034E-02	1.06E-03	2.076E-02	1.74E-03	2.153E-02	1.09E-03
2.893E-02	1.586E-02	1.23E-03	1.487E-02	4.45E-04	1.530E-02	7.65E-04
2.868E-02	1.419E-02	2.78E-04	9.866E-03	1.50E-04	8.201E-03	2.28E-04
2.789E-02	1.285E-02	7.85E-04	1.343E-02	3.17E-04	1.305E-02	3.21E-04

 Tab. E.1: Continued.

CAS(8,8)	sm4	444	sm666 sm888		388	
$ c_i $	$ c_i $	Error	$ c_i $	Error	$ c_i $	Error
2.711E-02	4.392E-03	3.76E-04	2.544E-04	1.96E-04	4.582E-04	3.15E-04
2.664E-02	1.826E-02	1.23E-03	2.086E-02	7.48E-04	1.812E-02	1.46E-03
2.546E-02	1.089E-02	7.51E-04	1.057E-02	6.86E-04	9.673E-03	4.57E-04
2.466E-02	1.166E-02	3.90E-04	1.143E-02	6.86E-04	1.203E-02	8.41E-04
2.064E-02	1.434E-02	8.87E-04	1.331E-02	6.38E-04	1.363E-02	8.62E-04
1.973E-02	1.647E-02	4.17E-04	1.449E-02	9.23E-04	1.413E-02	1.49E-04
1.689E-02	9.288E-03	5.33E-04	9.059E-03	5.18E-04	8.133E-03	7.50E-04
1.646E-02	1.412E-02	5.81E-04	1.396E-02	4.30E-04	1.365E-02	4.10E-04
1.617E-02	7.391E-03	2.82E-04	7.482E-03	2.92E-04	7.364E-03	4.47E-04
1.565E-02	1.165E-03	5.62E-04	4.420E-04	3.96E-04	4.075E-04	2.10E-04
1.502E-02	6.371E-03	3.80E-04	5.388E-03	3.28E-04	5.391E-03	6.32E-04
1.443E-02	1.576E-02	1.60E-03	1.601E-02	5.69E-04	1.570E-02	1.73E-03
1.405E-02	1.418E-02	4.90E-04	1.328E-02	5.07E-04	1.279E-02	5.59E-04
1.329E-02	1.073E-02	6.47E-04	1.001E-02	6.08E-04	9.850E-03	5.47E-04
1.277E-02	5.393E-03	2.30E-04	3.963E-03	3.37E-04	3.059E-03	5.46E-04
1.165E-02	5.662E-03	8.95E-04	6.262E-03	4.41E-04	5.990E-03	7.35E-04
1.155E-02	4.432E-03	2.12E-04	3.761E-03	2.30E-04	3.651E-03	4.94E-04
1.120E-02	8.625E-03	6.08E-04	7.986E-03	2.78E-04	7.864E-03	3.75E-04
1.102E-02	1.755E-03	4.06E-04	6.637E-04	2.98E-04	6.778E-04	7.56E-05
1.089E-02	6.774E-03	3.40E-04	6.895E-03	3.83E-04	7.219E-03	9.95E-04
1.080E-02	1.386E-02	5.40E-04	1.442E-02	1.51E-03	1.394E-02	4.83E-04
1.076E-02	3.547E-03	2.97E-04	2.945E-03	4.47E-04	3.057E-03	4.67E-04
1.062E-02	4.592E-03	1.89E-04	4.287E-03	2.57E-04	4.253E-03	3.46E-04
1.058E-02	1.031E-03	7.44E-04	2.579E-03	4.41E-04	2.626E-03	7.01E-04
1.056E-02	6.805E-03	8.27E-04	7.399E-03	9.00E-04	6.914E-03	5.06E-04
1.011E-02	3.222E-03	3.15E-04	3.304E-03	5.23E-04	2.975E-03	3.78E-04
1.011E-02	2.173E-04	1.82E-04	7.661E-04	2.87E-04	1.358E-03	5.97E-04
9.573E-03	3.276E-03	2.89E-04	2.372E-03	3.36E-04	3.309E-03	6.29E-04
9.558E-03	1.007E-02	8.21E-04	1.050E-02	1.51E-03	1.073E-02	1.31E-03
9.301E-03	3.617E-03	6.76E-04	3.286E-03	1.91E-04	3.036E-03	5.15E-04
9.161E-03	2.562E-03	2.40E-04	2.559E-03	5.34E-04	2.425E-03	2.70E-04
9.041E-03	2.212E-03	1.98E-04	2.021E-03	2.02E-04	2.204E-03	2.60E-04
8.814E-03	2.676E-03	4.05E-04	1.880E-03	3.86E-04	1.974E-03	1.58E-04
8.544E-03	4.309E-03	4.49E-04	3.509E-03	4.32E-04	3.390E-03	5.97E-04

 Tab. E.1: Continued.

CAS(8,8)	sm ²	144	sm6	666	sm8	388
$ c_i $	$ c_i $	Error	$ c_i $	Error	$ c_i $	Error
8.239E-03	4.419E-03	6.85E-04	4.546E-03	6.43E-04	4.607E-03	2.98E-04
8.187E-03	5.322E-03	5.16E-04	5.296E-03	6.46E-04	4.986E-03	2.81E-04
7.831E-03	1.197E-03	4.44E-04	7.335E-04	1.45E-04	7.027E-04	2.90E-04
7.712E-03	2.534E-03	3.52E-04	1.918E-03	2.99E-04	1.651E-03	4.02E-04
7.626E-03	3.895E-03	4.45E-04	4.165E-03	6.66E-04	4.428E-03	7.69E-04
7.475E-03	4.158E-03	4.21E-04	3.600E-03	1.39E-04	3.700E-03	3.46E-04
7.282E-03	2.548E-03	4.72E-04	1.583E-03	2.24E-04	1.986E-03	2.76E-04
7.067E-03	5.847E-04	3.79E-04	7.156E-04	2.80E-04	5.690E-04	3.57E-04
7.026E-03	6.316E-03	2.68E-04	5.700E-03	2.44E-04	5.369E-03	2.71E-04
6.420E-03	1.380E-03	3.29E-04	1.674E-03	5.26E-04	1.662E-03	9.90E-05
5.692E-03	1.657E-03	4.82E-04	1.331E-03	3.41E-04	1.279E-03	1.68E-04
5.690E-03	2.138E-03	4.93E-04	1.860E-03	5.02E-04	2.437E-03	6.14E-04
5.424E-03	1.500E-03	2.45E-04	1.279E-03	1.58E-04	1.365E-03	1.96E-04
5.286E-03	2.899E-03	2.64E-04	2.525E-03	3.53E-04	2.366E-03	2.53E-04
5.177E-03	1.106E-03	2.83E-04	9.658E-04	3.69E-04	5.273E-04	2.32E-04
5.113E-03	2.102E-04	1.79E-04	6.852E-04	5.15E-04	7.835E-04	4.25E-04
5.109E-03	1.390E-03	2.89E-04	1.064E-03	2.39E-04	9.121E-04	3.34E-04
4.910E-03	7.005E-03	7.68E-04	6.155E-03	1.90E-03	6.408E-03	6.88E-04
4.889E-03	1.916E-03	3.09E-04	1.162E-03	3.70E-04	1.031E-03	2.34E-04
4.796E-03	8.555E-04	6.48E-04	9.581E-04	2.59E-04	7.732E-04	4.82E-04
4.622E-03	5.635E-04	3.83E-04	1.116E-03	3.68E-04	1.021E-03	5.74E-04
4.613E-03	3.639E-04	2.01E-04	3.017E-04	1.94E-04	3.389E-04	2.06E-04
4.484E-03	1.001E-03	4.17E-04	5.727E-04	3.10E-04	4.988E-04	1.91E-04
4.339E-03	1.357E-03	3.18E-04	1.399E-03	3.77E-04	1.229E-03	4.71E-04
3.974E-03	1.334E-03	4.39E-04	1.818E-03	3.65E-04	1.778E-03	2.69E-04
3.810E-03	3.130E-03	4.85E-04	3.090E-03	4.93E-04	3.237E-03	4.17E-04
3.695E-03	1.105E-03	2.89E-04	1.071E-03	4.76E-04	1.469E-03	1.19E-04
3.539E-03	7.024E-04	2.71E-04	7.268E-04	4.82E-04	9.320E-04	1.93E-04
3.392E-03	1.155E-03	4.06E-04	6.383E-04	4.17E-04	5.428E-04	2.24E-04
3.389E-03	1.917E-03	3.49E-04	1.543E-03	2.02E-04	2.313E-03	4.53E-04
3.268E-03	6.364E-04	4.24E-04	5.785E-04	1.32E-04	4.499E-04	1.96E-04
3.096E-03	3.200E-04	2.03E-04	3.511E-04	1.47E-04	2.864E-04	3.47E-04
3.096E-03	1.059E-03	2.90E-04	4.885E-04	3.67E-04	5.037E-04	2.67E-04
3.068E-03	1.189E-03	8.95E-05	7.098E-04	3.56E-04	7.378E-04	3.92E-04

Tab. E.1: Continued.

CAS(8,8)	sm4	144	sm6	666	sm8	sm888	
$ c_i $	$ c_i $	Error	$ c_i $	Error	$ c_i $	Error	
3.068E-03	9.355E-04	4.77E-04	1.197E-03	2.42E-04	1.048E-03	2.14E-04	
2.957E-03	2.090E-03	2.46E-04	2.130E-03	3.36E-04	2.236E-03	4.48E-04	
2.912E-03	7.361E-04	2.40E-04	5.676E-04	3.41E-04	6.037E-04	4.79E-04	
2.867E-03	2.057E-03	3.19E-04	1.907E-03	6.47E-04	1.972E-03	4.66E-04	
2.850E-03	4.486E-04	2.59E-04	2.600E-04	1.39E-04	3.027E-04	6.08E-05	
2.847E-03	1.943E-04	1.17E-04	4.134E-04	2.81E-04	3.834E-04	3.05E-04	
2.659E-03	2.004E-03	3.11E-04	1.941E-03	4.48E-04	2.321E-03	3.39E-04	
2.638E-03	5.094E-04	4.19E-04	3.686E-04	2.13E-04	4.342E-04	3.07E-04	
2.586E-03	6.269E-04	1.97E-04	3.301E-04	2.97E-04	5.945E-04	2.31E-04	
2.543E-03	6.745E-04	1.33E-04	3.356E-04	3.12E-04	4.255E-04	2.72E-04	
2.540E-03	1.751E-03	2.94E-04	1.525E-03	2.97E-04	1.501E-03	4.18E-04	
2.337E-03	5.839E-04	1.65E-04	2.858E-04	1.43E-04	3.478E-04	1.95E-04	
2.302E-03	1.414E-03	4.00E-04	1.363E-03	2.77E-04	1.577E-03	2.46E-04	
2.222E-03	1.471E-03	5.72E-04	8.784E-04	1.84E-04	1.012E-03	4.69E-04	
2.189E-03	1.259E-03	1.07E-04	1.342E-03	4.45E-04	1.582E-03	3.41E-04	
2.134E-03	3.920E-04	2.66E-04	1.727E-04	5.64E-05	4.841E-04	2.00E-04	
2.080E-03	3.620E-04	1.79E-04	3.138E-04	3.03E-04	2.706E-04	1.44E-04	
1.956E-03	5.954E-04	2.99E-04	2.753E-04	1.21E-04	1.579E-04	8.55E-05	
1.930E-03	1.741E-03	1.95E-04	1.357E-03	3.08E-04	1.185E-03	6.15E-04	
1.907E-03	2.104E-04	1.87E-04	1.705E-04	1.33E-04	2.491E-04	1.63E-04	
1.885E-03	6.429E-04	3.47E-04	7.194E-04	3.41E-04	3.700E-04	2.14E-04	
1.864E-03	5.627E-04	4.78E-04	2.844E-04	2.85E-04	3.542E-04	2.82E-04	
1.856E-03	1.115E-03	3.23E-04	1.176E-03	3.45E-04	1.192E-03	3.94E-04	
1.847E-03	6.385E-04	2.67E-04	3.866E-04	1.94E-04	3.681E-04	3.51E-04	
1.795E-03	2.806E-04	1.27E-04	1.675E-04	8.49E-05	3.266E-04	1.17E-04	
1.696E-03	1.735E-03	5.68E-04	1.323E-03	8.24E-04	1.116E-03	6.51E-04	
1.655E-03	1.089E-03	2.47E-04	7.442E-04	3.86E-04	7.835E-04	3.98E-04	
1.629E-03	1.106E-03	4.19E-04	9.059E-04	3.25E-04	5.939E-04	3.54E-04	
1.598E-03	9.690E-04	3.89E-04	8.794E-04	2.77E-04	7.838E-04	2.65E-04	
1.540E-03	1.253E-03	5.46E-04	1.024E-03	4.15E-04	1.188E-03	7.22E-05	
1.520E-03	2.576E-04	1.62E-04	2.670E-04	2.05E-04	3.536E-04	2.31E-04	
1.470E-03	4.814E-04	3.03E-04	3.554E-04	2.50E-04	2.553E-04	2.27E-04	
1.467E-03	2.665E-04	1.94E-04	2.458E-04	1.78E-04	2.360E-04	1.30E-04	
1.434E-03	8.636E-04	5.02E-04	1.151E-03	2.23E-04	7.758E-04	3.29E-04	

 Tab. E.1: Continued.

CAS(8,8)	sm ²	144	sm6	666	sm8	388
$ c_i $	$ c_i $	Error	$ c_i $	Error	$ c_i $	Error
1.417E-03	2.741E-04	1.73E-04	1.496E-04	1.80E-04	2.339E-04	1.16E-04
1.302E-03	3.405E-04	2.22E-04	2.991E-04	1.30E-04	3.343E-04	2.38E-04
1.219E-03	8.121E-04	4.66E-04	5.705E-04	1.22E-04	4.449E-04	2.17E-04
1.157E-03	2.641E-04	2.41E-04	4.255E-04	1.27E-04	1.846E-04	1.81E-04
1.152E-03	3.884E-04	3.18E-04	1.713E-04	1.19E-04	2.409E-04	2.26E-04
1.140E-03	5.410E-04	3.62E-04	4.385E-04	2.17E-04	2.637E-04	2.49E-04
1.015E-03	2.194E-04	2.13E-04	2.262E-04	1.54E-04	3.224E-04	2.20E-04
1.001E-03	2.431E-04	1.73E-04	3.862E-04	3.49E-04	1.373E-04	1.56E-04
9.883E-04	1.697E-04	9.47E-05	2.519E-04	1.89E-04	2.507E-04	1.47E-04
9.348E-04	8.328E-04	2.05E-04	1.058E-03	3.10E-04	7.411E-04	5.08E-04
8.581E-04	3.253E-04	2.43E-04	3.780E-04	7.78E-05	3.059E-04	1.88E-04
8.563E-04	4.847E-04	1.62E-04	3.203E-04	3.54E-04	2.142E-04	2.09E-04
8.540E-04	8.666E-04	1.76E-04	7.513E-04	2.31E-04	5.218E-04	2.86E-04
8.532E-04	7.151E-04	3.83E-04	3.339E-04	1.88E-04	7.797E-04	3.43E-04
8.344E-04	3.838E-04	2.82E-04	1.992E-04	1.79E-04	2.819E-04	2.80E-04
8.253E-04	1.035E-03	6.85E-04	1.003E-03	3.82E-04	1.107E-03	2.92E-04
7.649E-04	2.733E-04	1.83E-04	3.459E-04	1.93E-04	1.540E-04	7.63E-05
6.471E-04	5.907E-04	3.68E-04	2.028E-04	2.24E-04	3.460E-04	1.66E-04
6.457E-04	1.277E-03	4.63E-04	6.732E-04	3.17E-04	7.196E-04	3.60E-04
5.818E-04	7.298E-04	2.40E-04	8.402E-04	1.96E-04	9.998E-04	9.64E-05
5.580E-04	2.695E-03	3.94E-04	2.324E-03	2.95E-04	1.657E-03	2.15E-04
5.424E-04	4.244E-04	4.85E-04	4.783E-04	3.57E-04	3.252E-04	2.23E-04
5.102E-04	1.937E-04	1.89E-04	2.251E-04	1.01E-04	1.470E-04	1.16E-04
5.033E-04	6.299E-04	3.68E-04	6.475E-04	4.26E-04	5.538E-04	2.43E-04
4.869E-04	5.386E-04	2.15E-04	2.262E-04	2.33E-04	1.596E-04	1.29E-04
4.677E-04	2.527E-04	2.42E-04	1.563E-04	1.30E-04	3.134E-04	2.15E-04
4.187E-04	2.939E-04	1.66E-04	2.600E-04	2.73E-04	2.287E-04	3.32E-04
3.960E-04	2.526E-04	1.34E-04	2.613E-04	2.01E-05	1.577E-04	9.17E-05
3.526E-04	2.541E-04	2.65E-04	1.594E-04	1.28E-04	2.372E-04	2.11E-04
2.637E-04	6.212E-04	4.24E-04	9.211E-04	3.68E-04	3.427E-04	2.11E-04
2.328E-04	2.021E-04	1.63E-04	2.426E-04	2.03E-04	3.633E-04	1.56E-04
2.027E-04	4.010E-04	2.13E-04	6.438E-04	3.28E-04	8.158E-04	1.81E-04
1.396E-04	4.618E-04	2.52E-04	4.498E-04	2.42E-04	2.406E-04	1.95E-04
1.055E-04	4.457E-04	2.94E-04	2.929E-04	1.69E-04	2.084E-04	1.83E-04

Tab. E.1: Continued.

CAS(8,8)	sm444		8,8) sm444 sm666		sm888	
$ c_i $	$ c_i $	Error	$ c_i $	Error	$ c_i $	Error
9.900E-05	4.230E-04	3.13E-04	2.548E-04	1.86E-04	2.262E-04	1.58E-04
7.000E-05	3.714E-04	3.14E-04	2.026E-04	1.30E-04	3.153E-04	1.94E-04
6.390E-05	3.324E-04	2.98E-04	2.028E-04	1.33E-04	2.266E-04	2.33E-04
0.000E+00	3.612E-04	2.90E-04	1.791E-04	7.62E-05	3.217E-04	2.35E-04
0.000E+00	4.658E-04	4.87E-04	3.975E-04	1.68E-04	2.661E-04	8.39E-05
0.000E+00	3.814E-04	3.53E-04	1.669E-04	2.24E-04	2.955E-04	1.76E-04
0.000E+00	3.247E-04	1.70E-04	2.237E-04	2.34E-04	2.530E-04	1.25E-04
0.000E+00	4.205E-04	4.81E-04	1.737E-04	3.81E-05	5.785E-04	3.20E-04
0.000E+00	2.390E-04	2.04E-04	2.817E-04	2.02E-04	2.621E-04	1.76E-04
0.000E+00	6.766E-04	3.56E-04	5.866E-04	2.24E-04	5.263E-04	4.60E-04
0.000E+00	4.342E-04	3.64E-04	4.103E-04	2.46E-04	3.842E-04	2.06E-04
0.000E+00	3.693E-04	2.60E-04	3.335E-04	2.18E-04	1.637E-04	1.45E-04

Using the Linear Optimization Method

Tab. E.2: Absolute values of Hamilton matrix elements together with the energy contributions $\delta e_i^{(2)}$. The quantities are given in $E_{\rm h}$. The *Error* columns correspond to one standard deviation.

$ar{H}_{0i}$	Error	$ar{H}_{i0}$	Error	$ig ar{H}_{ii}$	Error	$\delta e_i^{(2)}$	Error
1.1316E-01	1.19E-04	1.1246E-01	1.24E-04	7.2249E+01	1.17E-01	3.6483E-03	1.30E-04
1.3766E-01	7.66E-05	1.3722E-01	1.42E-04	6.2969E+01	2.93E-01	1.4797E-03	3.28E-05
8.4355E-02	8.71E-05	8.4062E-02	9.70E-05	4.8082E+01	1.70E-01	2.5639E-04	1.50E-06
6.0992E-02	1.71E-04	6.0875E-02	2.15E-04	7.4973E+01	2.17E-01	5.1405E-03	1.35E-03
9.8826E-03	8.66E-05	9.9862E-03	1.29E-04	7.3570E+01	2.29E-01	4.5807E-05	4.04E-06
2.8377E-02	7.62E-05	2.8348E-02	1.39E-04	4.6167E+01	2.27E-02	2.7202E-05	1.82E-07
2.2542E-02	2.12E-04	2.2319E-02	2.61E-04	7.1363E+01	3.93E-01	1.1558E-04	9.00E-06
6.0203E-03	1.07E-04	6.2168E-03	1.68E-04	7.2122E+01	7.49E-02	1.0350E-05	4.41E-07
7.3663E-02	2.83E-04	7.3707E-02	1.30E-04	6.5569E+01	3.08E-01	5.3426E-04	1.92E-05
5.9004E-02	1.09E-04	5.9007E-02	5.13E-05	6.8565E+01	1.48E-01	4.8539E-04	9.47E-06
5.7737E-02	7.65E-05	5.7202E-02	9.98E-05	4.8777E+01	2.26E-01	1.2250E-04	1.14E-06
4.1468E-02	1.79E-04	4.1322E-02	1.50E-04	6.1284E+01	3.22E-01	1.1859E-04	3.41E-06
1.1927E-02	1.61E-04	1.1816E-02	1.74E-04	6.6371E+01	4.33E-01	1.5069E-05	7.88E-07
3.2218E-02	1.07E-04	3.2129E-02	6.15E-05	6.5780E+01	2.13E-01	1.0396E-04	2.55E-06
1.2018E-02	9.03E-05	1.1928E-02	1.75E-04	3.4204E+01	2.02E-01	3.4514E-06	6.86E-08
2.7402E-02	1.36E-04	2.7341E-02	1.00E-04	3.1591E+01	1.02E-01	1.6969E-05	9.36E-08
4.3006E-03	1.53E-04	3.8278E-03	1.16E-04	7.1693E+01	8.97E-02	4.0757E-06	3.29E-07
3.3248E-02	2.47E-04	3.2786E-02	1.09E-04	6.9247E+01	2.26E-01	1.6806E-04	6.68E-06
6.0945E-03	1.01E-04	6.0934E-03	5.24E-05	3.2291E+01	7.14E-02	8.5479E-07	2.17E-08
1.6770E-02	1.73E-04	1.6709E-02	1.68E-04	6.4041E+01	2.77E-01	2.3964E-05	7.55E-07
2.1627E-02	8.94E-05	2.1425E-02	1.71E-04	5.3616E+01	1.15E+00	2.0986E-05	1.04E-06
1.1683E-02	8.09E-05	1.1501E-02	1.28E-04	6.8767E+01	1.54E-01	1.9280E-05	6.54E-07
1.0339E-02	1.61E-04	1.1233E-02	2.47E-04	6.2068E+01	1.65E-01	8.4968E-06	3.19E-07
1.7031E-02	8.77E-05	1.6959E-02	1.24E-04	6.9479E+01	3.13E-01	4.6203E-05	1.87E-06
9.2641E-03	2.02E-04	9.2234E-03	1.40E-04	6.9146E+01	1.73E-01	1.2968E-05	5.60E-07
5.8864E-03	1.39E-04	5.9647E-03	1.88E-04	7.1827E+01	6.04E-01	9.1763E-06	1.63E-06
5.6708E-03	2.71E-04	5.6045E-03	7.74E-05	3.1285E+01	2.37E-01	7.1523E-07	4.31E-08
1.6895E-02	2.83E-04	1.7180E-02	1.99E-04	6.2067E+01	2.64E-01	2.1241E-05	8.44E-07
4.3035E-03	1.52E-04	4.4312E-03	1.92E-04	6.8635E+01	4.53E-01	2.7015E-06	3.37E-07
2.7398E-02	1.28E-04	2.7148E-02	2.10E-04	4.6905E+01	2.44E-01	2.5795E-05	2.37E-07
1.3929E-02	2.91E-04	1.3745E-02	1.32E-04	6.5533E+01	6.17E-01	1.8819E-05	1.37E-06
4.9113E-03	2.40E-04	4.8893E-03	1.22E-04	6.3007E+01	3.33E-01	1.8864E-06	1.02E-07

Tab. E.2: Continued.

$ar{H}_{0i}$	Error	$ar{H}_{i0}$	Error	$ar{H}_{ii}$	Error	$\delta e_i^{(2)}$	Error
1.6712E-02	1.20E-04	1.6735E-02	2.33E-04	6.0767E+01	3.60E-01	1.8686E-05	4.68E-07
2.8508E-02	6.15E-05	2.7973E-02	1.47E-04	3.3605E+01	6.69E-01	1.8929E-05	2.37E-07
1.2881E-02	1.78E-04	1.2858E-02	1.64E-04	6.3701E+01	4.82E-01	1.3776E-05	6.42E-07
3.8448E-03	2.87E-04	3.9743E-03	2.98E-04	6.6359E+01	3.80E-01	1.6368E-06	2.41E-07
1.4051E-02	1.02E-04	1.3996E-02	7.71E-05	5.1501E+01	1.47E+00	8.1394E-06	5.41E-07
8.1059E-03	1.03E-04	8.1434E-03	4.62E-05	6.7280E+01	9.60E-01	7.8936E-06	1.01E-06
7.1733E-03	1.82E-04	6.5899E-03	1.54E-04	6.3535E+01	3.35E-01	3.8791E-06	2.52E-07
2.6978E-02	1.24E-04	2.6664E-02	1.50E-04	4.3854E+01	1.83E-01	2.2561E-05	2.97E-07
4.5734E-03	1.63E-04	4.5701E-03	8.27E-05	6.5393E+01	3.82E-01	2.0227E-06	1.22E-07
3.1447E-03	1.52E-04	3.1946E-03	8.69E-05	6.5488E+01	3.66E-01	9.8244E-07	8.95E-08
3.0331E-03	1.75E-04	2.8804E-03	1.03E-04	7.0625E+01	4.20E-01	1.7275E-06	2.91E-07
5.5609E-03	2.42E-04	5.4932E-03	8.76E-05	4.3076E+01	2.11E-01	9.3587E-07	5.85E-08
1.2956E-02	3.04E-04	1.3037E-02	8.66E-05	6.0857E+01	3.34E-01	1.1358E-05	5.22E-07
6.1608E-03	3.30E-05	6.1301E-03	1.88E-04	4.6774E+01	1.13E+00	1.3063E-06	8.46E-08
6.1040E-03	3.96E-04	6.2085E-03	1.61E-04	6.0988E+01	2.10E-01	2.5710E-06	2.14E-07
8.9956E-03	3.40E-04	8.9052E-03	5.82E-05	6.5445E+01	7.06E-01	7.8208E-06	7.63E-07
2.2493E-03	1.27E-04	2.2650E-03	9.38E-05	7.4131E+01	7.39E-01	5.0249E-06	5.34E-06
1.7526E-02	1.82E-04	1.7441E-02	1.93E-04	6.4433E+01	3.08E-01	2.7044E-05	6.36E-07
2.3682E-03	8.45E-05	2.3528E-03	2.54E-04	4.9754E+01	4.18E+00	2.1634E-07	1.58E-08
7.9179E-03	2.53E-04	7.8314E-03	1.56E-04	5.9668E+01	3.50E-01	3.8622E-06	2.30E-07
4.5860E-03	3.04E-04	4.6725E-03	2.22E-04	6.6210E+01	1.52E+00	2.3026E-06	4.60E-07
6.9057E-03	1.91E-04	6.8861E-03	5.48E-05	4.2125E+01	3.14E-01	1.4145E-06	3.49E-08
2.0198E-03	2.13E-04	2.0694E-03	1.47E-04	6.5193E+01	2.92E-01	3.9768E-07	6.04E-08
9.6244E-03	1.66E-04	9.6016E-03	1.26E-04	6.5814E+01	2.89E-01	9.3179E-06	3.97E-07
1.2092E-03	2.32E-04	1.3383E-03	1.32E-04	6.9951E+01	5.99E-01	2.7661E-07	3.76E-08
5.2753E-03	2.94E-04	5.3566E-03	1.12E-04	6.4818E+01	2.77E-01	2.5889E-06	1.74E-07
8.3897E-03	1.53E-04	8.3760E-03	9.64E-05	5.8502E+01	2.85E-01	4.0764E-06	5.48E-08
1.0803E-02	1.04E-04	1.0734E-02	3.04E-04	5.6093E+01	1.74E-01	5.9043E-06	2.40E-07
3.2083E-03	1.14E-04	3.2372E-03	1.67E-04	6.7659E+01	5.13E-01	1.2930E-06	1.60E-07
6.4574E-03	1.42E-04	6.5297E-03	2.53E-04	6.5334E+01	4.79E-01	4.0556E-06	1.89E-07
1.2014E-02	2.45E-04	1.2210E-02	5.86E-05	6.1884E+01	3.09E-01	1.0592E-05	3.97E-07
6.8405E-03	1.77E-04	6.9054E-03	1.94E-04	6.3827E+01	5.01E-01	3.9668E-06	1.09E-07
1.4355E-02	1.06E-04	1.4589E-02	1.36E-04	6.7560E+01	8.31E-01	2.5868E-05	3.30E-06
3.3626E-03	2.01E-04	3.4761E-03	1.03E-04	4.5013E+01	2.88E-01	3.8052E-07	2.73E-08
2.0478E-04	8.54E-05	1.6243E-04	1.31E-04	6.6909E+01	4.76E-01	4.0447E-09	3.30E-09

 Tab. E.2: Continued.

$ar{H}_{0i}$	Error	$ar{H}_{i0}$	Error	$ar{H}_{ii}$	Error	$\delta e_i^{(2)}$	Error
9.6855E-03	9.59E-05	9.5679E-03	8.02E-05	6.9543E+01	3.17E-01	1.4982E-05	7.33E-07
7.4249E-03	2.04E-04	7.2866E-03	9.96E-05	6.1476E+01	2.57E-01	3.7941E-06	1.49E-07
6.4985E-03	2.89E-04	6.6875E-03	4.11E-05	6.3896E+01	3.55E-01	3.6752E-06	2.61E-07
3.1231E-03	3.25E-04	3.1536E-03	1.55E-04	6.3428E+01	3.76E-01	8.0255E-07	1.13E-07
1.4101E-03	2.31E-04	1.4497E-03	1.61E-04	6.2848E+01	8.37E-01	1.5790E-07	2.50E-08
2.7682E-03	2.57E-04	2.8712E-03	1.42E-04	4.0669E+01	1.65E-01	2.2718E-07	3.01E-08
2.3079E-03	3.05E-04	2.2768E-03	8.08E-05	6.5568E+01	3.46E-01	5.1726E-07	7.35E-08
1.9213E-03	1.12E-04	1.9758E-03	8.20E-05	4.9545E+01	4.44E-01	1.4493E-07	1.02E-08
4.2653E-03	2.15E-04	4.2711E-03	2.16E-04	6.4059E+01	3.55E-01	1.5621E-06	1.41E-07
3.2511E-03	2.17E-04	3.2841E-03	1.41E-04	6.5483E+01	2.67E-01	1.0441E-06	1.20E-07
1.3190E-04	1.09E-04	1.6169E-04	1.96E-04	6.8362E+01	3.11E-01	4.0297E-09	7.47E-09
5.4526E-03	1.09E-04	5.3895E-03	2.02E-04	6.9065E+01	1.32E+00	4.5285E-06	7.92E-07
2.4728E-03	2.90E-04	2.1750E-03	1.93E-04	6.3183E+01	8.27E-01	4.3021E-07	7.64E-08
2.6277E-03	1.62E-04	2.8107E-03	1.71E-04	6.4084E+01	8.08E-01	6.3884E-07	9.84E-08
4.1174E-03	1.59E-04	4.3593E-03	1.25E-04	6.3922E+01	2.02E-01	1.5190E-06	7.66E-08
1.9117E-03	1.86E-04	1.9526E-03	1.37E-04	6.6362E+01	1.35E+00	4.0216E-07	5.25E-08
4.5920E-03	1.69E-04	4.7113E-03	2.00E-04	6.4462E+01	3.97E-01	1.9210E-06	1.40E-07
8.9714E-03	1.36E-04	9.0403E-03	1.54E-04	6.3489E+01	3.18E-01	6.6239E-06	2.38E-07
6.4799E-03	4.33E-04	6.5481E-03	2.53E-04	5.9642E+01	2.80E-01	2.6367E-06	2.14E-07
4.8113E-03	2.48E-04	4.6520E-03	5.76E-05	6.7210E+01	8.20E-01	2.6461E-06	3.28E-07
3.1594E-03	2.21E-04	3.1700E-03	2.67E-04	7.1144E+01	2.07E+00	3.2538E-06	3.10E-06
6.2752E-03	3.99E-04	6.2525E-03	1.69E-04	5.8544E+01	3.85E-01	2.2825E-06	1.65E-07
7.7562E-03	8.53E-05	7.8087E-03	8.67E-05	6.5375E+01	1.20E-01	5.8440E-06	1.30E-07
1.0825E-03	1.47E-04	1.0712E-03	5.62E-05	3.0835E+01	2.36E-01	2.5882E-08	4.29E-09
1.1820E-03	4.03E-04	1.2342E-03	1.53E-04	6.0514E+01	2.34E-01	9.8580E-08	4.17E-08
4.6508E-03	2.81E-04	4.6449E-03	1.93E-04	6.0098E+01	9.46E-01	1.3810E-06	5.55E-08
2.5417E-03	2.36E-04	2.5197E-03	9.24E-05	6.0178E+01	6.27E-01	4.1093E-07	2.87E-08
1.3751E-03	4.76E-04	1.0802E-03	1.78E-04	6.2760E+01	3.03E-01	1.1394E-07	3.95E-08
4.0803E-03	2.71E-04	4.1034E-03	9.95E-05	6.3237E+01	5.45E-01	1.3411E-06	1.11E-07
2.9707E-03	2.63E-04	2.8739E-03	1.96E-04	6.0672E+01	9.17E-01	5.6704E-07	5.94E-08
3.8430E-03	2.90E-04	3.6349E-03	5.81E-05	5.8363E+01	5.03E-01	8.0605E-07	8.93E-08
1.0074E-03	2.90E-04	1.1402E-03	1.20E-04	6.1338E+01	5.23E-01	7.9043E-08	2.17E-08
1.6846E-03	2.34E-04	1.4262E-03	2.10E-04	7.0850E+01	1.49E+00	5.1736E-07	1.27E-07
9.0998E-04	2.01E-04	9.0726E-04	1.83E-04	6.6238E+01	1.25E+00	8.7981E-08	3.05E-08
1.4906E-03	1.90E-04	1.3853E-03	9.91E-05	3.5491E+01	1.71E+00	5.1828E-08	1.10E-08

Tab. E.2: Continued.

$ar{ar{H}_{0i}}$	Error	$ar{H}_{i0}$	Error	$ar{H}_{ii}$	Error	$\delta e_i^{(2)}$	Error
3.7170E-03	3.51E-04	3.7458E-03	2.09E-04	5.9241E+01	2.01E-01	8.4562E-07	1.13E-07
3.0355E-03	3.12E-04	3.1919E-03	1.06E-04	6.0320E+01	1.30E-01	6.2969E-07	8.20E-08
3.7944E-03	4.19E-04	3.8305E-03	1.32E-04	5.4954E+01	4.12E-01	6.9927E-07	8.01E-08
7.8405E-04	2.89E-04	8.5168E-04	1.10E-04	2.9330E+01	1.28E-01	1.4708E-08	7.30E-09
2.0434E-03	2.41E-04	2.1590E-03	1.10E-04	4.4976E+01	4.40E-01	1.4371E-07	2.12E-08
7.5875E-04	3.20E-04	7.6344E-04	2.18E-04	4.0951E+01	2.55E-01	1.7171E-08	9.98E-09
3.9300E-04	2.45E-04	4.4457E-04	4.10E-05	7.0171E+01	1.99E+00	4.3058E-08	4.16E-08
1.2205E-03	1.02E-04	1.4456E-03	2.40E-04	7.0587E+01	9.94E-01	3.5334E-07	9.37E-08
2.2849E-03	2.42E-04	2.1323E-03	1.40E-04	6.6189E+01	6.25E-01	5.1114E-07	6.64E-08
1.3258E-03	2.07E-04	1.1507E-03	1.60E-04	6.6141E+01	1.02E+00	1.5851E-07	2.38E-08
2.8259E-03	2.09E-04	2.8423E-03	5.65E-05	4.2560E+01	2.20E-01	2.4233E-07	2.26E-08
1.5157E-04	2.15E-04	9.4243E-05	5.81E-05	3.0522E+01	9.35E-02	3.4468E-10	4.37E-10
3.6844E-03	2.87E-04	3.6324E-03	2.03E-04	6.5862E+01	1.82E-01	1.3584E-06	1.72E-07
1.4555E-03	1.51E-04	1.3777E-03	1.50E-04	7.4997E+01	3.85E-01	3.4262E-06	2.07E-06
3.9834E-04	2.39E-04	7.0141E-04	2.61E-04	6.9760E+01	4.13E-01	5.0187E-08	3.47E-08
1.5419E-03	2.31E-04	1.5249E-03	6.81E-05	4.5505E+01	1.76E+00	7.7480E-08	8.98E-09
4.6014E-04	1.97E-04	6.1631E-04	1.39E-04	4.2914E+01	5.30E-01	8.6326E-09	4.52E-09
2.2927E-03	1.90E-04	2.1782E-03	1.93E-04	4.2536E+01	3.78E-01	1.5113E-07	2.36E-08
3.6407E-03	3.69E-04	3.7128E-03	1.74E-04	6.5855E+01	1.06E+00	1.3774E-06	1.84E-07
1.7097E-03	3.44E-04	1.8511E-03	1.85E-04	6.2159E+01	4.54E-01	2.3370E-07	5.50E-08
5.5006E-04	1.07E-04	3.6392E-04	1.28E-04	6.6799E+01	2.81E-01	2.2748E-08	9.63E-09
3.0578E-03	2.03E-04	3.1196E-03	1.66E-04	4.2594E+01	4.95E-01	2.8839E-07	3.25E-08
1.0869E-03	4.09E-04	1.1893E-03	1.62E-04	6.0778E+01	3.65E-01	8.8623E-08	4.08E-08
3.9150E-04	1.67E-04	2.8512E-04	6.63E-05	6.1189E+01	5.11E-01	8.0907E-09	5.05E-09
3.6573E-04	2.24E-04	1.7828E-04	1.08E-04	3.0994E+01	4.61E-01	1.5394E-09	1.62E-09
3.7428E-04	1.93E-04	4.2276E-04	6.17E-05	3.8232E+01	6.55E-01	4.3100E-09	2.26E-09
1.2309E-03	2.39E-04	1.5533E-03	2.05E-04	6.9966E+01	2.41E+00	4.4631E-07	3.57E-07
2.1923E-03	2.47E-04	1.9305E-03	1.75E-04	5.9294E+01	2.64E-01	2.5953E-07	5.32E-08
1.0050E-02	1.36E-04	1.0097E-02	1.44E-04	6.9339E+01	1.23E-01	1.5858E-05	3.97E-07
3.6282E-04	9.31E-05	3.5105E-04	2.31E-04	6.4015E+01	3.57E-01	1.1218E-08	7.29E-09
9.0874E-04	2.13E-04	7.4512E-04	1.76E-04	7.3394E+01	1.50E+00	1.7368E-06	3.46E-06
2.5817E-03	2.16E-04	2.4939E-03	1.25E-04	5.7251E+01	4.54E-01	3.4841E-07	3.59E-08
4.6997E-04	7.43E-05	5.9542E-04	1.84E-04	7.4001E+01	1.30E+00	2.9845E-06	6.37E-06
3.1083E-04	2.82E-04	3.9084E-04	9.98E-05	6.5570E+01	1.28E+00	1.1759E-08	1.04E-08
1.1342E-03	1.97E-04	1.1139E-03	1.04E-04	4.5858E+01	5.88E-01	4.2400E-08	8.50E-09

 Tab. E.2: Continued.

$ar{H}_{0i}$	Error	$ar{H}_{i0}$	Error	$ar{H}_{ii}$	Error	$\delta e_i^{(2)}$	Error
1.0850E-02	1.54E-04	1.0677E-02	9.15E-05	3.2964E+01	2.34E-01	2.7083E-06	5.33E-08
6.9473E-04	3.13E-04	8.0782E-04	2.30E-04	4.3445E+01	3.23E-01	1.8243E-08	9.47E-09
6.4743E-04	1.72E-04	6.6612E-04	1.78E-04	4.5394E+01	9.19E-01	1.3913E-08	4.03E-09
5.5130E-04	2.78E-04	5.5429E-04	1.96E-04	6.2234E+01	1.32E+00	2.1925E-08	1.27E-08
1.7051E-03	2.04E-04	1.5843E-03	7.62E-05	4.3789E+01	2.04E+00	8.5089E-08	1.42E-08
1.0574E-03	1.42E-04	8.8395E-04	1.64E-04	7.2287E+01	4.56E+00	1.7655E-07	4.29E-08
4.4520E-04	3.25E-04	4.9585E-04	2.01E-04	4.1952E+01	1.02E+00	6.4125E-09	6.21E-09
2.5532E-04	2.43E-04	1.9991E-04	1.75E-04	6.6131E+01	4.24E-01	4.3200E-09	6.69E-09
5.0962E-04	3.60E-04	1.4586E-04	1.71E-04	4.2733E+01	2.48E-01	1.6470E-09	1.79E-09
1.8654E-03	1.85E-04	1.9581E-03	1.32E-04	6.1634E+01	4.80E-01	2.5967E-07	3.67E-08
2.7462E-04	3.01E-04	1.7529E-04	1.56E-04	6.6646E+01	4.30E-01	9.6934E-09	1.72E-08
2.5189E-04	1.62E-04	2.1689E-04	1.37E-04	6.6925E+01	7.13E-01	5.7441E-09	4.92E-09
1.3447E-04	8.27E-05	2.5740E-04	1.69E-04	4.2614E+01	5.13E-01	1.1314E-09	8.08E-10
2.8262E-03	2.58E-04	2.6328E-03	2.84E-04	6.0879E+01	7.42E-01	5.0471E-07	9.39E-08
6.8101E-03	1.01E-04	6.8279E-03	1.26E-04	7.1745E+01	1.58E-01	1.1653E-05	5.70E-07
4.7138E-04	2.26E-04	5.1289E-04	2.12E-04	6.3675E+01	8.02E-01	2.0063E-08	1.32E-08
3.0965E-04	2.20E-04	2.4224E-04	1.86E-04	6.5463E+01	1.07E+00	6.9653E-09	6.73E-09
5.2595E-04	1.14E-04	3.9541E-04	2.85E-04	6.4109E+01	2.38E+00	1.9848E-08	1.77E-08
2.1287E-04	1.91E-04	1.2832E-04	1.04E-04	6.7365E+01	4.87E-01	3.9301E-09	5.75E-09
3.4417E-04	2.93E-04	3.7480E-04	1.86E-04	6.4391E+01	4.51E-01	1.2412E-08	1.33E-08
3.6479E-04	2.07E-04	3.0255E-04	1.74E-04	6.6528E+01	1.35E+00	1.4081E-08	1.49E-08
8.7675E-05	5.93E-05	1.1638E-04	1.07E-04	6.9509E+01	5.35E-01	1.8412E-09	1.67E-09
9.0881E-05	8.47E-05	9.6910E-05	7.64E-05	7.1296E+01	3.44E-01	2.3129E-09	2.55E-09
2.5461E-04	1.34E-04	8.1818E-05	6.76E-05	6.3571E+01	7.04E-01	2.2456E-09	2.05E-09
1.6294E-04	1.26E-04	1.3305E-04	9.42E-05	6.3397E+01	4.07E-01	1.3271E-09	1.52E-09
1.2365E-04	7.41E-05	1.3234E-04	6.90E-05	6.5587E+01	5.29E-01	1.6497E-09	1.25E-09
2.0945E-04	1.14E-04	1.7344E-04	1.34E-04	6.6975E+01	3.37E-01	4.6941E-09	5.96E-09
1.2495E-04	5.48E-05	1.8343E-04	1.46E-04	6.9280E+01	5.15E-01	3.1805E-09	3.05E-09
1.4901E-04	1.09E-04	6.3043E-05	6.55E-05	6.8505E+01	3.38E-01	1.1376E-09	1.90E-09
1.7839E-04	1.33E-04	1.9285E-04	1.49E-04	6.7450E+01	1.09E+00	2.8758E-09	2.55E-09

CIPSI-Jastrow Wave Functions

VMC and DMC Energies

Tab. E.3: C_2 VMC and DMC energies in E_h for truncated CIPSI wave functions using SDs.

Threshold	VMC	DMC
0.0100	-75.6276(4)	-75.9007(6)
0.0075	-75.6484(4)	-75.9032(6)
0.0050	-75.6793(4)	-75.9041(5)
0.0025	-75.7049(4)	-75.9066(5)

Tab. E.4: C_2 VMC and DMC energies in E_h for CIPSI-Jastrow wave functions (Determinant and CSF expansions) at various optimization levels using two different Jastrow factors.

		VMC			DMC				
Threshold	Jas	Jas+CI	Jas+MO+CI	Jas	Jas+CI	Jas+MO+CI			
0.0100	-75.8463(4)	-75.8525(3)	-75.8763(3)	-75.9007(5)	-75.9064(5)	-75.9122(5)			
0.0075	-75.8531(4)	-75.8614(4)	-75.8816(3)	-75.9034(5)	-75.9089(5)	-75.9141(5)			
0.0050	-75.8619(3)	-75.8725(3)	-75.8869(3)	-75.9050(5)	-75.9119(5)	-75.9171(5)			
0.0025	-75.8683(3)	-75.8801(3)	-75.8892(3)	-75.9066(5)	-75.9152(5)	-75.9160(5)			
			Det, sm666						
0.0100	-75.8597(3)	-75.8669(3)	-75.8842(3)	-75.9011(5)	-75.9065(5)	-75.9120(5)			
0.0075	-75.8658(3)	-75.8746(3)	<i>-</i> 75.8895(3)	-75.9040(5)	-75.9090(5)	-75.9135(5)			
0.0050	-75.8718(3)	-75.8838(2)	-75.8936(3)	-75.9066(5)	-75.9118(5)	-75.9162(5)			
0.0025	-75.8768(3)	-75.8902(3)	-75.8940(3)	-75.9067(5)	-75.9142(5)	-75.9167(5)			
			CSF, sm444						
0.0100	-75.8482(4)	-75.8557(3)	-75.8785(3)	-75.9023(5)	-75.9083(5)	-75.9125(5)			
0.0075	-75.8561(4)	-75.8651(3)	-75.8832(3)	-75.9034(5)	-75.9099(5)	-75.9149(5)			
0.0050	-75.8637(3)	-75.8756(3)	-75.8891(3)	-75.9049(5)	-75.9128(5)	-75.9161(5)			
0.0025	-75.8702(3)	-75.8816(3)	-75.8917(3)	-75.9076(5)	-75.9149(5)	-75.9183(5)			
	CSF, sm666								
0.0100	-75.8621(3)	-75.8705(3)	-75.8875(3)	-75.9024(5)	-75.9084(5)	-75.9130(5)			
0.0075	-75.8677(3)	-75.8780(3)	-75.8913(3)	-75.9042(5)	-75.9104(5)	-75.9148(5)			
0.0050	-75.8725(3)	-75.8863(3)	-75.8953(3)	-75.9045(5)	-75.9147(5)	-75.9158(5)			
0.0025	-75.8775(3)	-75.8916(3)	-75.8959(3)	-75.9071(5)	-75.9161(5)	-75.9182(5)			
0.0010			-75.9025(3)			-75.9197(5)			

Tab. E.5: C VMC and DMC energies in E_h for fully optimized (Jas+MO+CI) truncated CIPSI-Jastrow CSF wave functions. An sm666 Jastrow factor was used.

Truncation Scheme <i>a</i>			Tru	ncation Scher	me b	Truncation Scheme <i>c</i>		
Threshold	VMC	DMC	Threshold	VMC	DMC	Threshold	VMC	DMC
0.0100	-37.8378(2)	-37.8432(5)	0.1000	-37.8240(2)	-37.8365(5)	0.1000	-37.8240(2)	-37.8365(5)
0.0075	-37.8400(2)	-37.8438(5)	0.0870	-37.8240(2)	-37.8365(5)	0.0550	-37.8231(3)	-37.8346(5)
0.0050	-37.8397(3)	-37.8438(5)	0.0710	-37.8240(2)	-37.8365(5)	0.0380	-37.8321(2)	-37.8408(5)
0.0025	-37.8401(3)	-37.8448(5)	0.0500	-37.8238(3)	-37.8364(5)	0.0340	-37.8330(3)	-37.8415(5)
0.0010	-37.8391(2)	-37.8430(5)	0.0320	-37.8329(3)	-37.8424(5)	0.0230	-37.8362(2)	-37.8424(5)

Tab. E.6: C_2 VMC and DMC energies in E_h for truncated CIPSI-Jastrow wave functions using Slater determinants for different sets of initial orbitals.

			VMC	D:	MC				
Threshold	# Dets	Jas	Jas+CI	Jas+MO+CI	Jas+CI	Jas+MO+CI			
B3LYP									
0.0100	191	-75.8721(3)	-75.8781(3)	-75.8844(3)	-75.9109(5)	-75.9120(5)			
0.0075	300	-75.8740(3)	-75.8832(2)	-75.8890(3)	-75.9118(5)	-75.9142(4)			
0.0050	589	-75.8769(3)	-75.8882(2)	-75.8938(3)	-75.9140(5)	-75.9161(5)			
0.0025	1377	-75.8815(3)	-75.8942(2)	-75.8983(3)	-75.9174(5)	-75.9173(5)			
			PBE0						
0.0100	189	-75.8706(3)	-75.8775(3)	-75.8843(3)	-75.9107(5)	-75.9123(5)			
0.0075	286	-75.8732(3)	-75.8809(3)	-75.8891(3)	-75.9119(5)	-75.9129(5)			
0.0050	581	-75.8760(3)	-75.8871(2)	-75.8941(3)	-75.9137(5)	-75.9153(5)			
0.0025	1379	-75.8807(3)	-75.8938(2)	-75.8983(3)	-75.9161(5)	-75.9175(5)			
CAS(8,8)									
0.0100	143	-75.8671(3)	-75.8744(3)	-75.8848(3)	-75.9094(5)	-75.9128(4)			
0.0075	240	-75.8700(3)	-75.8794(3)	-75.8895(3)	-75.9123(5)	-75.9139(5)			
0.0050	510	-75.8745(3)	-75.8862(3)	-75.8937(3)	-75.9140(5)	-75.9167(4)			
0.0025	1201	-75.8788(3)	-75.8913(2)	-75.8983(3)	-75.9157(5)	-75.9185(5)			